

Bridging the gap: combined optical tweezers with free standing lipid membrane

Marin Lizarraga, Victor

DOI

[10.4233/uuid:38f761f4-6d73-4ca9-9cca-8de432184f0c](https://doi.org/10.4233/uuid:38f761f4-6d73-4ca9-9cca-8de432184f0c)

Publication date

2018

Document Version

Final published version

Citation (APA)

Marin Lizarraga, V. (2018). *Bridging the gap: combined optical tweezers with free standing lipid membrane*. [Dissertation (TU Delft), Delft University of Technology]. <https://doi.org/10.4233/uuid:38f761f4-6d73-4ca9-9cca-8de432184f0c>

Important note

To cite this publication, please use the final published version (if applicable). Please check the document version above.

Copyright

Other than for strictly personal use, it is not permitted to download, forward or distribute the text or part of it, without the consent of the author(s) and/or copyright holder(s), unless the work is under an open content license such as Creative Commons.

Takedown policy

Please contact us and provide details if you believe this document breaches copyrights. We will remove access to the work immediately and investigate your claim.

Bridging the gap: combined optical tweezers with free standing lipid membrane

Victor Manuel Marin Lizarraga

**Bridging the gap: combined optical tweezers with free standing lipid
membrane**

Dissertation

**for the purpose of obtaining the degree of doctor
at Delft University of Technology
by the authority of the Rector Magnificus Prof. dr. ir. T.H.J.J. Van der Hagen
chair of the Board for Doctorates
to be defended publicly on
Friday 23 of February 2018 at 12:30 o'clock**

by

**Victor Manuel MARIN LIZARRAGA
Master of Biomedical Engineering and Physics, Center for Research and
Advanced Studies campus Monterrey, Mexico**

born in Merida, Mexico

This dissertation has been approved by the promotor.

Composition of the doctoral committee:

Rector Magnificus,	chairperson
Prof. dr. S. J. Tans	Delft University of Technology/ AMOLF, promotor
Dr. Marie-Eve Aubin-Tam	Delft University of Technology, copromotor

Independent memers:

Prof. dr. M. Dogterom	Delft University of Technology
Prof. dr. C. Wyman	Delft University of Technology/Erasmus University
Prof. dr. ir. M.W.J. Prins	Eindhoven University of Technology
Dr. C. Danelon	Delft University of Technology
Dr. L. Segerink	Twente University



Bionanoscience Department
Think big about life at the smallest scale



Keywords: Optical tweezers, NOA81, lipid membrane, lipid nanotube, microfluidics

Printed by: Ridderprint

Cover by: Victor Manuel Marin Lizarraga

Copyright © 2018 by Victor Manuel Marin Lizarraga

Casimir PhD series, delft-Leiden 2018-05

ISBN 978-90-8593-337-3

An electronic copy of this dissertation is available at:

<http://repository.tudelft.nl/>.

Contents

Introduction	1
1.1 Membranes of living systems	2
1.2 Methods to assemble model membranes	3
1.2.1 Liposomes	3
1.2.2 Lipid bilayer supported on a surface.	4
1.2.3 Free standing lipid bilayers on apertures	4
1.2.4 Applications of model membranes	5
1.3 Mechanical studies of membranes	5
1.3.1 Analysis of membrane fluctuations	5
1.3.2 Membrane mechanical deformation	6
1.4 This thesis	8
1.5 References	9
Microfluidic approaches for the formation of lipid membranes	13
2.1 Microfluidic devices for assembling lipid membranes	14
2.1.1 Soft polymers	14
2.1.2 Glass	15
2.1.3 UV curable polymers	15
2.2 Surface properties and modifications for microfluidics	15
2.3 Methods to assemble lipid membranes in microfluidics	18
2.3.1 Double emulsion droplet system to form lipid vesicles	18
2.3.2 Lipid bilayers in a cross-geometry	19
2.3.3 Lipid bilayers spanning apertures	19
2.4 Characterization of lipid bilayers formed in microdevices	22

2.4.1 Electrophysiology: electrical properties of lipid membranes	22
2.4.2 Membrane visualization by confocal microscopy.	24
2.5 References	26
Free standing lipid bilayers formation in Norland optical adhesive (NOA81) microchannels	31
3.1 Introduction	32
3.2 Material and Methods	33
3.2.1 PDMS microfluidic device formation.	33
3.2.2 Glass microfluidic device.	33
3.2.3 NOA81 microfluidic device formation.	35
3.2.4 Lipid bilayer formation.	36
3.2.5 Sessile drop experiment.	36
3.2.6 Fluorescence confocal microscopy.	36
3.2.7 Capacitance measurements.	37
3.2.8 Electrophysiology measurements with α -Hemolysin.	37
3.3 Results and Discussion	38
3.3.1 Attempts to form free standing lipid bilayers in PDMS microdevices .	38
3.3.2 Formation of free standing lipid bilayers in glass microdevices	39
3.3.3 Formation of free standing lipid bilayers in NOA81 microdevices. . . .	42
3.3.3.1 Characterization of the silanized-NOA81 surface	43
3.3.3.2 Formation of free standing DPhPC and DOPC/DPPC bilayers	44
3.3.3.3 Measurement of lipid bilayer surface area with fluorescence confocal microscopy.	45
3.3.3.4 Electrical measurements of free standing lipid bilayers	48
3.3.3.5 Single protein pore insertion	49

3.4 Conclusions	51
3.5 Reference	52
3.6 Appendix	55
Combination of free standing lipid membranes with optical tweezers	57
4.1 Introduction	58
4.1.1 General configuration of optical tweezers	59
4.1.2 Optical tweezers stiffness calibration	60
4.1.2.1 Drag force method	61
4.1.2.2 Power spectrum method	62
4.1.2.3 Equipartition theorem method	63
4.2 Material and methods.	65
4.2.1 Microfluidic device description, fabrication and surface functionalization.	65
4.2.2 Lipid membrane formation.	66
4.2.3 Lipid membrane visualization	66
4.2.4 Capacitance measurements	66
4.2.5 Optical tweezers experiments	67
4.3 Results and discussion.	69
4.4 Conclusion	75
4.5 References	77
Lipid nanotube formation on planar lipid membranes	81
5.1. Introduction	82
5.1.1 Lipid nanotubes in cells	82
5.1.2 Lipid nanotube formation triggered by an external force	83

5.2 Material and Methods	87
5.2.1 Microfluidic device fabrication	87
5.2.2 Free standing lipid membrane formation	87
5.2.3 Optical tweezers experiments	87
5.2.4. Image particle tracking of retracting lipid nanotubes	88
5.3 Results and discussion.	89
5.4 Conclusion	95
5.5 References	96
5.6 Appendix	99
Conclusion and Outlook	103
6.1 Summary	104
6.2 Contributions to the field	104
6.2.1 Development of artificial lipid membranes in microfluidics	104
6.2.2 Optical tweezers combined with artificial lipid membrane	105
6.3 Future work	106
6.4 References	107
Glossary	109
Acknowledgements	111
Curriculum vitae.	113
Publications	114

Chapter 1

Introduction

“Imagination will often carry us to worlds that never were, but without it we go nowhere.”

Carl Sagan

All known living organisms are contained and protected by lipidic barriers. These lipidic barriers or membranes exhibit multiple intriguing properties, and their study have benefited from interdisciplinary approaches at the interface of physics, chemistry and biology. The importance of lipid membranes in many vital cell processes highlights the need of developing technologies to facilitate the study of their properties. This introductory chapter describes the technologies currently available to form, study and characterize artificial lipidic systems, and then leads to a general description of this thesis.

1.1 Membranes of living systems

Cells are complex living systems, which make use of semipermeable barriers known as biological membranes for protection and for communication with the environment. The role of membranes goes far beyond enclosing and defining cells and organelles. Many essential processes for organisms, such as transport, sensing and energy conversion, are carried out on biological membranes. Amphipathic lipidic molecules constitute the fundamental building blocks of these biological barriers. The intrinsic amphipathic nature of these molecules grants them with an elegant self-assembling mechanism, in which they form a lipid bilayer to wrap off the cell. In addition, a broad variety of functions and mechanical capabilities are enabled due to specific lipids and liposoluble molecules found in membranes. There is a large variety of lipid molecules found in cell membranes. The basic chemical characteristic of lipid molecules consists of having one hydrophilic head and one or several hydrophobic tails. The more abundant lipidic molecules that constitute the cell membranes are the glycerophospholipids which contains a glycerol molecule joined to two fatty acid tails by a phosphate ester bond.

Nonpolar molecules like O_2 and CO_2 can diffuse across the membrane allowing cells to perform the respiration process. In contrast, ions and polar molecules are impermeable to membranes. These molecules require the use of transmembrane proteins to cross the lipid bilayer to participate in physiological processes. Such transport across transmembrane proteins can be categorized into either *passive transport*, if a gradient of solute is driving the translocation, or *active transport* if additional energy is needed. Transport across the membrane is not only a process vital for cells, but also a mechanism for killing host cells accomplished by pathogenic microorganisms. Transmembrane proteins can be secreted by pathogens and used as toxins to lyse cells or translocate cargo proteins to stop specific metabolic pathways. For example, α -Hemolysin secreted by *Staphylococcus aureus*, kills cells by forming transmembrane channels, producing lethal changes in osmotic pressure [1]. However, transport regulation is not the only function of proteins in the lipid membranes. Communication among cells is achieved by surface receptors hosted into the membrane that can recognize specific chemical signals. Specific membrane receptors also enable the immune system to detect pathogens like viruses or microorganisms. External or internal stimulus can trigger different phenomena in cells like an increase in the production of receptors and transporters, influencing the overall functionality of the membrane [2].

Cells are continuously under the influence of external mechanical, chemical or electrical stimuli, happening at the membrane interface. The mechanical properties of lipid bilayers enable cells to rapidly adjust their mechanics and morphology in response to these signals. For instance, in response to a specific stimulus, a cell can modify its cytoskeletal configuration in order to generate small membrane protrusion, eventually leading to cell motion. Pseudopodia and pili are good illustrations of biomechanical cell motion induced by a change in membrane conformation. Another example is phagocytosis and endocytosis, where a membrane invagination is needed

to wrap solid particles into membrane sacks for digestion. Additionally, the formation of cylindrical or tube-like elongated structures have been observed in cells for inter-cellular communication. Such cylindrical lipid membrane consists of few nanometers in diameter (~50 nm) but can be extended in length to up to the micrometer scale. Their formation can be initiated by applying a force on the membrane.

The study of cell membranes is key to unravel complex biological processes. Several approaches have been developed to study lipid membranes' properties, starting from the identification of their chemical structure using mass spectroscopy [3, 4], ensemble properties with X-ray diffraction studies [5], up to their mechanical properties [6, 7]. Membrane investigations began with *in vivo* studies. However, the highly complex composition of membranes in living systems brought major challenges. For this reason, the development of more controlled systems became needed. Artificial lipidic systems allowed performing systematic studies with adjustable lipid compositions into controlled environments. The increasing need for those conditions gave birth to artificial lipid bilayers assembled *in vitro*, also known as model lipid membranes.

1.2 Methods to assemble model membranes

The goal of artificial lipid membranes is to mimic cell membranes. Depending on the required application, different levels in complexity can be achieved. However, each method has shown different advantages and disadvantages. Model lipid membranes help us to understand complex processes carried out by cell membranes, in a more controlled environment and systematic approach. Different methods have been developed to self-assemble lipids into model membranes with different properties (Fig. 1.1) [8]. These approaches rely on the amphipathic nature of lipids, which self-assemble into bilayers to minimize the interaction between the hydrophobic tails and the aqueous medium. Current model lipid membranes can be generally classified as liposomes, supported lipid bilayers and free standing lipid bilayers on apertures [9, 10].

1.2.1 Liposomes

It is energetically unfavorable for lipid bilayers to expose free edges to water. Therefore, thin films of bilayers tend to bend themselves to form vesicles (Fig. 1.1a) in aqueous medium. This configuration is more stable because it avoids hydrophobic regions, in the cross-section of the bilayer, to be exposed to the aqueous medium. Although bending the lipid bilayer requires energy, the edge energy is usually more energetically costly. Liposomes can be classified as: small unilamellar vesicles (SUV) [11], giant unilamellar vesicles (GUV) [12] and multilamellar vesicles (MLV) [13]. Liposomes have found applications as drug delivery systems, as synthetic cells and as precursors for other model membranes. Their mechanical properties depend on the nature of the phospholipid, the liposome size and the buffer conditions. Methods to produce liposomes include natural swelling [14], extrusion of GUV [15]

and electroswelling [16].

1.2.2 Lipid bilayer supported on a surface

When membranes are fully spanned on a surface, they are considered to be *supported* membranes [17]. Electrostatic interactions between the hydrophilic head of the phospholipid and the surface are usually used to achieve supported membranes [18]. The process consists of letting SUVs deposit on a surface (Fig. 1.1b). As soon as the SUVs interact with the surface, they deform and cover the maximum area until they eventually break and span on the surface [19]. Hydrophilic surfaces such as mica are used to span films of lipid membranes. It should be noted that this method can result in stacks of membranes as well as parts of the surface without any membrane. Also, modifying surface properties (e.g., hydrophobicity) can be done to control whether the membrane is a monolayer or a bilayer.

1.2.3 Free standing lipid bilayers on apertures

Lipid bilayers can also be formed over an aperture. These membranes are planar and usually require organic solvent for their formation. This type of membranes is also known as black lipid membranes (BLM) because they appear to be black, from the destructive interference of light reflected by the two sides of the membrane, which has a thickness in the nanometer scale [20]. Different approaches have been designed, but most of them consist of the formation of monolayers at a solvent/water interface, followed by the “zipping” of the two monolayers into a bilayer, when the two make contact at the aperture (Fig. 1.1c). The size and the surface properties (e.g., electrostatic, hydrophobic) of the aperture play an important role on membrane stability [21]. Higher stability is achieved as the aperture size reduces and its hydrophobicity increases [22].

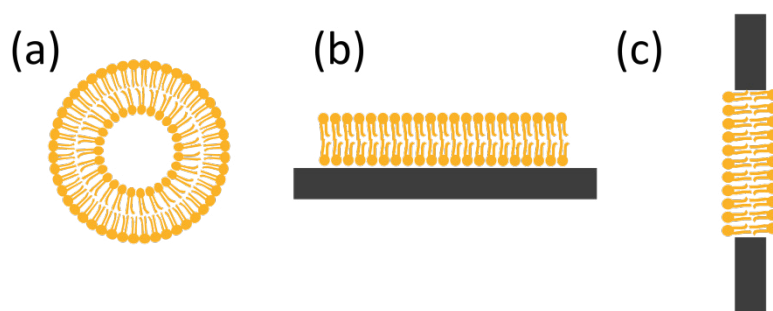


Figure 1.1: Overview of different model lipid membranes. Assembly of artificial phospholipid bilayers into: (a) vesicles, (b) supported bilayer and (c) lipid bilayers on apertures. Stable flat lipid membranes in aqueous solution are accomplished with the help of a rigid material. Vesicles and flat lipid bilayer on apertures are both considered as free standing lipid bilayers. Picture adapted from [10].

1.2.4 Applications of model membranes

Biophysical studies of model lipid membranes demonstrate their versatility in mimicking cell membranes [10, 23]. Combination with other methods like fluorescence enables the study of lipid rafts and of phase transition in complex membranes. Model membranes with access to both sides of the membrane, such as vesicles and free standing lipid membranes on apertures enable electrophysiology studies, which allow to investigate transport mechanisms across the membranes. Model membranes are not only used to understand the electrical properties but also the mechanical properties of cell membranes. Technological advances in micromanipulation have enabled studies that show how shape deformation of lipid membranes is relevant to biological processes [24]. Fusion vesicle studies have shown that vesicles are promising systems to deliver certain drugs into the human body [25] therefore model membranes have also found applications in drug delivery [26]. Additionally, model membranes have shown potential application as sensors [27, 28]. The sensing application of lipid membranes together with membrane nanopores [29, 30] shows promisingly uses for sequencing of DNA on a single molecule level [31-33].

1.3 Mechanical studies of membranes

Cell membranes undergo important morphological changes during cell replication, motility and phagocytosis. *In vivo* mechanical studies of the membranes of red blood cells have shown a crucial link between functionality and membrane morphological transition [34]. Detailed understanding of these processes requires the study of membrane mechanical properties. The increasing need for these types of investigation has driven the development of biophysical tools to unravel the mechanics of cell membranes. Combining observation and/or manipulation techniques with artificial membrane systems have demonstrated to be a suitable manner to study their mechanical properties (bending rigidity, elasticity). While early efforts have been done to model and predict these properties [35, 36] and study them experimentally [37-40], the mechanical properties of complex membrane systems are not fully understood. Different types of artificial lipid membranes show different properties. For example, GUVs are popular model membranes because of their solvent free condition. However GUVs are limited in the types of lipids that can easily form GUVs and their difficulty to form asymmetric bilayers. When studying the mechanical properties of membranes, different types of assays result in different model membrane requirements. These assays are briefly described hereafter.

1.3.1 Analysis of membrane fluctuations

Elastic properties of lipid membranes make them susceptible to fluctuations under certain thermal conditions. Fluctuation spectroscopy of GUVs measures the contour variations under the influence of heat to determine properties like tension and bending elasticity modulus [20, 27]. However, this method cannot be performed

on GUVs in gel phase, restricting this method to vesicles with low tension at room temperatures. Membrane fluctuations in free standing lipid bilayers formed over apertures can also be used similarly to reveal membrane tension [41].

1.3.2 Membrane mechanical deformation

Imposing a deformation on the membrane is a common method to assess its mechanical properties. There is a large diversity of tools employed to impose the deformation (Fig. 1.2). Electrical and magnetic fields can modify vesicle shape and the induced deformation can be correlated to the strength of the field in order to determine the membrane tension. Micropipette aspiration (Fig. 1.2a) consists of grabbing a single GUV with a glass micropipette and generating a suction in such way to obtain insights on the membrane tension [42]. The tension induced by the suction is used to control the area loaded inside the micropipette.

Other approaches use optical tweezers to apply a deformation force [43], such as out-of-plane deformation (Fig. 1.2b) which consists of deforming a membrane by contacting two particles onto the membrane, with one particle being pulled while the other one remaining fixed within the trap [44]. Bending rigidity can be determined via a measure of the relative particles displacement. In similar way, bending rigidity can be calculated via pulling a membrane tube from a GUV with an optically trapped bead. Using the optical tweezers to measure the force required to extend the tube, or “tethering” force, the bending rigidity can then be determined from the linear slope of this tethering force as a function of the square root of the membrane tension [45].

Supported lipid bilayers can also be used, though access is limited to only one side of the membrane. The elastic response of a lipid bilayer spanned onto a surface is usually measured with atomic force microscopy (AFM). This technique also allows imaging the topography of the surface [46], detecting lipid rafts [47], resolving the interaction of ligands with receptors on the membrane [48] and studying material properties (e.g., stiffness) [49]. However, interactions between the lipid bilayer and the surface can be a source of artefacts. To overcome this issue an alternative technique uses AFM on lipid bilayers spanned over apertures on a surface (Fig. 1.2c). In this technique, the AFM tip is displaced to apply a defined normal force on the membrane, which reveals local elastic properties of the free standing lipid membrane [40].

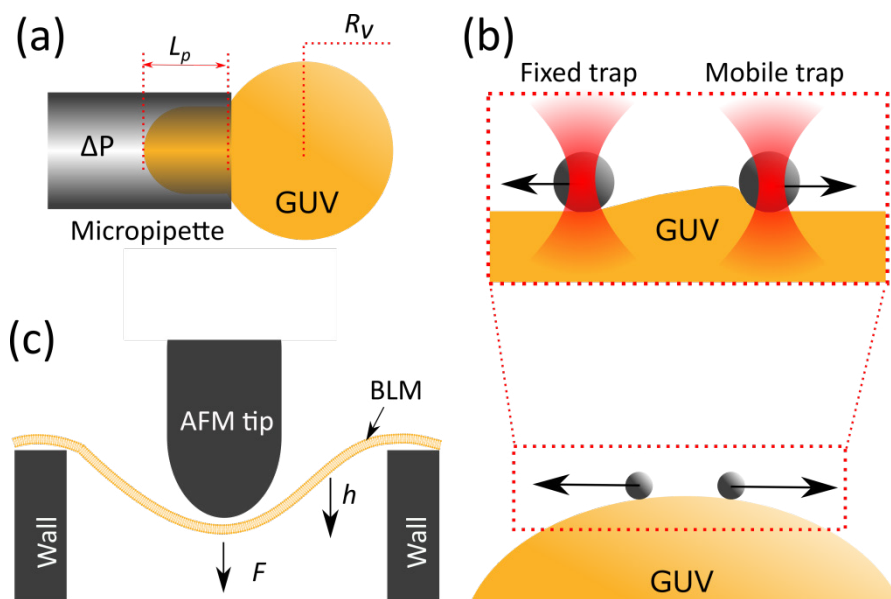


Figure 1.2: Biophysical methods to impose mechanical stress on model membranes. (a) Glass micropipette suction represents an easy method to manipulate GUVs and to measure mechanical properties. Mechanical stress and GUV deformation can be imposed by applying negative pressure (ΔP) and observing the proportion of the lipid bilayer introduced into the pipette aperture (L_p). (b) Drawing of a section of a GUV where two microparticles are adhered to a bilayer and manipulated with an optical tweezers. A force is imposed by rolling one particle, while the other remains fixed within the trap. (c) The tip of an AFM cantilever applies a force (F) over a free black lipid membrane (BLM). This method is restricted to assess a local region of the bilayer.

1.4 This thesis

Current methods to form model membranes show some limitations, such as complex manipulation and restriction to one side of the membrane. To address these issues, new methodology must be developed. For example, in the context of this thesis, it was proposed to form lipid bilayers over apertures inside a microfluidic device to gain free access to both sides of the membranes, and to design this device for integration into an optical tweezers to impose and measure forces and displacements with high resolution.

In chapter 2, a review of some of the current technologies to form artificial lipid membranes in microfluidics devices is presented. A big variety of methods are described in the literature, however the selection of the methods that are described in Chapter 2 is based on what it is considered more suitable for this specific project. The importance of the manufacturing conditions like flow cell material and surface chemistry is highlighted. A comparative review of such techniques opens the possibility for improvements. This chapter also introduces electrical and optical techniques commonly used to characterize artificial lipid membranes. Chapter 3 presents the development of a microfluidic device to assemble stable lipid membranes on apertures, using different flow cell materials like polydimethylsiloxane (PDMS), glass or Norland optical adhesive 81 (NOA81). Electrophysiology and confocal microscopy are used to characterize lipid bilayers formation. Chapter 4 demonstrates the combination of free standing lipid membranes formed over an aperture with an optical tweezers, which enables dynamic control and monitoring over conditions on both sides of the membrane. In chapter 5, the device is used to form lipid nanotubes. The easy access to both sides of the membrane enables not only to *pull*, but also to *push* membrane nanotubes of hundreds of microns in length, much longer than those formed from GUVs. Such long tubes open novel possibilities for the formation of artificial lipid tube networks that mimic the ones found in cellular organelles, as for instance in the endoplasmic reticulum (ER). A final summary is presented in chapter 6, as well as future possible studies to further develop this novel method.

1.5 References

1. Lubkin, A. and V.J. Torres, The ever-emerging complexity of α -toxin's interaction with host cells. *Proceedings of the National Academy of Sciences*, 2015. 112(46): p. 14123-14124.
2. Arcuino, G., et al., Intercellular calcium signaling mediated by point-source burst release of ATP. *Proceedings of the National Academy of Sciences*, 2002. 99(15): p. 9840-9845.
3. Harkewicz, R. and E.A. Dennis, Applications of Mass Spectrometry to Lipids and Membranes. *Annual Review of Biochemistry*, 2011. 80(1): p. 301-325.
4. Leão, B.C.S., et al., Membrane lipid profile monitored by mass spectrometry detected differences between fresh and vitrified in vitro-produced bovine embryos. *Zygote*, 2014. 23(5): p. 732-741.
5. Bhattacharya, S. and S. Haldar, Interactions between cholesterol and lipids in bilayer membranes. Role of lipid headgroup and hydrocarbon chain-backbone linkage. *Biochimica et Biophysica Acta (BBA) - Biomembranes*, 2000. 1467(1): p. 39-53.
6. Picas, L., F. Rico, and S. Scheuring, Direct Measurement of the Mechanical Properties of Lipid Phases in Supported Bilayers. *Biophysical Journal*, 2012. 102(1): p. L01-L03.
7. Garcia-Manyes, S. and F. Sanz, Nanomechanics of lipid bilayers by force spectroscopy with AFM: A perspective. *BBA - Biomembranes*, 2010. 1798(4): p. 741-749.
8. Chan, Y.-H.M. and S.G. Boxer, Model Membrane Systems and Their Applications. *Current opinion in chemical biology*, 2007. 11(6): p. 581-587.
9. Khan, M.S., N.S. Dosoky, and J.D. Williams, Engineering Lipid Bilayer Membranes for Protein Studies. *International Journal of Molecular Sciences*, 2013. 14(11): p. 21561-21597.
10. Peetla, C., A. Stine, and V. Labhasetwar, Biophysical Interactions with Model Lipid Membranes: Applications in Drug Discovery and Drug Delivery. *Molecular Pharmaceutics*, 2009. 6(5): p. 1264-1276.
11. Lin, C.-M., et al., Size-Dependent Properties of Small Unilamellar Vesicles Formed by Model Lipids. *Langmuir*, 2012. 28(1): p. 689-700.
12. Akbarzadeh, A., et al., Liposome: classification, preparation, and applications.

-
- Nanoscale Research Letters, 2013. 8(1): p. 102.
13. Agnihotri, S.A., K.S. Soppimath, and G.V. Betageri, Controlled release application of multilamellar vesicles: a novel drug delivery approach. *Drug Delivery*, 2010. 17(2): p. 92-101.
 14. Le Meins, J.F., et al., Hybrid polymer/lipid vesicles: state of the art and future perspectives. *Materials Today*, 2013. 16(10): p. 397-402.
 15. Patil, Y.P., M.D. Kumbhalkar, and S. Jadhav, Extrusion of electroformed giant unilamellar vesicles through track-etched membranes. *Chemistry and Physics of Lipids*, 2012. 165(4): p. 475-481.
 16. Pereno, V., et al., Electroformation of Giant Unilamellar Vesicles on Stainless Steel Electrodes. *ACS Omega*, 2017. 2(3): p. 994-1002.
 17. Lind, T.K., M. Cárdenas, and H.P. Wacklin, Formation of Supported Lipid Bilayers by Vesicle Fusion: Effect of Deposition Temperature. *Langmuir*, 2014. 30(25): p. 7259-7263.
 18. Jass, J., T. Tjärnhage, and G. Puu, From Liposomes to Supported, Planar Bilayer Structures on Hydrophilic and Hydrophobic Surfaces: An Atomic Force Microscopy Study. *Biophysical Journal*, 2000. 79(6): p. 3153-3163.
 19. Castellana, E.T. and P.S. Cremer, Solid supported lipid bilayers: From biophysical studies to sensor design. *Surface Science Reports*, 2006. 61(10): p. 429-444.
 20. Tien, H.T., S. Carbone, and E.A. Dawidowicz, Formation of Black Lipid Membranes by Oxidation Products of Cholesterol. *Nature*, 1966. 212(5063): p. 718-719.
 21. Winterhalter, M., Black lipid membranes. *Current Opinion in Colloid & Interface Science*, 2000. 5(3): p. 250-255.
 22. Jeong, D.-W., et al., Enhanced stability of freestanding lipid bilayer and its stability criteria. *Scientific Reports*, 2016. 6: p. 38158.
 23. Knobloch, J., et al., Membrane–drug interactions studied using model membrane systems. *Saudi Journal of Biological Sciences*, 2015. 22(6): p. 714-718.
 24. Jarsch, I.K., F. Daste, and J.L. Gallop, Membrane curvature in cell biology: An integration of molecular mechanisms. *The Journal of Cell Biology*, 2016. 214(4): p. 375-387.
 25. Sinico, C. and A.M. Fadda, Vesicular carriers for dermal drug delivery. *Expert*

-
- Opinion on Drug Delivery, 2009. 6(8): p. 813-825.
26. Sercombe, L., et al., Advances and Challenges of Liposome Assisted Drug Delivery. *Frontiers in Pharmacology*, 2015. 6: p. 286.
 27. Nikolelis, D.P. and U.J. Krull, Bilayer lipid membranes for electrochemical sensing. *Electroanalysis*, 1993. 5(7): p. 539-545.
 28. Hirtz, M., et al., Self-limiting multiplexed assembly of lipid membranes on large-area graphene sensor arrays. *Nanoscale*, 2016. 8(33): p. 15147-15151.
 29. Howorka, S., Building membrane nanopores. *Nature Nanotechnology*, 2017. 12: p. 619.
 30. Kukwikila, M. and S. Howorka, Nanopore-Based Electrical and Label-Free Sensing of Enzyme Activity in Blood Serum. *Analytical Chemistry*, 2015. 87(18): p. 9149-9154.
 31. Bello, J., et al., Lipid bilayer membrane technologies: A review on single-molecule studies of DNA sequencing by using membrane nanopores. *Microchimica Acta*, 2017. 184(7): p. 1883-1897.
 32. Cao, C., et al., Construction of an aerolysin nanopore in a lipid bilayer for single-oligonucleotide analysis. *Nature Protocols*, 2017. 12: p. 1901.
 33. Baker, C.A. and C.A. Aspinwall, Emerging trends in precision fabrication of microapertures to support suspended lipid membranes for sensors, sequencing, and beyond. *Analytical and Bioanalytical Chemistry*, 2015. 407(3): p. 647-652.
 34. Sosa, J.M., et al., The relationship between red blood cell deformability metrics and perfusion of an artificial microvascular network. *Clinical hemorheology and microcirculation*, 2014. 57(3): p. 291-305.
 35. Helfrich, W., Elastic Properties of Lipid Bilayers: Theory and Possible Experiments, in *Zeitschrift für Naturforschung C*. 1973. p. 693.
 36. Méléard, P., et al., Advantages of statistical analysis of giant vesicle flickering for bending elasticity measurements. *The European Physical Journal E*, 2011. 34(10): p. 116.
 37. Venable, R.M., F.L.H. Brown, and R.W. Pastor, Mechanical properties of lipid bilayers from molecular dynamics simulation. *Chemistry and Physics of Lipids*, 2015. 192: p. 60-74.

-
38. Diz-Muñoz, A., D.A. Fletcher, and O.D. Weiner, Use the force: Membrane tension as an organizer of cell shape and motility. *Trends in cell biology*, 2013. 23(2): p. 47-53.
 39. Koster, G., et al., Membrane tube formation from giant vesicles by dynamic association of motor proteins. *PNAS*, 2003. 100(26): p. 15583-15588.
 40. Steltenkamp, S., et al., Mechanical Properties of Pore-Spanning Lipid Bilayers Probed by Atomic Force Microscopy. *Biophysical Journal*, 2006. 91(1): p. 217-226.
 41. Takei, T., et al., Measurement of membrane tension of free standing lipid bilayers via laser-induced surface deformation spectroscopy. *Soft Matter*, 2015. 11(44): p. 8641-8647.
 42. Henriksen, J.R. and J.H. Ipsen, Measurement of membrane elasticity by micro-pipette aspiration. *The European Physical Journal E*, 2004. 14(2): p. 149-167.
 43. Shitamichi, Y., M. Ichikawa, and Y. Kimura, Mechanical properties of a giant liposome studied using optical tweezers. *Chemical Physics Letters*, 2009. 479(4-6): p. 274-278.
 44. Rumiana, D., et al., A practical guide to giant vesicles. Probing the membrane nanoregime via optical microscopy. *Journal of Physics: Condensed Matter*, 2006. 18(28): p. S1151.
 45. Heinrich, V. and R.E. Waugh, A piconewton force transducer and its application to measurement of the bending stiffness of phospholipid membranes. *Annals of Biomedical Engineering*, 1996. 24(5): p. 595-605.
 46. Giocondi, M.-C., et al., Surface topography of membrane domains. *Biochimica et Biophysica Acta (BBA) - Biomembranes*, 2010. 1798(4): p. 703-718.
 47. Orsini, F., et al., Atomic force microscopy imaging of lipid rafts of human breast cancer cells. *Biochimica et Biophysica Acta (BBA) - Biomembranes*, 2012. 1818(12): p. 2943-2949.
 48. Horton, M., G. Charras, and P. Lehenkari, ANALYSIS OF LIGAND-RECEPTOR Interactions in cells by Atomic Force Microscopy. *Journal of Receptors and Signal Transduction*, 2002. 22(1-4): p. 169-190.
 49. Vinckier, A. and G. Semenza, Measuring elasticity of biological materials by atomic force microscopy. *FEBS Letters*, 1998. 430(1): p. 12-16.

Chapter 2

Microfluidic approaches for the formation of lipid membranes

Technologies to assemble model membranes into microsystems are relatively new and are gaining interest due to the wide range of applications that they offer. Novel materials and manufacturing processes are continuously being developed to improve the methods to assemble and characterize artificial lipid membranes. This chapter includes a description and comparison of microfluidic technologies to assemble artificial lipid membranes. Techniques to characterize and visualize artificial lipid membranes formed in microdevices are then presented.

2.1 Microfluidic devices for assembling lipid membranes

Microfluidics is considered as set of techniques that allow precise control of confined fluids in microchambers in the range of 1-500 μm . Miniaturize methodologies to assemble lipid membranes grant the possibility of increasing control and robustness. At the microscale, sample volumes are reduced and parallelism becomes more easily implemented. In order to find a successful approach to fabricate a microfluidic device to assemble lipid membranes, the fabrication technique and the material to use need to be properly chosen [1]. An increasing development in this area has been observed in past years due to expansion in electronics techniques and 3D printing technologies [2]. Examples of technologies to manufacture microsystems are soft-lithography [3], electron beam lithography [4], drill craving [5], paper patterning [6] and recently 3D patterning [7]. Microfluidics systems have shown to be a powerful technique to sort cells [8] and to study cell motility [9] and cell-cell interactions [10]. It has also found applications as biological sensors, microbioreactors and droplets generators. The importance of using microfluidics is based on its reduced size, parallelism and faster processes compared with larger scale. Common materials for the fabrication of microchambers are polydimethylsiloxane (PDMS) [11], glass [12], poly(methyl-methacrylate) (PMMA) [13] and paper [14]. The behavior of the fluid inside the chambers depends on surface properties, pressure and flow [15]. Surface treatment is often required to grant specific functionalities to the material [16]. Table 2.1 gives a general overview of the advantages and disadvantages of materials commonly used to assemble lipid membranes.

2.1.1 Soft polymers

Most common soft materials are microfabricated using a technique called soft lithography [17, 18]. This technique consists of fabricating a polymer mold (e.g., with the photoresist SU-8) on a silicon wafer. To cast the pattern onto the microfluidic device, a polymer with fast curing properties is poured onto the patterned mold [19]. As an example, polydimethylsiloxane (PDMS) is one of the most used elastomers in microfluidics, because of its low cost, transparency, easy manufacturing and biocompatibility. Once a PDMS replica is fully cured, it is demolded, drilled to form inlets and outlets, and sealed off on a glass surface pre-treated with oxygen plasma. The treatment with oxygen plasma is done to facilitate the formation of bonds via free radical on both surfaces.

Most technologies to assemble lipid membranes in microfluidic devices are adaptations of common methodologies at the macroscale (see 1.2), which often make use of organic solvents to form lipid membranes. The use of PDMS to form lipid bilayers in presence of organic solvent presents major problems as PDMS swells due to the absorption of many of these solvents [20,21]. Therefore, in order to work with PDMS, the solvent should be carefully selected.

2.1.2 Glass

As mentioned, PDMS has disadvantages because of chemical incompatibility with some organic solvents like ether, acetone, tetrahydrofuran and chloroform. In circumstances where it is needed to stream one of those chemicals, another more inert material should be used, such as glass. Transparency, chemical inertness and rigidity are some of the advantageous properties of glass that favors its use in microfluidic devices. However, patterning and sealing glass chambers present some difficulties. The patterning of glass can be achieved by etching with strong acids [22], bases or plasma [23], or with the use of lasers [24]. In addition, the sealing of the chamber is frequently carried out at high temperatures or very strong plasma treatments, making the fabrication process complex and expensive. Lipid membrane formation in glass has been more developed in the context of glass micropipettes rather than through the fabrication of an entire microdevice out of glass [25, 26]. Glass micropipette studies have generated insights concerning the materials and surface chemistry required to assemble lipid membranes at the interface with glass.

2.1.3 UV curable polymers

Photopolymers have shown to be a promising alternative for low cost microfluidic fabrication [13]. Due to its curing ability when exposed to UV light and its resistance of numerous chemicals, UV curable polymers can be a suitable candidate to assemble lipid membranes using solvents. For instance, Norland Optical Adhesive (NOA81) is a material that gains popularity in the microfluidics field because of its resistance to organic solvents, low susceptibility to swelling and possibility of surface modifications [14]. The process of fabrication is similar to the soft lithography of other polymers like PDMS [15]. However, as NOA81 is more rigid, an additional step is required. Casting a pattern onto NOA81 requires the fabrication of a PDMS doomy master made with soft lithography. After polymerization of the NOA81 onto the PDMS master, the PDMS mold is removed and the device can be sealed with a NOA81 covered glass slide.

2.2 Surface properties and modifications for microfluidics

Hydrophobic surfaces have been reported to help lipid membrane formation [25]. Materials like teflon have been shown to be well suited materials for assembling lipid membranes on apertures [27]. Teflon is known for its hydrophobicity and its resistance to solvents. In a similar way, hydrophobic microchamber inner walls can enhance lipid bilayer formation in microfluidics devices. Teflon as material for fabrication of microfluidics devices turns out to be complex because of the mechanical and chemical properties of the teflon. In addition to that, teflon is not transparent and its use would hinder optical techniques. However, using a thin film of teflon

sandwiched between two layers of glass having NOA81 as UV-curable adhesive is a common approach for this material to fully isolate the different chambers [28].

Alternatively, hydrophobic chambers can be obtained by coating the inner walls with a hydrophobic molecule. There are different processes which go from making free radical with plasma or chemical deposition, nonetheless, a covalent link between the molecule and the surface is required to maintain the effect as long as possible. To characterize surface hydrophobicity, the sessile drop technique can be used [29], which consists of placing a droplet of liquid onto the surface of interest (Fig. 2.1a). The contact angle of the droplet with the surface (angle at the intersection of the three interfaces: liquid, solid and gas) is measured. When water is used, high contact angles signify higher surface hydrophobicity.

Silanization is a method that allows covering surfaces with alkoxy groups in order to make hydrophilic or hydrophobic surfaces (Fig. 2.1b). Materials like PDMS, glass, silicon and some oxide metals possess hydroxyl groups which can interact with the alkoxy groups (methoxy or ethoxy) to form a covalent bond. Previous work has shown that the use of silane molecules with long carbon chains of fluoromethyl increases the hydrophobic effect and leads to more stable lipid membranes [25].

Microfluidic material	Advantages	Disadvantages
PDMS [29-31]	<ul style="list-style-type: none"> *Easy and cheap manufacturing *Optically transparent 	<ul style="list-style-type: none"> *Swelling with solvents *Less stable membranes
Glass [24, 32]	<ul style="list-style-type: none"> *No swelling in presence of solvents *Optically transparent *Stable membranes 	<ul style="list-style-type: none"> *Expensive and complex manufacturing
NOA 81 [33]	<ul style="list-style-type: none"> *Easier and cheaper than glass *Optically transparent *No swelling in presence of solvents *Stable membranes 	<ul style="list-style-type: none"> *Less flexible than PDMS
Teflon [26, 34]	<ul style="list-style-type: none"> *Stable lipid membranes *Chemically inert *No swelling in presence of solvents *Stable membranes 	<ul style="list-style-type: none"> *Not transparent *Complex manufacturing
SU-8 [35]	<ul style="list-style-type: none"> *Stable lipid membranes *Some swelling in presence of solvent *Stable membranes 	<ul style="list-style-type: none"> *Semi transparent *Complex manufacturing

Table 2.1: Compilation of materials used to assemble lipid membrane in microfluidics. This table describes the advantages and disadvantages of materials commonly used to assemble lipid membranes. These represent the most popular materials used for lipid membrane formation. However other materials like PMMA [37, 38], silicon [39-41] and polyamides [42], also used to assemble lipid membranes, will not be covered in this thesis.

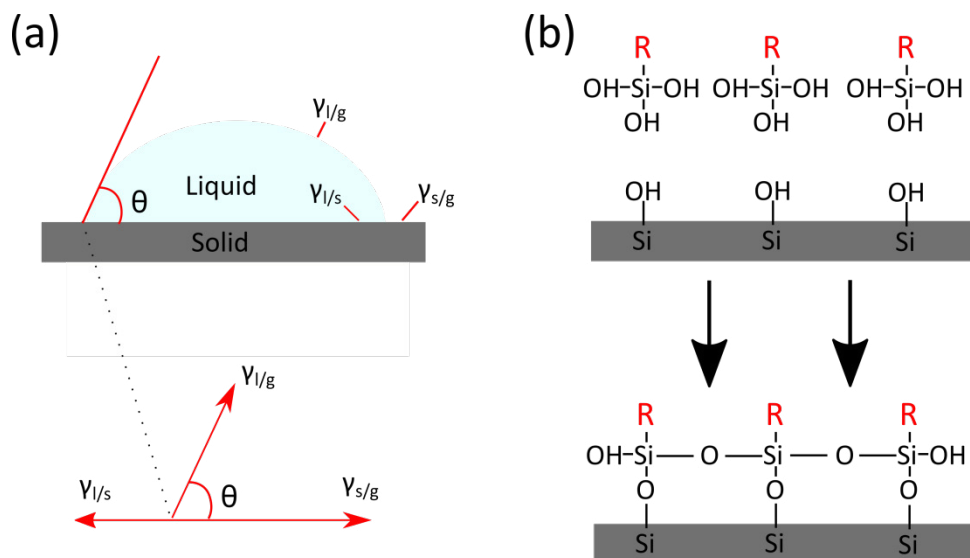


Figure 2.1: Characterization and modification of hydrophobic surface. (a) Schematic of a water droplet onto a surface, where $\gamma_{l/g}$ represents surface tension at liquid-gas, liquid-solid ($\gamma_{l/s}$) and solid-gas ($\gamma_{s/g}$) interface. Below, a force diagram showing the tension contribution of different interfaces is shown. (b) Process of silanization, which is used to functionalize glass surfaces and modify the surface chemistry, for instance to increase hydrophobicity [25].

2.3 Methods to assemble lipid membranes in microfluidics

Different approaches have been developed to form long lived stable model membranes in microfluidic devices [43], sometimes with the aim of accessing both side of the membrane [1]. The overall goal of using microfluidics consists of reduced incubation times and sample volumes, easy manipulation, enhanced parallelism and combination with other instruments. Several approaches have been developed in order to reproduce model membranes with the help of different microfluidics approaches. A summary of popular systems used for formation of model membranes in microfluidics devices is presented below.

2.3.1 Double emulsion droplet system to form lipid vesicles

Current methods for producing lipid vesicles have the disadvantages of low size control, difficulties in manipulation, difficulties in getting unilamellar vesicles and requirement of long periods of incubation. Microfluidics addresses these difficulties by using microfluidic devices capable of making lipid vesicles with high throughput, controlled monodispersity and in a continuous process [44, 45].

The double emulsion-droplet approach (Fig 2.2a) consists of a drop of aqueous solution (vesicle inner solution) formed with a sheath flow of lipid solvent (usually oil) focused into a narrower stream, followed by second sheath flow of another aqueous solution (vesicle outer solution) to form a double emulsion drop. In addition, double emulsion-droplet can be combined with a layer-by-layer artificial membrane assembly [18]. This method is based on the deposition of a lipid monolayer over droplets trapped in a microfluidic array (Fig. 2.2b), enabling the formation of multilamellar and asymmetric membranes in a more straightforward and controlled manner compared with traditional methods.

In a similar way, a monolayer can be formed at the interface of water droplets into an organic solvent. An approach consists of forming monolayers at the interface of water droplets submerged in organic solvent. Usually, conductive electrodes are coated with wet agarose of aqueous solution to carry small drops inside a solution of lipids in oil (Fig. 2.2c). A monolayer is formed at the interface of the aqueous solution and the lipid in oil [46, 47] and the lipid bilayer forms when the two drops make contact and zip a bilayer [48]. Electrophysiology experiments can be performed with this approach because electrodes are isolated by the lipid membrane and nonconductive medium. Adaptations of this method have been done by carefully exchanging the droplet content of each drop accessing both sides of the membrane.

2.3.2 Lipid bilayers in a cross-geometry

Another approach consists of contacting lipid monolayers inside straight channels (Fig 2.2d), as is shown in a microfluidic device with a cross-geometry (rectangular channels that intersect forming a cross intersection) [47]. When forming a lipid bilayer in a cross-geometry device, firstly the device is filled with a solution of lipid in oil, and a lipid monolayer will form when pushing an aqueous solution in the perpendicular channel. A bilayer is formed when the monolayers make contact at the intersection. Electrodes have been incorporated into such devices, but a successful method to enable continuous exchange of solution has not been implemented yet.

2.3.3 Lipid bilayers spanning apertures

Lipid bilayers formed on microapertures inside microfluidic channels are especially useful when parallelism and easy access to both sides of the membrane is required. Briefly, this method consists of either zipping (Fig 2.2e) or spanning (Fig. 2.2f) a lipid bilayer on an aperture. The spanning of lipid bilayers to cover nanowells (Fig. 2.2f) on a surface is comparable to the formation of supported lipid bilayers [33]. One advantage is that free standing lipid bilayers are formed every time a nanowell is closed. This method does not require solvents but has some disadvantages like access to only one side of the membrane, the necessity of fabricating very small (nanosized) wells to obtain stable membranes, and the difficulty in performing electrophysiology measurements, which are only possible with complex techniques [49].

On the other hand, zipping of lipid membranes on apertures (Fig. 2.2e) requires solvent, but is not limited to nanoscale dimensions [32]. This method is adapted from the traditional “painting method” technique, which uses a teflon thin film separating two chambers of millimeter scale, into which a small aperture is made over which the lipid bilayer forms. Two frequent microfabrication methods for zipping bilayers in microdevices with an aperture are: (1) to contact two monolayers over a cavity [50]; and (2) to sandwich a thin film.

In approach (1), cavities are preferably made at the bottom of the chamber for direct observation, microchambers are filled with an aqueous solution, followed by flowing a lipid in oil solution which results in the formation of a monolayer. Finally, formation of the bilayer is carried out via contact of a second monolayer at the aperture [32, 51]. Easy access to one side of the membrane and implementation of electrodes is possible. Surface hydrophobicity is an important requirement for bilayer formation.

The second approach (2) consists of a thin film, with an aperture, sandwiched in between two open chambers. Access to both sides of the membrane enable continuous perfusion, pressure control and the possibility to perform electrophysiology measurements [38]. Teflon is one of the most used materials, but it has the drawbacks of being non-transparent and being difficult to bind to other materials [52]. Research is currently being done to further improve the technologies to form artificial membranes in order to reach longer membrane lifetime and for combination with other techniques. Microdevice materials and surface chemistry are parameters to consider for increasing membrane stability and success in membrane formation. Furthermore, futures technologies should allow the combination with powerful biophysical tools opening up new possible investigations on lipid membranes and membrane associated biological macromolecules.

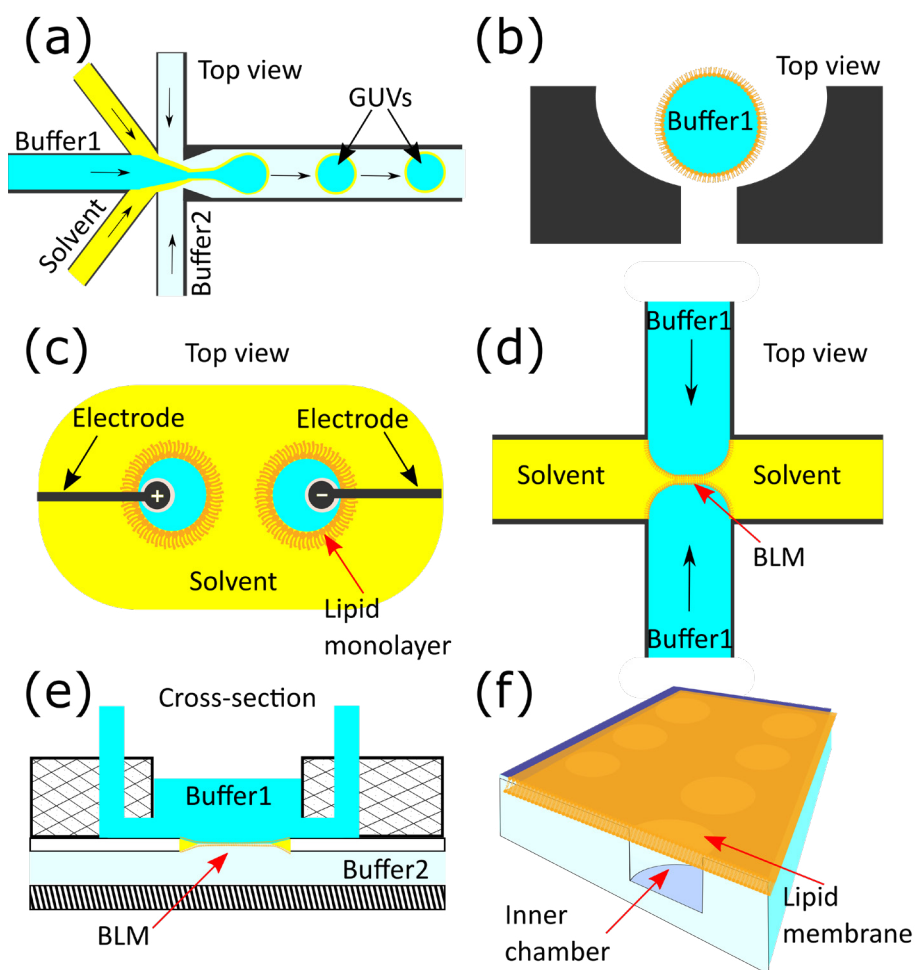


Figure 2.2: Methodologies for lipid membrane formation in microfluidic devices. (a) Double emulsion-droplet system produces GUVs in a continuous manner by supplying an inner aqueous flow together with a solvent source containing lipids. (b) Formation of GUVs in a layer-by-layer approach allows the assembly of asymmetric and multilamellar vesicles. (c) Droplet contact represents an easy and reproducible method to form lipid membranes via the contact of lipid monolayers. The large amount of organic solvent makes it difficult to combine with optical techniques. (d) Contacting monolayers inside microchannels is a common method but results in large amounts of solvent remaining inside the channel. (e) Teflon film containing a free standing lipid bilayer separating two chambers. A teflon film is interconnecting two cavities allowing independent perfusion in each side of the membrane. (f) Array of wells which are sealed with a lipid bilayer making a separation between the inner side of the well and the outside.

2.4 Characterization of lipid bilayers formed in microdevices

2.4.1 Electrophysiology: electrical properties of lipid membranes

The study of the electrical properties of cells and tissues is known as electrophysiology. The excitability of certain tissues under an electrical stimulus has fascinated scientists for many decades. Famous experiments from Luigi Galvani (1780s) and Jan Swammerdam (1660s) showed a correlation between muscular contraction and electrical stimulus. One of the most controversial electrophysiology experiments at the time, consisted of using frog legs to trigger a strong muscular contraction via mechanical and electrical stimulation. These observations led to many theories on bioelectricity, and together with technological advances to measure electrical current marked the beginning of the field of electrophysiology. Following this, new terms like action potential [53], electrical signal propagation [54] and membrane theory of excitation started to appear among scientists.

After the demonstration that Na^+ and K^+ ions exchange is required to produce an electrical potential, the lipid bilayer model [55] was proposed together with the idea that the exchange of ions is carried out by proteins that transport ions. Thanks to the development of the voltage-clamp technique, it became possible to demonstrate the “ion theory”, which assumed selective permeability of the lipid membrane by specific transmembrane pores or carriers. However, it was not until the beginning of 1960s that it became possible to perform direct recording of single currents associated to the insertion of ion channels onto artificial lipid bilayers [56]. Another popular technique was the use of liquid filled micropipettes, which consisted of glass micropipettes pressed against cell membranes to electrically isolate the membrane patch underneath [57]. With similar techniques, also known as patch-clamp, it became possible to measure the membrane impedance and the current flowing across the patch of membrane isolated by the tip of the micropipette (Fig. 2.3a). These methods were rapidly adopted and changed modern cell electrophysiology into what is known nowadays.

Insertion of pore proteins (e.g., toxins, ion channels) in lipid bilayer membranes can be monitored with a set of intracellular and extracellular electrodes to monitor the electrical activity across the membrane. However, there are many factors that make this approach very complicated, for example, a mixture of different proteins or fluctuations in ion concentration. It is often important to isolate a single type of ion channel to avoid noise contribution from others types of proteins. It is also advantageous to have the flexibility to have an adjustable and stable ion concentration. The benefits of studying ion channels in artificial membranes rather than in their natural membrane environment (e.g., with a patch-clamp approach) is that both membrane sides are accessible and can be modified in real-time.

Patch clamp and voltage clamp are versatile ways to monitor the activity of single ion channels by measuring currents or potentials (Fig. 2.4a). Similar techniques can also be applied in systems with artificial membranes formed over an aperture (Fig. 2.3b), known as black lipid membranes [58]. These techniques are very sensitive to small changes in current (in the order of pA) and noise filtering is required. In addition, they are often subject to poor seals and fluctuations in membrane capacitance. In general, membranes by themselves have very high resistance (in the order of G Ω) or little conductance (in the order of nS), however they behave as a capacitor. If we consider each monolayer of the bilayer as a charged plate, such a configuration resembles a plain capacitor and its properties depend on the separation between the two plates as well as on the charges on the plates and the potential applied (Fig. 2.4b).

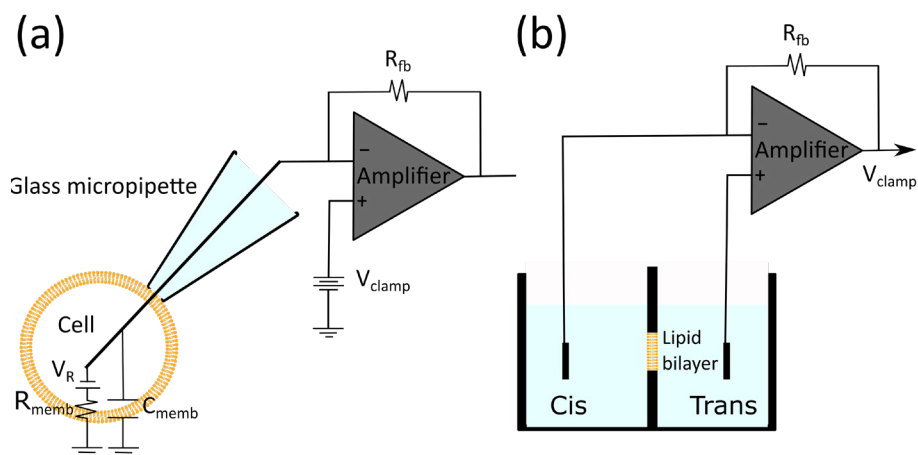


Figure 2.3: Simplified circuit diagram for electrophysiology of lipid membranes.

(a) A glass micropipette is used to isolate a membrane patch on a cell membrane to achieve a Giga seal (R_{memb}). Amplification is used with a feedback loop that holds a clamp voltage (V_{clamp}). The ion channel current is monitored taking into account the fluctuations due to membrane capacity (C_{memb}) [59]. (b) Similar voltage clamp implemented in a lipid membrane assembled inside a traditional chamber [58, 60].

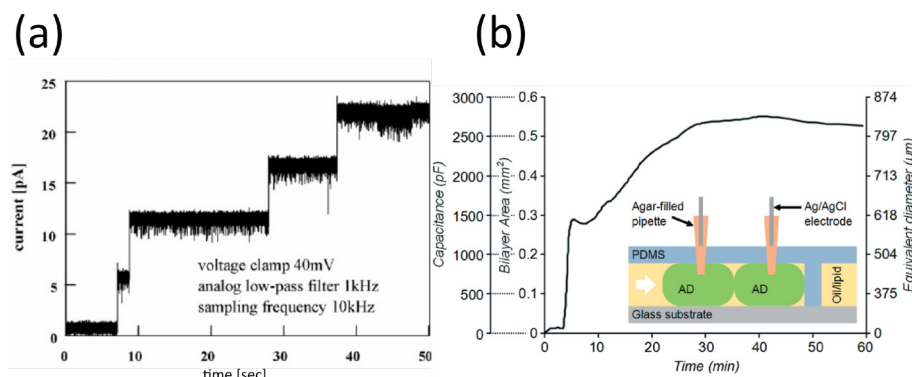


Figure 2.4: Electrophysiology recordings. (a) Voltage clamp recording of α -Hemolysin pores inserted in a black lipid membrane. Each increase in current represents an insertion event [38]. (b) Capacitance measurements in an emulsion-droplets system. The lipid bilayer capacitance is monitored over time with a plateau reached after ~30-40 minutes [30].

2.4.2 Membrane visualization by confocal microscopy

Fluorescence microscopy is used to enhance contrast in a system or to localize specific molecules or components of the cell [61]. This can be done by using fluorescent dyes that label specific structures. Light is used to excite the dye, which then emits light at a longer wavelength (lower energy), ideally in the visible range for easier detection. The difference between the wavelength for maximum excitation and the wavelength with maximum emission is known as the Stokes shift. An important technical aspect to consider when performing an experiment with fluorescence is the photobleaching effect, which results in an attenuation of the emission light over time [62]. In conventional fluorescence microscopy, fluorescent signals come from different focal points (Fig. 2.8a). To obtain an image that corresponds to a specific plane in the sample, techniques like optical sectioning and confocal microscopy are frequently used.

Optical sectioning consists of imaging slices of an object, ending up with a stack of images that corresponds to slices from the top to the bottom of the object [63]. A pin hole allows blocking light coming from different focal planes (Fig. 2.8 b). Only the light originating from a single spot reaches the detector. The sample is scanned in order to create an image. As standard microscopy illumination is not bright enough, a collimated laser is used to illuminate a single spot with the possibility to scan an area by moving the sample or manipulating the incidence angle of the laser. The major limitation of this technique is the scanning speed, which limits the time resolution. An

alternative is known as a spinning disk confocal, which consists of multiple pinholes to illuminate more spots on the sample for a faster scanning [64].

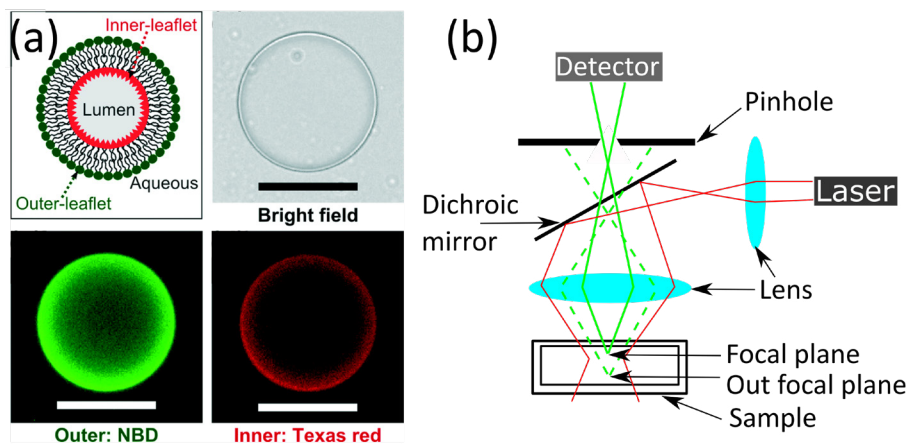


Figure 2.5: Fluorescence techniques to visualize membranes. a) Picture of asymmetric vesicle using different dyes on each leaflet of the lipid membrane (green: outer membrane leaflet; and red: inner membrane leaflet), and in comparison with a bright field image (upper right corner), scale bar 50 μm , figure from [65]. b) Simplified schematics of the confocal microscopy technique.

2.5 References

1. Zagnoni, M., Miniaturised technologies for the development of artificial lipid bilayer systems. *Lab on a Chip*, 2012. 12(6): p. 1026-1039.
2. Whitesides, G.M., The origins and the future of microfluidics. *Nature*, 2006. 442(7101): p. 368-373.
3. Qin, D., Y. Xia, and G.M. Whitesides, Soft lithography for micro- and nanoscale patterning. *Nat. Protocols*, 2010. 5(3): p. 491-502.
4. Robinson, A., Electron-beam lithography: Going green with silk. *Nat Nano*, 2014. 9(4): p. 251-252.
5. Bings, N.H., et al., Microfluidic Devices Connected to Fused-Silica Capillaries with Minimal Dead Volume. *Analytical Chemistry*, 1999. 71(15): p. 3292-3296.
6. Yetisen, A.K., M.S. Akram, and C.R. Lowe, Paper-based microfluidic point-of-care diagnostic devices. *Lab on a Chip*, 2013. 13(12): p. 2210-2251.
7. Pavesi, A., et al., Engineering a 3D microfluidic culture platform for tumor-treating field application. 2016. 6: p. 26584.
8. Wyatt Shields Iv, C., C.D. Reyes, and G.P. Lopez, Microfluidic cell sorting: a review of the advances in the separation of cells from debulking to rare cell isolation. *Lab on a Chip*, 2015. 15(5): p. 1230-1249.
9. Yeh, C.F., et al., Towards an Endpoint Cell Motility Assay by a Microfluidic Platform. *IEEE Transactions on NanoBioscience*, 2015. 14(8): p. 835-840.
10. Zervantonakis, I.K., et al., Microfluidic devices for studying heterotypic cell-cell interactions and tissue specimen cultures under controlled microenvironments. *Biomicrofluidics*, 2011. 5(1): p. 013406.
11. Friend, J. and L. Yeo, Fabrication of microfluidic devices using polydimethylsiloxane. *Biomicrofluidics*, 2010. 4(2): p. 026502.
12. Jia, Z.-J., Q. Fang, and Z.-L. Fang, Bonding of Glass Microfluidic Chips at Room Temperatures. *Analytical Chemistry*, 2004. 76(18): p. 5597-5602.
13. Arshya, B., N. Alireza, and K. Hossein, A new simple and fast thermally-solvent assisted method to bond PMMA–PMMA in micro-fluidics devices. *Journal of Micromechanics and Microengineering*, 2016. 26(6): p. 065017.
14. Li, X., D.R. Ballerini, and W. Shen, A perspective on paper-based microfluidics:

-
- Current status and future trends. *Biomicrofluidics*, 2012. 6(1): p. 011301-011301-13.
15. Wu, L., et al., Wall effects in continuous microfluidic magneto-affinity cell separation. *Biotechnology and Bioengineering*, 2010. 106(1): p. 68-75.
 16. Beal, J.H.L., et al., A rapid, inexpensive surface treatment for enhanced functionality of polydimethylsiloxane microfluidic channels. *Biomicrofluidics*, 2012. 6(3): p. 036503.
 17. Kim, J., R. Surapaneni, and B.K. Gale, Rapid prototyping of microfluidic systems using a PDMS/polymer tape composite. *Lab on a Chip*, 2009. 9(9): p. 1290-1293.
 18. Wu, H., B. Huang, and R.N. Zare, Construction of microfluidic chips using polydimethylsiloxane for adhesive bonding. *Lab on a Chip*, 2005. 5(12): p. 1393-1398.
 19. Sollier, E., et al., Rapid prototyping polymers for microfluidic devices and high pressure injections. *Lab on a Chip*, 2011. 11(22): p. 3752-3765.
 20. Hung, L.-H., R. Lin, and A.P. Lee, Rapid microfabrication of solvent-resistant biocompatible microfluidic devices. *Lab on a Chip*, 2008. 8(6): p. 983-987.
 21. Lee, J.N., C. Park, and G.M. Whitesides, Solvent Compatibility of Poly(dimethylsiloxane)-Based Microfluidic Devices. *Analytical Chemistry*, 2003. 75(23): p. 6544-6554.
 22. John, M.N. and A.W. Daniel, Ultradeep fused silica glass etching with an HF-resistant photosensitive resist for optical imaging applications. *Journal of Micromechanics and Microengineering*, 2012. 22(3): p. 035011.
 23. Khan Malek, C., et al., Deep microstructuring in glass for microfluidic applications. *Microsystem Technologies*, 2007. 13(5): p. 447-453.
 24. Waddell, E.A., Laser Ablation as a Fabrication Technique for Microfluidic Devices, in *Microfluidic Techniques: Reviews and Protocols*, S.D. Minteer, Editor. 2006, Humana Press: Totowa, NJ. p. 27-38.
 25. Bright, L.K., et al., Decreased Aperture Surface Energy Enhances Electrical, Mechanical, and Temporal Stability of Suspended Lipid Membranes. *ACS Applied Materials & Interfaces*, 2013. 5(22): p. 11918-11926.
 26. Tunuguntla, R.H., et al., Synthesis, lipid membrane incorporation, and ion permeability testing of carbon nanotube porins. *Nat. Protocols*, 2016. 11(10):

-
- p. 2029-2047.
27. Mayer, M., et al., Microfabricated Teflon Membranes for Low-Noise Recordings of Ion Channels in Planar Lipid Bilayers. *Biophysical Journal*, 2003. 85(4): p. 2684-2695.
 28. Bomer, J.G., et al., Wafer-scale fabrication of glass-FEP-glass microfluidic devices for lipid bilayer experiments. *Lab on a Chip*, 2014. 14(23): p. 4461-4464.
 29. Kaufmann, T.C., A. Engel, and H.-W. Rémigy, A Novel Method for Detergent Concentration Determination. *Biophysical Journal*. 90(1): p. 310-317.
 30. King, P.H., et al., Interdroplet bilayer arrays in millifluidic droplet traps from 3D-printed moulds. *Lab on a Chip*, 2014. 14(4): p. 722-729.
 31. Malmstadt, N., et al., Automated Formation of Lipid-Bilayer Membranes in a Microfluidic Device. *Nano Letters*, 2006. 6(9): p. 1961-1965.
 32. Sadao, O., et al. Microfluidic formation of lipid bilayer array for membrane transport analysis. in 2008 IEEE 21st International Conference on Micro Electro Mechanical Systems. 2008.
 33. Jönsson, P., M.P. Jonsson, and F. Höök, Sealing of Submicrometer Wells by a Shear-Driven Lipid Bilayer. *Nano Letters*, 2010. 10(5): p. 1900-1906.
 34. Marin, V., et al., Stable Free-Standing Lipid Bilayer Membranes in Norland Optical Adhesive 81 Microchannels. *Analytical Chemistry*, 2016. 88(15): p. 7466-7470.
 35. Honigmann, A., et al., Characterization of Horizontal Lipid Bilayers as a Model System to Study Lipid Phase Separation. *Biophysical Journal*. 98(12): p. 2886-2894.
 36. Kalsi, S., et al., Shaped Apertures in Photoresist Films Enhance the Lifetime and Mechanical Stability of Suspended Lipid Bilayers. *Biophysical Journal*, 2014. 106(8): p. 1650-1659.
 37. Le Pioufle, B., et al., Lipid Bilayer Microarray for Parallel Recording of Transmembrane Ion Currents. *Analytical Chemistry*, 2008. 80(1): p. 328-332.
 38. Suzuki, H., et al., Electrophysiological recordings of single ion channels in planar lipid bilayers using a polymethyl methacrylate microfluidic chip. *Biosens. Bioelectron*, 2007. 22(6): p. 1111-1115.
 39. Simon, A., et al., Formation and stability of a suspended biomimetic lipid bilayer on silicon submicrometer-sized pores. *Journal of Colloid and Interface*

-
- Science, 2007. 308(2): p. 337-343.
40. Azusa, O., et al., Mechanically Stable Lipid Bilayers in Teflon-Coated Silicon Chips for Single-Channel Recordings. *Micro and Nanosystems*, 2012. 4(1): p. 2-7.
 41. Buchholz, K., et al., Silicon-on-insulator based nanopore cavity arrays for lipid membrane investigation. *Nanotechnology*, 2008. 19(44): p. 445305.
 42. Eray, M., et al., Highly stable bilayer lipid membranes (BLMs) formed on microfabricated polyimide apertures. *Biosensors and Bioelectronics*, 1994. 9(4): p. 343-351.
 43. Osaki, T. and S. Takeuchi, Artificial Cell Membrane Systems for Biosensing Applications. *Analytical Chemistry*, 2017. 89(1): p. 216-231.
 44. Carugo, D., et al., Liposome production by microfluidics: potential and limiting factors. *Scientific Reports*, 2016. 6: p. 25876.
 45. Deshpande, S., et al., Octanol-assisted liposome assembly on chip. *Nature Communications*, 2016. 7: p. 10447.
 46. Czekalska, M.A., et al., A droplet microfluidic system for sequential generation of lipid bilayers and transmembrane electrical recordings. *Lab on a Chip*, 2015. 15(2): p. 541-548.
 47. Vargas, J.N., R. Seemann, and J.-B. Fleury, Fast membrane hemifusion via dewetting between lipid bilayers. *Soft Matter*, 2014. 10(46): p. 9293-9299.
 48. Leptihn, S., et al., Constructing droplet interface bilayers from the contact of aqueous droplets in oil. *Nat. Protocols*, 2013. 8(6): p. 1048-1057.
 49. Watanabe, R., et al., Arrayed lipid bilayer chambers allow single-molecule analysis of membrane transporter activity. *Nature Communications*, 2014. 5: p. 4519.
 50. Funakoshi, K., H. Suzuki, and S. Takeuchi, Lipid Bilayer Formation by Contacting Monolayers in a Microfluidic Device for Membrane Protein Analysis. *Analytical Chemistry*, 2006. 78(24): p. 8169-8174.
 51. Baaken, G., et al., Planar microelectrode-cavity array for high-resolution and parallel electrical recording of membrane ionic currents. *Lab on a Chip*, 2008. 8(6): p. 938-944.
 52. Kendall, E.L., C. Shao, and D.L. DeVoe, Visualizing the Growth and Dynamics

-
- of Liquid-Ordered Domains During Lipid Bilayer Folding in a Microfluidic Chip. *Small*, 2012. 8(23): p. 3613-3619.
53. Bean, B.P., The action potential in mammalian central neurons. *Nat Rev Neurosci*, 2007. 8(6): p. 451-465.
 54. Debanne, D., Information processing in the axon. *Nat Rev Neurosci*, 2004. 5(4): p. 304-316.
 55. Danielli, J.F. and H. Davson, A contribution to the theory of permeability of thin films. *Journal of Cellular and Comparative Physiology*, 1935. 5(4): p. 495-508.
 56. Mueller, P., et al., Reconstitution of Cell Membrane Structure in vitro and its Transformation into an Excitable System. *Nature*, 1962. 194(4832): p. 979-980.
 57. Strickholm, A., Impedance of a Small Electrically Isolated Area of the Muscle Cell Surface. *The Journal of General Physiology*, 1961. 44(6): p. 1073.
 58. Montal, M. and P. Mueller, Formation of Bimolecular Membranes from Lipid Monolayers and a Study of Their Electrical Properties. *Proceedings of the National Academy of Sciences*, 1972. 69(12): p. 3561-3566.
 59. Zhao, Y., et al., Patch clamp technique: Review of the current state of the art and potential contributions from nanoengineering. *Journal of Nanoengineering and Nanosystems*, 2008. 222(1): p. 1-11.
 60. Bartsch, P., et al., Horizontal Bilayer for Electrical and Optical Recordings. *Materials*, 2012. 5(12).
 61. Bachmann, L., et al., Fluorescence Spectroscopy of Biological Tissues—A Review. *Applied Spectroscopy Reviews*, 2006. 41(6): p. 575-590.
 62. Nathalie, B.V., et al., Photobleaching correction in fluorescence microscopy images. *Journal of Physics: Conference Series*, 2007. 90(1): p. 012068.
 63. Mertz, J., Optical sectioning microscopy with planar or structured illumination. *Nat Meth*, 2011. 8(10): p. 811-819.
 64. Jonkman, J. and C.M. Brown, Any Way You Slice It—A Comparison of Confocal Microscopy Techniques. *JBT*, 2015. 26(2): p. 54-65.
 65. Lu, L., J.W. Schertzer, and P.R. Chiarot, Continuous microfluidic fabrication of synthetic asymmetric vesicles. *Lab on a Chip*, 2015. 15(17): p. 3591-3599.

Chapter 3

Free standing lipid bilayers formation in Norland optical adhesive (NOA81) microchannels

There is an increasing interest in the development of methods to form artificial lipid membranes in microdevices, especially for their use in combination with optical, electrophysiological, and/or force spectroscopy single-molecule techniques. Current technologies to assemble lipid bilayers in microfluidic devices usually rely on complex fabrication processes using materials that are difficult to microfabricate, like glass or Teflon. In this chapter we report a simple and reproducible method to form free standing lipid bilayer membranes in microdevices made with Norland optical adhesive (NOA81). Surface treatment with either alkylsilane or fluoroalkylsilane enables the self-assembly of stable DPhPC and DOPC/DPPC membranes. Capacitance measurements are used to characterize the lipid bilayer and to follow its formation in real-time. With current recordings, the insertion of single α -Hemolysin pores into the bilayer membrane are detected, showing that this device can be used for single-channel electrophysiology sensing applications*.

*Parts of this chapter have been published in *Analytical Chemistry*, 2016. 88(15): p. 7466-7470.

3.1 Introduction

Artificial lipid bilayers are commonly used to mimic cellular membranes in biophysical studies [1, 2], synthetic biology [3, 4], drug delivery [5] and diagnostic applications [6]. In particular, free standing lipid membranes are often required in biophysical applications that necessitate control over the physical and chemical conditions on both sides of the membrane (e.g., electrophysiology). Free standing lipid bilayers are traditionally formed over small apertures in Teflon thin sheets by “painting” a droplet of lipid dissolved in organic solvent over the orifice [7].

There is an increasing interest in using microfluidic devices, as they offer the benefit of sub-microliter reagents volumes handling, high-sensitive sensing and simple parallelization [8, 9]. In addition, advances in microtechnologies allow a faster and more efficient manufacturing of microfluidic devices. For these reasons, various traditional “large scale” technologies are moving towards miniaturization. In particular, several biophysical techniques now use microfluidic devices to carry out experimental assays. Although materials like Teflon and glass confer mechanical robustness and long-term stability to the membrane [10, 11], they lack straightforward cost-efficient micro-patterning techniques. Alternatively, polymethylsiloxane (PDMS) is a biocompatible material, which allows low-cost and simple fabrication, but its use for the formation of free standing lipid bilayers is hindered by swelling and deformability issues in several organic solvents [12], which are often required for artificial lipid bilayer formation [13, 14].

Different technologies have been developed to make these microdevices suitable for assembling artificial lipid membranes in presence of organic solvents. Recently, the photopolymer Norland optical adhesive 81 (NOA81) has gained attention as a material for fabricating microfluidic systems [15]. Owing to its solvent resistance, optical transparency and easy fabrication, we find NOA81 to be a well-suited material for microfluidic devices hosting lipid bilayers.

In this chapter, attempts to form lipid bilayers into PDMS or glass flow cells are first described. Afterwards, a method to assemble free standing long-lived lipid membranes in channels entirely made with NOA81 is presented. This simple and cost-efficient approach does not require gluing between layers, avoiding alignment and layers attachment, alleviating the risks of leakage and simplifying the fabrication process compared to other reported methods [16-18]. Kinetics of membrane formation is monitored in capacitance measurements. High-resolution current recordings show the insertion of single pores of α -Hemolysin in the membrane, demonstrating the potential of this methodology.

3.2 Material and Methods

3.2.1 PDMS microfluidic device formation.

PDMS microfluidic devices are made with standard soft lithography, consisting basically of three steps: (1) Printing the design onto a photopolymer film, (2) transferring the pattern on a PDMS mold (Fig. 3.1a-d) and (3) sealing of the flowcell. Chrome-mask transparency is purchased from a micro lithography company. SU-8 photoresist is used due to its capability to reach a thickness between 5-100 μm . Sealing of the microchambers is carried out by coating a thin layer of semi liquid PDMS on a clean cover slip (number 1.5, $\sim 170 \mu\text{m}$ thickness) and binding the patterned PDMS side with the semi liquid PDMS. The semi liquid PDMS makes a covalent bond after baking the flowcell at 90 °C for 20 minutes. To increase hydrophobicity, the final flowcell is baked at 120 °C for about 1 h. To avoid swelling effect, flowcells are coated with a sol-gel layer or saturated with solvent. To coat a layer of sol-gel inside the flowcell a solution of tetraethoxysilane (TEOS), methyltriesilane (MTES), ethanol, and pH 2.6 deionized water (D.I.), adjusted with hydrochloric acid (HCl) in a 1:1:1:1 volume ratio is flowed into the flow cell. To start the sol-gel process, the flowcell is placed onto a hotplate at 60 °C and after 10 seconds the sol is flushed out with a stream of air. Saturation with solven is carried out via submerging the flowcell into decane overnight.

3.2.2 Glass microfluidic device.

A microfluidic device fully made of glass is purchased from Translume Advanced Glass Micromachine. Device dimensions are 75 mm long by 24 mm wide with 6 access holes that are 1 mm in diameter. The entire device is made of two silica plates thermally bonded together. The top plate is about 1 mm thick and contains the microcavities and access holes. The bottom plate is 120-140 μm thick and has no access hole. The glass device consists of two rectangular channels connected by five apertures in series, with aperture widths of 150, 50, 75, 100 and 200 μm . The average depth of the microchambers is 30 μm and the top surface is translucent but not optically transparent due to roughness imperfection onto the surface.

Glass microchannels are filled and submerged in 0.1 M of HNO_3 solution during 30 minutes followed by rising with D.I. water, then with acetone, and finally dried in a convection oven at 70 °C during 30 minutes. Immediately the chambers are filled and submerged in tri-chloro(1H,1H,2H,2H-perfluorooctyl)silane (PFOTS, Sigma-Aldrich) at 2% V/V PFOTS in toluene and incubate for 6-12 hr. After incubation, it is rinsed with toluene followed by 100 % ethanol and D.I. water, and finally dried in a oven at 70 °C for 30 minutes.

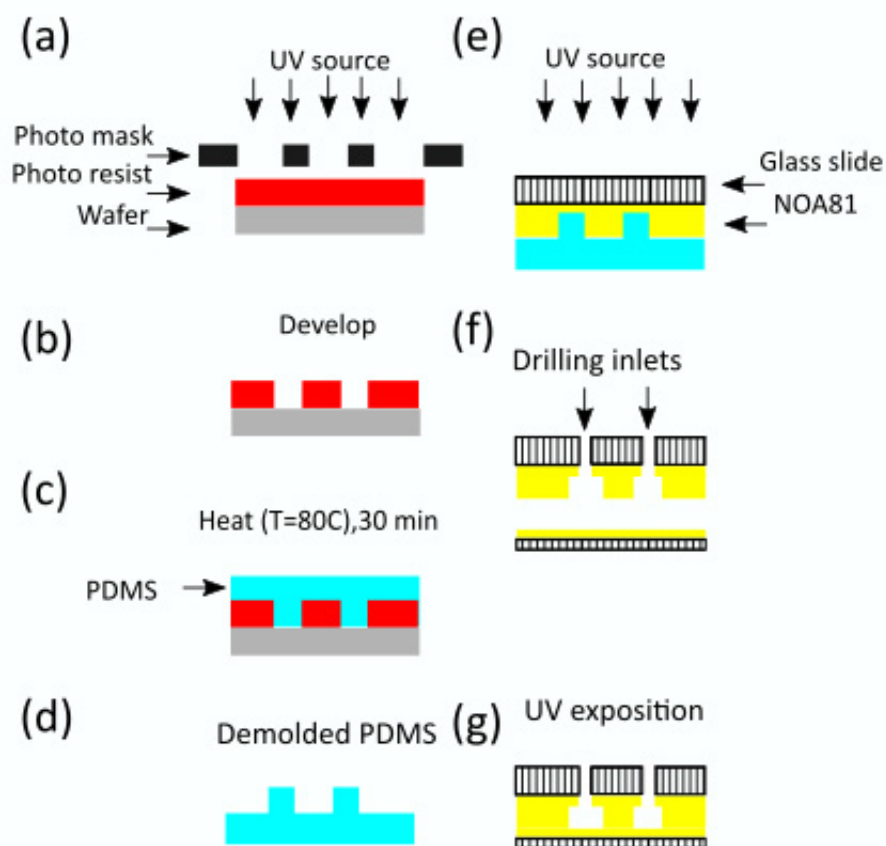


Figure 3.1: Soft lithography microfabrication scheme. Microfluidic designs are printed on a grain emulsion chrome mask high resolution film. A thin film of the photoresist SU-8 2075 is deposited on a silicon wafer with a spin coater at a speed of 2000 rpm during 60 seconds, followed by a pre-bake time on a hot plate at 95°C during 15 minutes. Patterning of the photoresist is carried out with an EVG 620 automated mask aligner system (a). After UV exposure, a post-bake treatment at 95°C during 15 minutes improves fixation of the printed pattern before development (b). SU-8 2075 patterns are used as master molds for PDMS negative replicas. The PDMS negative replicas are cured onto SU-8 patterns at 80°C for 30 minutes and used as master molds for the NOA81 microchannels (c, d). UV exposure is required to cure NOA81 and to seal the microchambers (e-g).

3.2.3 NOA81 microfluidic device formation.

Microchannels entirely made of NOA81 (Norland products) are sandwiched in between two glass slides (Fig. 3.1g) to enhance robustness. Device fabrication follows a straightforward process consisting of three steps:

(1) Fabrication of the PDMS mold. Parallel microchannels connected by one or multiple apertures are etched on a SU-8 2075 photoresist layer using conventional lithography [19]. Devices are made with aperture widths of 30, 60, 85, 90, 120 μm , and all microchannels have a height of 100 μm . Three different SU-8 masters are made; a master mold with different apertures size (30, 60, 90, 120 μm wide), a second mold with multiple apertures with the same size aperture (85 μm wide) and third master with a single aperture 85 μm wide. A PDMS negative replica is made by curing PDMS onto the SU-8 patterns, gently peeling it off, and subsequently using it as mold for NOA81 [15] (Fig. 3.1 a-d). Due to its flexibility, PDMS is a suitable reusable mold that is easily removed from the NOA81 channels.

(2) Fabrication of the NOA81 device. Liquid NOA81 is poured onto the PDMS replica, and covered with a microscope glass slide, which is previously cleaned with Hellmanex III, rinsed with ethanol, and finally treated with oxygen plasma at 30% power for 25 s (Plasma Preen I). The NOA81 layer thickness is controlled with thin metal spacers between the glass slide and the PDMS. NOA81 is cured by a 3-min UV exposition at a wavelength of 365 nm, with 36 W of power (Promed UVL-36 with four UV-9W-L bulbs). The PDMS mold is then removed from the NOA81 microchannels. The channels are washed with ethanol and holes are made for inlets/outlets with a sandblaster. Secondly, a clean glass cover slide is coated with a partially cured NOA81 layer. This is done by spin-coating a thin layer of NOA81 during 5 s at 500 rpm followed by 20 s at 4000 rpm (Spin150i POLOS) and partially curing by UV exposition during 30 s. The partially cured NOA81 layer is gently pressed against the fully cured NOA81, thus closing the channels (Fig. 3.1e-g). To permanently seal the two layers of NOA81, the device is subject to a final UV exposition during 8 min, followed by heating at 50°C during 12 h.

(3) Surface treatment. NOA81 microchannels are cleaned by rinsing the channels with ethanol, followed by flowing nitrogen, and drying at 80°C. To reduce the surface hydrophilicity of the device, the hydroxyl groups present on the NOA81 are functionalized with tri-chloro(1H,1H,2H,2H-perfluorooctyl)silane (PFOTS, Sigma-Aldrich) or with trichloro(octyl)silane (OTS, Sigma-Aldrich). For this silanization treatment, a 1.5 % V/V PFOTS or OTS solution in isooctane is injected inside clean microchannels and incubated for 15 min. After incubation, microchannels are cleaned as before.

3.2.4 Lipid bilayer formation.

Lipids (1,2-diphytanoyl-sn-glycero-3-phosphocholine (DPhPC) (Appendix Fig. 1a), 1,2-di-(9Z-octadecenoyl)-sn-glycero-3-phosphocholine (DOPC) (Appendix Fig. 1b) and 1,2-dihexadecanoyl-sn-glycero-3-phosphocholine (DPPC) (Appendix Fig. 1c)) in chloroform are purchased from Avanti lipids. Chloroform is evaporated with a stream of nitrogen gas during 20 min, followed by incubation in a vacuum chamber for at least 2 h. Dried lipids are suspended in aqueous buffer (150 mM of KCl, 10 mM of HEPES at pH of 7.4) and stored at 4°C for later use. Microchannels are first filled with organic solvent using a pressure pump (Fluigent MFCS-EZ) pushing at ~ 0.5 mbar in both channels. Afterwards, at the same pressure, we flow a previously sonicated aqueous solution, which contains lipids in 150 mM KCl, 10mM HEPES at pH 7.4.

Membranes are composed of DPhPC, or of a mixture of DOPC and DPPC in a 1:1 molar ratio. For the formation of the DPhPC lipid membrane, the organic solvent is decane, and the aqueous phase contains 3.0 mg/ml DPhPC. For the formation of the DOPC/DPPC lipid membrane, the organic solvent is a mixture of decane/chloroform/methanol at 7:2:1 v/v [20], and the aqueous phase contains 3.0 mg/ml DOPC and 2.8 mg/ml DPPC. Bilayer membrane formation is observed with bright field microscopy when lipid monolayers enter in contact at the water-solvent interface in the aperture between the channels. To evaluate success rates of lipid bilayer formation under different conditions, a microdevice with series of multiple rectangular apertures with same geometry is used however to study the effect of aperture size a second device with multiple apertures with different sizes are used. For electrophysiology experiments a device with a single aperture is required.

3.2.5 Sessile drop experiment.

For the sessile drop measurements done on NOA81, glass slides (cleaned as described before) are coated with NOA81, exposed to UV during 10 min and fully cured on a hotplate at 80°C overnight [21]. Half the samples are further treated with either the PFOTS or the OTS silane. Hydrophobicity is characterized by depositing a 7 μ l droplet of water (MilliQ, 18.2M Ω .cm at 25°C) on the NOA81 coated slides and the contact angle of the drop is measured [22]. Similarly, lipophilicity is characterized by depositing a 7 μ l droplet of decane on the substrate.

3.2.6 Fluorescence confocal microscopy.

To image the lipid bilayer in the aperture, 0.15 mg/ml N-(Fluorescein-5-thiocarbonyl)-1,2-dihexadecyl-sn-glycero-3-phosphoethanolamine (Fluor-DHPE, Avanti lipids) is added to the lipid containing aqueous solution used for membrane formation. A Nikon A1R confocal microscope is used for imaging.

3.2.7 Capacitance measurements.

Capacitance is monitored with Ag/AgCl electrodes using triangular signal of 200 Hz at 100 mV peak-to-peak with signal generator (BK precision 4040A 20MHZ). A DLPCA 200 (Femto) is used for amplification and current-potential convertor. After a 5 KHz low-pass filter, acquisition is done by a DAQ USB-6009 (National Instrument) at a 20 KHz rate, and computing is done with homemade LabView script.

3.2.8 Electrophysiology measurements with α -Hemolysin.

For the electrophysiology measurements, 3.3 $\mu\text{g/ml}$ of α -Hemolysin (Sigma-Aldrich) is added to the DPhPC aqueous solution and flowed in one of the two channels. A Keithley 65117A is used as generator and picoammeter to measure the current flowing through the protein pores present in the bilayer membrane.

3.3 Results and Discussion

3.3.1 Attempts to form free standing lipid bilayers in PDMS microdevices

PDMS is a suitable material for fast prototyping in microfluidics. First attempts to assemble lipid membranes are carried out in PDMS microfluidics in order to explore promising geometries (Appendix Fig. II). The inner surface of PDMS is slightly hydrophobic [23, 24]. Its hydrophobicity can be temporally increased by exposing the microfluidics to high temperatures. Hydrophobicity enhances the chance to form stable lipid bilayers [11] as mentioned in chapter 2. Using the “contact of monolayers” approach (see 2.3.2) requires solvent to form lipid monolayers at the interface. Decane and mineral oil are examples of organic solvents for lipidic molecules [25]. However, when using decane in a PDMS microfluidic device, swelling is observed all over the PDMS walls [26], inducing deformation (Fig. 3.2a), increase in the hydrostatic pressure and closure of the channels. This creates difficulties in producing a continuous water-solvent interface travelling at a controlled speed through the microchamber. To overcome PDMS swelling of the inner wall, the interior of the microfluidic device is coated with a sol-gel layer but unfortunately fractures, cracks or non-coated patches eventually let the decane to leak resulting in the swelling of PDMS (Fig. 3.2b). In order to avoid adsorption of decane, saturation of the PDMS with solvent is attempted by immersing overnight the entry device in decane.

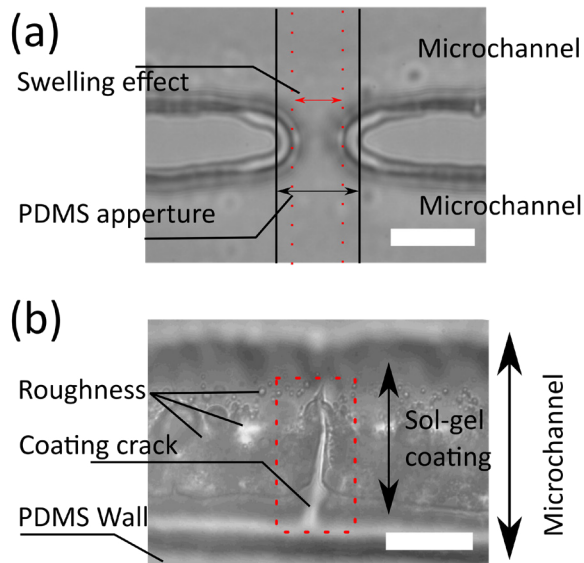


Figure 3.2: Solvent effect on PDMS microfluidic device. (a) Decreasing of aperture dimension due to swelling of PDMS wall aperture, scale bar 5 μm . (b) Fracture on the sol coated PDMS, resulting in solvent contact with the PDMS and additional roughness inside the microchannels, scale bar 200 μm .

Unfortunately, solvent saturation weakens the glass-PDMS bond resulting in the PDMS device desorbing from the glass surface. Using a less aggressive solvent like mineral oil does not swell the material; however the mineral oil increased the hydrodynamic resistance due to its viscosity, affinity to the hydrophobic PDMS and oil bubbles formation [27]. All these inconveniences required the use of pressure values above 25 mbar which is not suitable, because pressure misbalances in between the chambers could result on pressure differences of around 5 mbar between the two channels, which are high enough to disrupt or bend the membrane.

3.3.2 Formation of free standing lipid bilayers in glass microdevices

Microfluidic devices made of glass do not swell or dissolve in contact with organic solvents commonly used to form lipidic bilayers. In addition, glass can be treated to increase its hydrophobicity. Similar approaches have been followed to successfully assemble lipid membranes at the nozzle of glass micropipettes [11]. In a previous study, micropipettes have been treated to make them hydrophobic via silanization using a chlorosilane molecule bound to a long saturated fluoralkane [11]. Similarly, in this thesis, a glass microfluidic device is silanized to enhance lipid membrane formation using PFOTS (Fig. 3.6a). Formation of a lipid monolayer at the water-solvent interface is achieved by adding lipids either in the aqueous phase or into the solvent phase. Free standing membranes are formed by subsequently flowing an organic solvent and an aqueous solution of lipids (Fig. 3.3a). The lipid bilayer forms when the two lipid monolayers at the water-solvent interface contact one another in the aperture between the channels. A pocket of remaining solvent surrounding the lipid bilayer is observed (Fig. 3.3b). In addition, pressure values of ~ 10 mbar are required to flow the interface. The resistance can be reduced by expanding the width and the height of the channels. The presence of a membrane is suspected from the microscopic observations of the apertures (Fig. 3.4a), which is confirmed with electrophysiology tests. Once a membrane is assembled at the first aperture, the pressure source is stopped to perform electrophysiology experiments on that membrane. Stopping the formation of other lipid membranes over the next apertures allows studying a single membrane, as well as decreases the risk to close the circuit in the case of a membrane rupture.

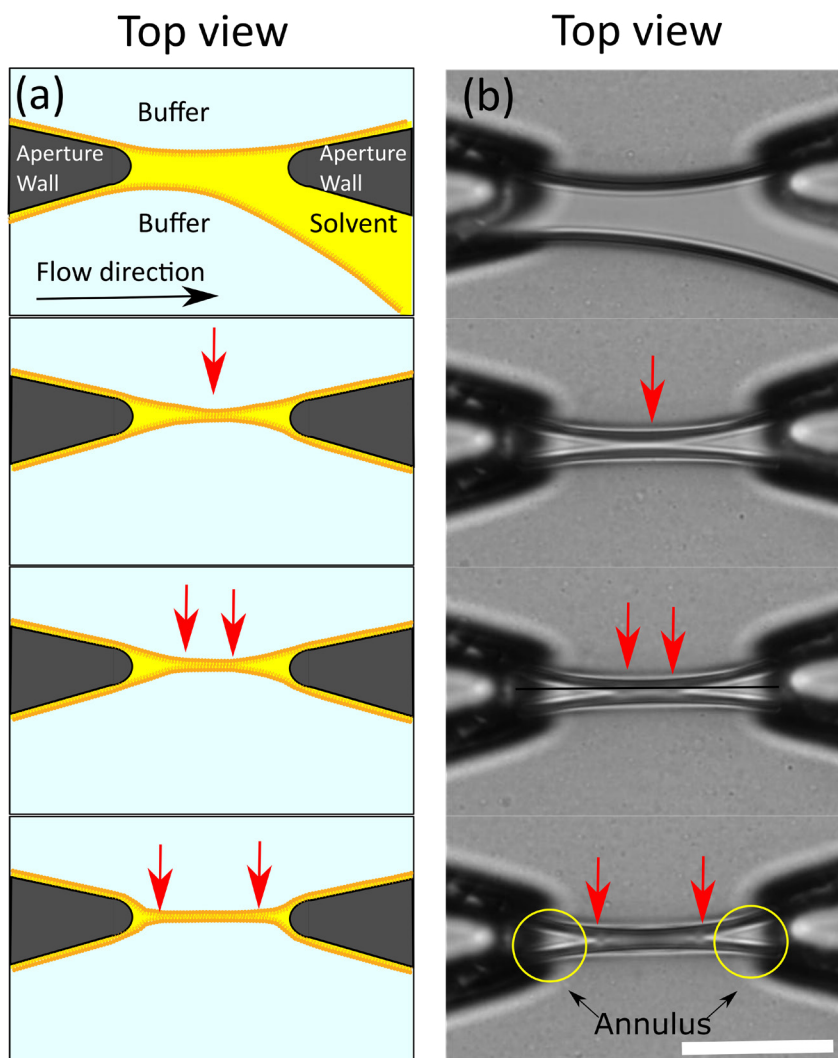


Figure 3.3: Lipid membrane formation via contacting of monolayers. (a) Schematics of the sequence for the assembly of lipid bilayers at a microaperture (grey). Lipid monolayers (orange) formed at the interface of aqueous solution (blue) and lipid solvent (yellow). Red arrows in both images delimit the region where the two monolayers are contacting one another. (b) Top view pictures of the microaperture in which the lipid membrane is assembled. Images from top to bottom represent the sequences of event leading to the contact of monolayers and lipid bilayer expansion. An annulus, or pocket of solvent (inside yellow circles), can be observed surrounding the membrane. Scale bar 50 μm .

α -Hemolysin proteins are added to one side of the membrane at a concentration of $3.3 \mu\text{g/ml}$ and the flux of ions across the membrane is measured to monitor the insertion of proteins in the membrane (Fig. 3.4b). α -Hemolysin can form pores into lipid bilayers and drive the translocation of ions across the membrane. The successful insertion of α -Hemolysin in the membrane ensures that a lipid bilayer covers the aperture, as opposed to two monolayers with a layer of organic solvent in between. However, as mentioned before, glass flowcells are much more fragile and their manufacturing is expensive compared to PDMS flowcells. The high price and complex manufacturing makes it a difficult material for prototyping and to explore the multiple geometries and conditions for improving lipid membrane formation. In addition, due to insufficient surface transparency, this device would not be well suited for studies in combination with optical techniques if surface roughness is not improved.

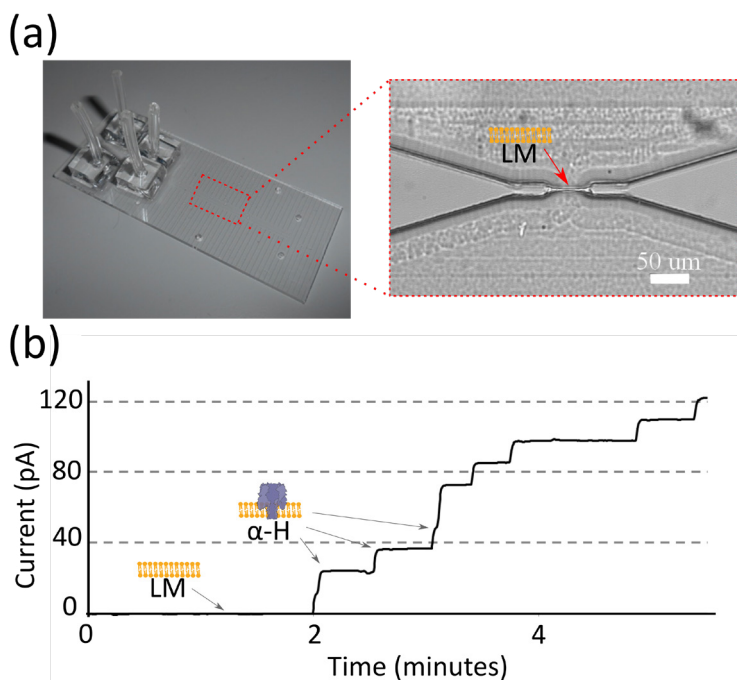


Figure 3.4: Formation and characterization of lipid membranes in glass microdevices. (a) Glass microfluidic device (left) with a close-up view on the aperture (right) with a lipid membrane (LM), PDMS blocks are glued onto the glass surface and used as inlets to hold the tubing of the solutions. (b) Electrophysiology recordings of α -Hemolysin pores (α -H) with an applied voltage of 80 mV (DC) in 150 mM KCl, 10 mM HEPES at pH of 7.4.

Assembling lipid bilayers in presence of solvent often results on the formation of an annulus. The annulus is a mixture of lipids and solvent that is trapped during the contact of monolayers. The annulus occupies a fraction of the total area of the aperture and it is reflected on the final area of the membrane. In other words, a larger annulus results in a smaller surface area for a bilayer membrane. Hypothetically the size of the annulus can be affected by the geometry of the channel and the speed of the water-solvent interface travelling in the channel; however these parameters are not covered in this study.

3.3.3 Formation of free standing lipid bilayers in NOA81 microdevices

Next, microchannels entirely made of NOA81 are fabricated, a material which prevents swelling and allows easy patterning. The microfluidic device with a single aperture consists of two 100 μm high and 1 mm-wide parallel channels connected by a rectangular aperture where a free standing lipid bilayer membrane is self-assembled (Fig. 3.5).

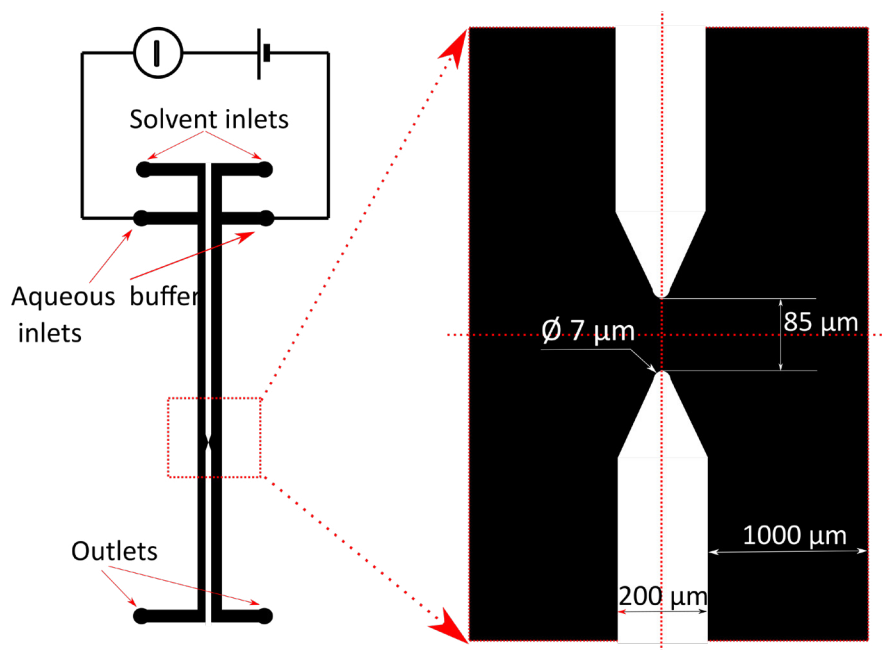
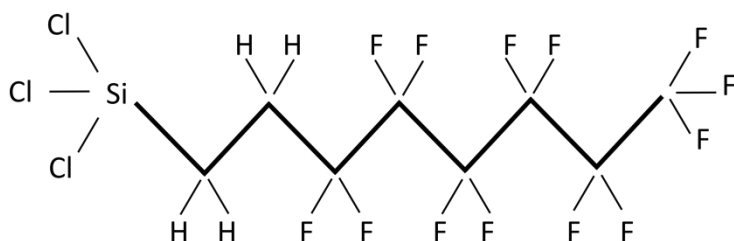


Figure 3.5: Single aperture microfluidic device. Rectangular NOA81 microchannels are interconnected by an aperture. Each side of the aperture is supplied with independent inlets for aqueous and organic solvent solutions. Electrodes are inserted into small PDMS blocks to grant a conductive medium to perform electrophysiology experiments. PDMS blocks are used over the inlets to hold the tubes with the solutions.

3.3.3.1 Characterization of the silanized-NOA81 surface

Prior to lipid membrane formation, a silanization of the surface of the channels is done with either the fluoroalkylsilane PFOTS (Fig. 3.6a) or the alkylsilane OTS (Fig. 3.6b).

(a)



(b)

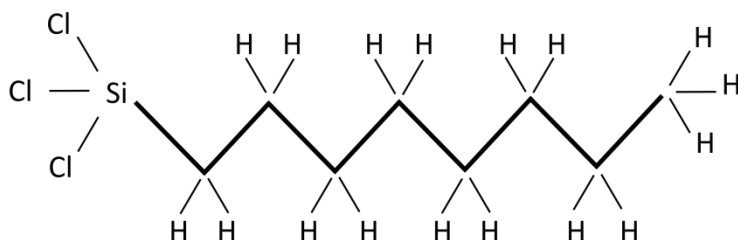


Figure 3.6: Chemical structure of silane molecules. Compounds used to modify the glass surface to induce hydrophobicity inside the microchambers: (a) PFOTS, previously reported to enhance stability of lipid membrane [11] and (b) OTS, a similar molecule with no fluor group present.

The resulting surface properties of silanized NOA81 are characterized by a sessile drop experiment. The contact angle values confirm that untreated NOA81 channels are mildly hydrophilic (Table 3.1) [21, 28]. Both surface treatments resulted in a more hydrophobic surface. With a drop of decane, a contact angle smaller than 10° is found for untreated NOA81 and for OTS-treated NOA81. However, we measured a contact angle of $\sim 70^\circ$ for PFOTS-treated NOA81.

Table 3.1: Contact angle values of water and decane on untreated and silanized NOA81.

		PFOTS-treated NOA81		OTS-treated NOA81	
Contact angle	NOA81	after surface treatment	7 days later	after surface treatment	7 days later
		water	69.3°±1.3°	107.8°±1.1°	109.8°±1.3°
decane	<10°	68.9°±1.5°	71.0°±1.5°	<10°	<10°

Therefore, the PFOTS treatment increases both the hydrophobic and lipophobic character of the surface. Surface properties are maintained after one week.

In agreement with these measurements, we observe that the treatment has an impact on the flow in the microchannels. When flowing decane followed by water in untreated NOA81 microchannels, droplets of organic solvent remain attached to the surface (Fig. 3.7a). In this condition, a pressure of ~10 mbar is required to push the water/decane interface, which prevents membrane formation. After surface treatment, significantly fewer droplets of decane are observed on the surface (Fig. 3.7b), and a pressure of 0.5 mbar is sufficient to push the solvent/buffer interface. Under this pressure, lipid bilayer formation in PFOTS- and OTS-treated NOA81 microchannels is reproducible.

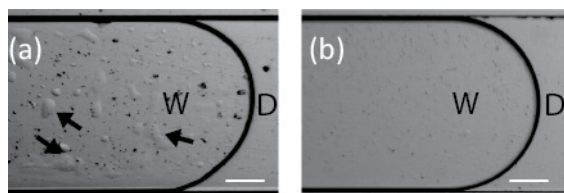


Figure 3.7: Microfluidic channel before and after surface treatment. Interface water (W)/decane(D) in a rectangular NOA81 microchannel, without (a) and with (b) PFOTS treatment, on different devices. Without surface treatment, droplets of decane are observed on the channel surface, as indicated with black arrows. Scale bar is 100 μm .

3.3.3.2 Formation of free standing DPhPC and DOPC/DPPC bilayers

Free standing membranes are formed similarly as in glass flowcells, by contacting two lipid monolayers at an aperture. The success rate of membrane formation is tested for DPhPC and for a 1:1 mixture of DOPC/DPPC using PFOTS- or OTS-treated multigap flowcells (Fig. 3.8). In both PFOTS- and OTS-treated flowcells, DPhPC membranes are formed in ~80% of the apertures. DOPC/DPPC membranes are formed in 66% of apertures of PFOTS-treated channels and 77% of apertures of OTS-treated channels.

For each condition 10 experiments are effected using 3 different flowcells for each treatment and mixture of lipid. The free standing lipid bilayers are stable for up to several days.

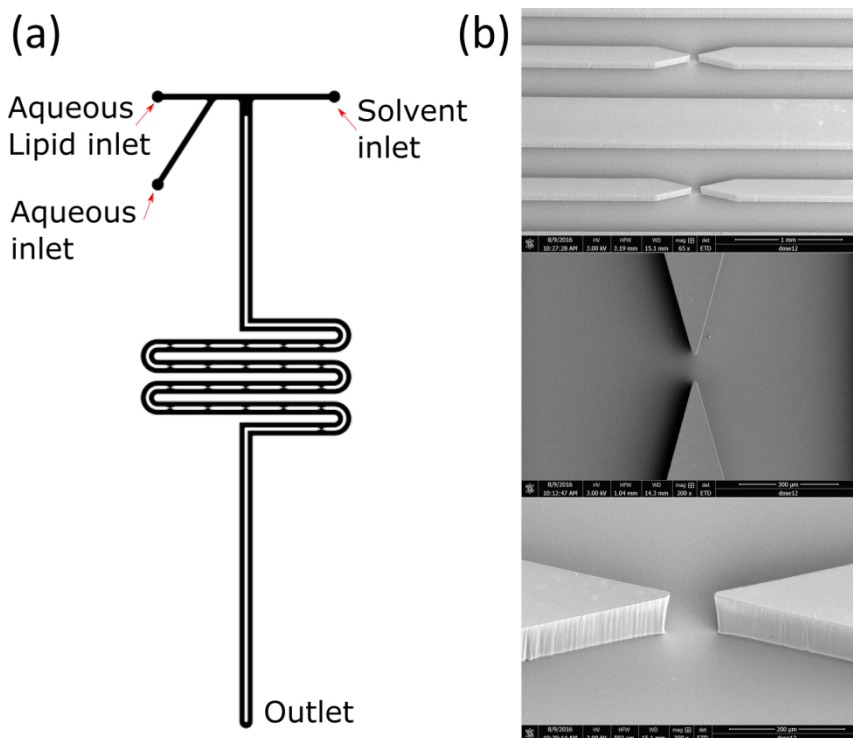


Figure 3.8: Flowcell used for measure success rate for membrane formation. Three different inlets are supplying lipid solutions, aqueous buffer or organic solvents (a). A total of 21 gaps are placed in a matrix of 5X4 for easy observation (b).

3.3.3.3 Measurement of lipid bilayer surface area with fluorescence confocal microscopy

Confocal fluorescence allows direct observation of fluorescent lipids which are included in the lipid bilayer on the aperture. Top-view allows an easier access and visualization of the lipid bilayer while it is forming. However, a full 3D view of the spanned lipid bilayer on the aperture can provide insight on the amount of solvent that might remain trapped between the lipid monolayers. Confocal microscopy is used to visualize lipids in specific planes. For that purpose, a small amount of fluorescently-labeled DHPE is added to the DPhPC solution. The aperture is scanned from bottom to top and then reconstructed in a 3D figure to be able to visualize from different perspectives.

The reconstructed 3D figure provides an estimation of the surface area of the lipid bilayer and the size of the annulus in the aperture. The geometry of the aperture is found to have an important effect on the size of the annulus (Fig. 3.9a). Little variations in the geometry of the gap are observed due to mold imperfection during the flow cell fabrication. The lipid bilayer has a maximum surface area of $8500 \mu\text{m}^2$, which corresponds to the size of the aperture. However, a smaller lipid bilayer area is expected due to the annulus and possibly also aperture imperfections. The analysis of a single lipid bilayer slice makes possible to estimate the size of the annulus, which can be approximated as a triangle with a height of $\sim 5 \mu\text{m}$ on average (Fig. 3.9b).

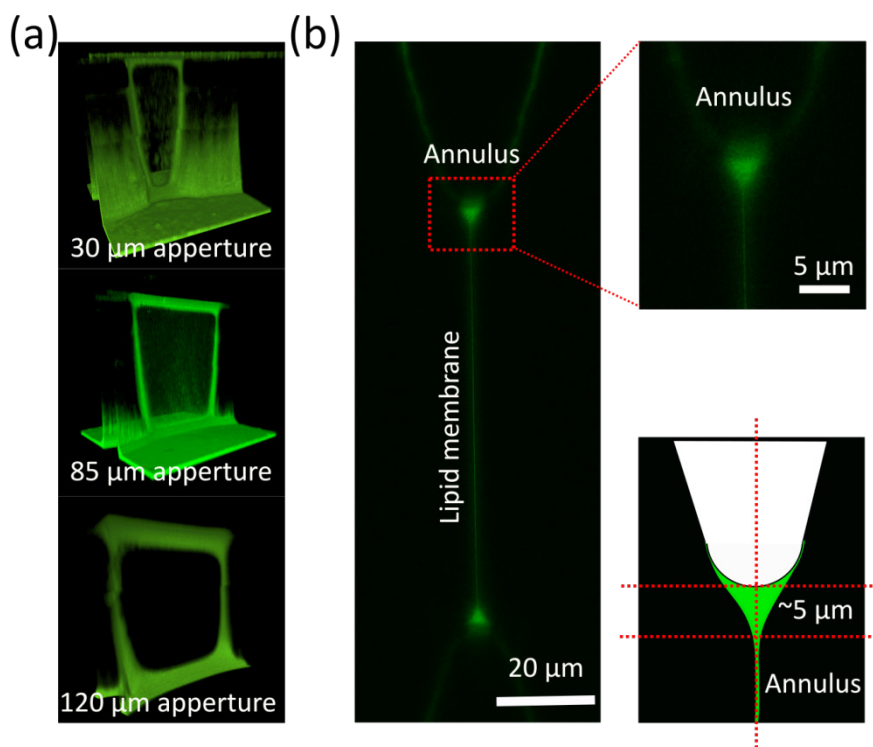


Figure 3.9: Fluorescence visualization of lipid bilayer by confocal microscopy. (a) Picture of the 3D reconstruction of free standing lipid membrane of DPhPC observed by fluorescence confocal microscopy. Fluorescent lipids (Fluor-DHPE) are used to visualize the lipid membrane and the annulus. Three different widths are shown in the picture: 30 μm , 85 μm and 120 μm . (b) Cross-section of lipid bilayer showing the reservoir of lipids in the organic solvent (annulus), which corresponds to the triangular area with higher fluorescent intensity.

To determine more precisely the size of the annulus, the intensity profile of each slice obtained from fluorescence confocal microscopy is analyzed. Horizontal planes are scanned from the bottom to the top of the aperture, by imaging slices spaced by 1

μm . The average (I_0) and the standard deviation (σ) of the intensity in a $10\ \mu\text{m} \times 10\ \mu\text{m}$ square area in the center of the membrane is calculated. To estimate the surface area of the lipid bilayer, we only considered the area with fluorescence intensity within 3σ from the average intensity. In each of the slices recorded, this criterion is used to determine the annulus/bilayer boundaries (Fig. 3.10).

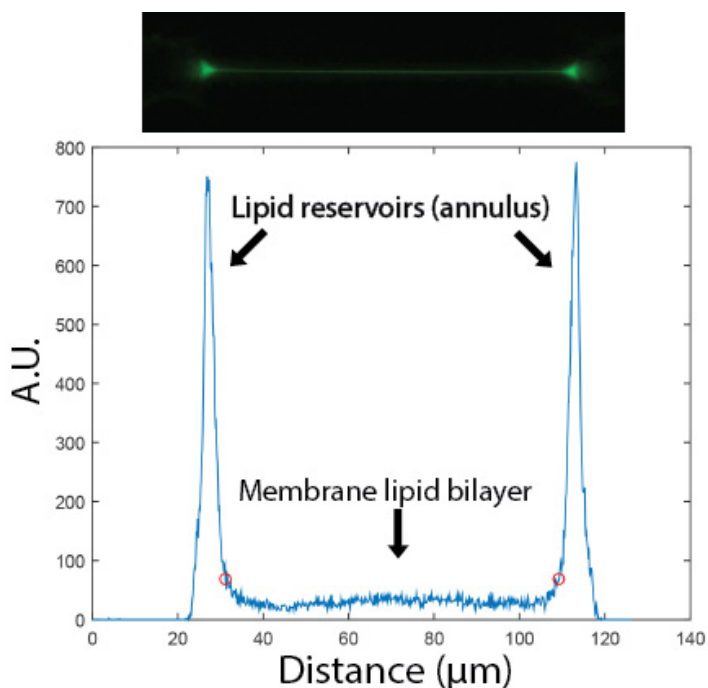


Figure 3.10: Intensity profile from fluorescence confocal microscopy. The picture (top) shows the fluorescent image at a height of $68\ \mu\text{m}$ from the bottom of the aperture. The graph (bottom) shows the corresponding cumulative intensity profile along the membrane axis. The central section corresponds to the lipid bilayer, while the edges correspond to the annulus. The analysis of the intensity profile of all microscope slices, after background subtraction, results in an average fluorescence intensity (I_0) of $45.7\ \text{A.U.}$ in the $10\ \mu\text{m} \times 10\ \mu\text{m}$ square area in the center of the membrane, with a standard deviation (σ) of $7.4\ \text{A.U.}$ The coordinates assigned as annulus/bilayer boundaries correspond to $I_0 + 3\sigma$ (i.e. $53.1\ \text{A.U.}$), as indicated with red circles. After computing each layer, the resulting lipid bilayer surface area is $6670\ \mu\text{m}^2$. Note: due to the sharp transition in intensity between the annulus and the lipid bilayer, the calculated area does not differ notably if the coordinates assigned as annulus/bilayer boundaries is 2σ , 3σ or 4σ higher than the average intensity, as shown in the table hereafter.

coordinates assigned as annulus/bilayer boundaries	Calculated bilayer area (μm^2)
$I_0 + 2\sigma$	6520
$I_0 + 3\sigma$	6670
$I_0 + 4\sigma$	6820

3.3.3.4 Electrical measurements of free standing lipid bilayers

Capacitance is monitored to follow the dynamics of bilayer formation of a DPhPC-membrane in single gap PFOTS-treated flow cells (Fig. 3.11). The measured capacitance reaches a steady state value after ~ 10 min, when the lipid bilayer reaches its maximum surface area. The average capacitance once the lipid bilayer is fully formed is 33 ± 2 pF. Considering the size of the aperture ($100 \mu\text{m} \times 85 \mu\text{m}$), we obtain a specific membrane capacitance of at least $\sim 0.4 \mu\text{F}\cdot\text{cm}^{-2}$. Taking into account the lipid bilayer surface area measured with confocal microscopy, we estimate a specific membrane capacitance of $\sim 0.5 \mu\text{F}\cdot\text{cm}^{-2}$, which is close to capacitance values previously reported for solvent-free DPhPC lipid membranes [29-31], indicating little decane in the bilayer membrane [32].

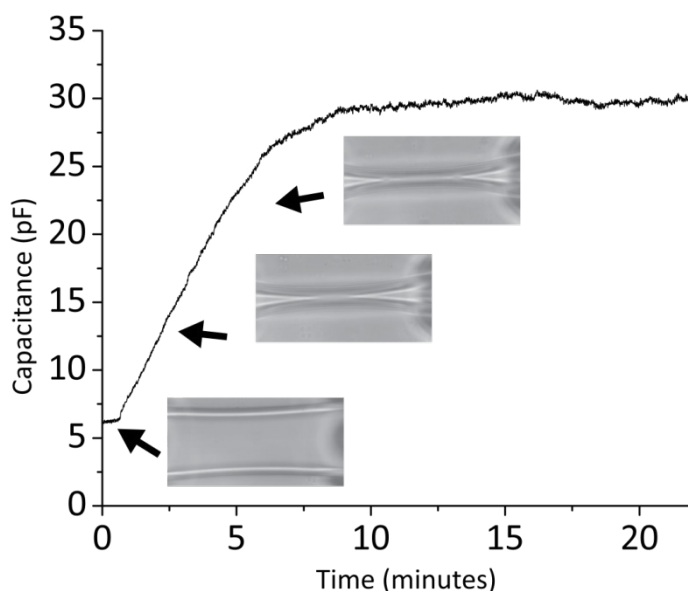


Figure 3.11: The capacitance increases when the lipid bilayer forms and spreads in size, until it reaches its maximum surface area. Pictures of the water/decane interfaces during membrane formation are shown.

3.3.3.5 Single protein pore insertion

Bilayer formation is also confirmed by inserting α -Hemolysin pores [29, 33] into the DPhPC lipid membrane formed in a PFOTS-treated single gap microdevice. In order to test the presence of a lipid bilayer, conductance experiments are performed. Transport of ions across the membrane can be monitored when biological pores are inserted in the membranes. Current is measured while ions are translocated from one side of the chamber to the other side. Without biological pores, the transport of ions can be neglected, since the membrane has a resistance in the order of $G\Omega$ (Fig. 3.12).

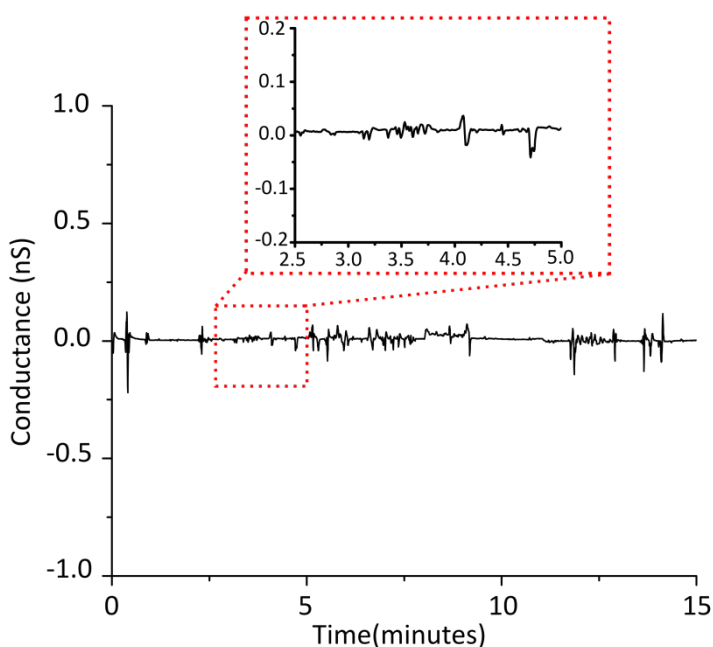


Figure 3.12: Conductance of a lipid membrane bilayer inside the NOA81 microfluidic device (in absence of proteins). For this dataset, the corresponding average seal resistance is $126 G\Omega$. For every lipid bilayer formed in the NOA81 device, the seal resistance is $>10 G\Omega$.

When $3.3 \mu\text{g/ml}$ α -Hemolysin is injected in one of the two channels, it results in discrete jumps in current (Fig. 3.13). With an applied potential of 40mV , the average single pore current measured from the electrophysiology recordings is $\sim 5 \text{ pA}$, in agreement with previously reported values [29]. The measure of discrete increments in ionic current due to the insertion of α -Hemolysin pores into the membrane is a strong evidence of the presence of a lipid bilayer. Without a lipid bilayer, α -Hemolysin

pores cannot be inserted and no current would be detected. Under lower pore concentration, this device could be used for single-channel current recording experiments.

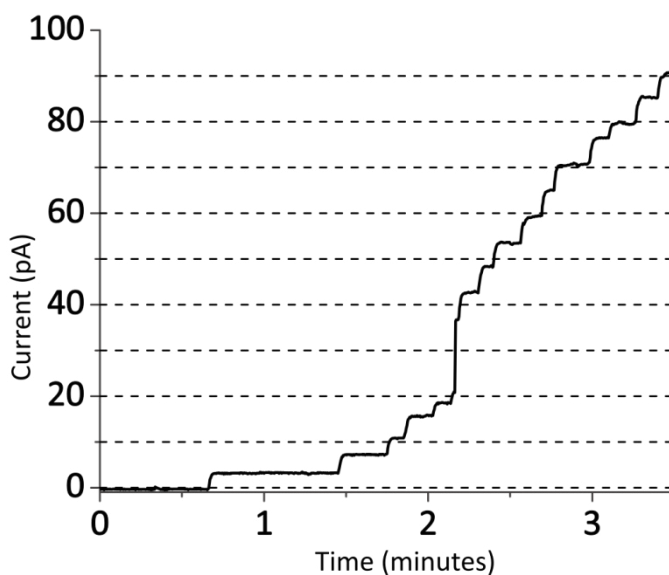


Figure 3.13: High-resolution current recording across the lipid membrane detects single α -Hemolysin pores inserting into the artificial lipid bilayer. Flowing $3.3 \mu\text{g/ml}$ α -Hemolysin in one channel results in discrete increments in the flux of ions across the lipid bilayer. The current is measured with a picoammeter at 40 mV DC.

Sudden changes of electrical potential above 300 mV, high concentration of biological proteins, presence of surfactants and changes in pH can affect the lifetime of lipid membranes assembled with this method. The success rate of membrane formation is likely related to the concentration of lipids into the solvent and the type of lipid used. It is observed that low lipid concentrations result in a lower success rate formation and that increasing the lipid concentration can improve success rate formation until a saturation concentration where success rate can be affected by others factors like flow speed and impurities in the solution. Perfusion of buffer in only one side of the membrane can be performed in order to increase the chance of pores insertion. However, as this is in the low Reynolds regime, the insertion of pores is mainly carried out by diffusion of the pores near the vicinity to the membrane.

3.4 Conclusions

In this chapter, newly developed methods to form model lipid bilayers membranes in microdevices are presented. In the search for a suitable material that can successfully support lipid bilayers stable for long periods of time, different materials are tested: PDMS, glass and NOA81. PDMS is relatively cheap and simple to manufacture, however it is incompatible with several solvents needed for lipid bilayer formation. To overcome this solvent incompatibility issue, glass flowcell are used, because glass does not swell in presence of organic solvent. It is found that glass is a suitable material to assemble lipid bilayers and electrophysiological investigations are performed using this technology. However, the high cost and complex manufacturing process makes it difficult to test several flow cell geometries that could enhance the lipid membrane formation. Nevertheless, the use of glass flowcells reveals basic requirements for lipid bilayer formation, such as geometry of the aperture, hydrophobicity properties and pressure limits.

Further investigations led to develop a technique based on NOA81 microdevices suitable to form long-lived free standing lipid bilayers, with easy control over the chemical and physical conditions on both sides of the membrane. For stable lipid bilayer formation, the NOA81 surface is treated with either a fluoroalkylsilane (PFOTS), which reproduces teflon surface properties, or with an alkylsilane (OTS). Electrophysiology measurements can detect the insertion of single α -Hemolysin protein pores. The lipid bilayer surface plane is perpendicular to the microscope focal plane, enabling direct observation of fluctuations in the membrane curvature. This highly reproducible method to form stable free standing lipid bilayers finds a wide range of applications, from drug screening to sensing devices, and membrane protein channels characterization. In addition, more investigations are needed to fully explore and exploit the potential of this system. Combination with optical techniques can help to explore the biophysical properties of lipid bilayers and proteins.

3.5 Reference

1. Weatherill, E.E. and M.I. Wallace, *Combining Single-Molecule Imaging and Single-Channel Electrophysiology*. Journal of Molecular Biology, 2015. **427**(1): p. 146-157.
2. Rajapaksha, S.P., X. Wang, and H.P. Lu, *Suspended Lipid Bilayer for Optical and Electrical Measurements of Single Ion Channel Proteins*. Analytical Chemistry, 2013. **85**(19): p. 8951-8955.
3. Sachse, R., et al., *Membrane protein synthesis in cell-free systems: From bio-mimetic systems to bio-membranes*. FEBS Letters, 2014. **588**(17): p. 2774-2781.
4. Nourian, Z., W. Roelofsen, and C. Danelon, *Triggered Gene Expression in Fed-Vesicle Microreactors with a Multifunctional Membrane*. Angewandte Chemie International Edition, 2012. **51**(13): p. 3114-3118.
5. Mizuno, M., et al., *Formation of Monodisperse Hierarchical Lipid Particles Utilizing Microfluidic Droplets in a Nonequilibrium State*. Langmuir, 2015. **31**(8): p. 2334-2341.
6. Kukwikila, M. and S. Howorka, *Nanopore-Based Electrical and Label-Free Sensing of Enzyme Activity in Blood Serum*. Analytical Chemistry, 2015. **87**(18): p. 9149-9154.
7. Mueller, P., et al., *METHODS FOR THE FORMATION OF SINGLE BIMOLECULAR LIPID MEMBRANES IN AQUEOUS SOLUTION*. The Journal of Physical Chemistry, 1963. **67**(2): p. 534-535.
8. Zagnoni, M., *Miniaturised technologies for the development of artificial lipid bilayer systems*. Lab on a Chip, 2012. **12**(6): p. 1026-1039.
9. Jonsson, P., M.P. Jonsson, and F. Hook, *Sealing of Submicrometer Wells by a Shear-Driven Lipid Bilayer*. Nano Letters, 2010. **10**(5): p. 1900-1906.
10. Göpfrich, K., et al., *Lipid Nanobilayers to Host Biological Nanopores for DNA Translocations*. Langmuir, 2012. **29**(1): p. 355-364.
11. Bright, L.K., et al., *Decreased Aperture Surface Energy Enhances Electrical, Mechanical, and Temporal Stability of Suspended Lipid Membranes*. ACS Applied Materials & Interfaces, 2013. **5**(22): p. 11918-11926.
12. Dangla, R., F. Gallaire, and C.N. Baroud, *Microchannel deformations due to solvent-induced PDMS swelling*. Lab on a Chip, 2010. **10**(21): p. 2972-2978.

13. King, P.H., et al., *Interdroplet bilayer arrays in millifluidic droplet traps from 3D-printed moulds*. Lab on a Chip, 2014. **14**(4): p. 722-729.
14. Tsuji, Y., et al., *Droplet-based lipid bilayer system integrated with microfluidic channels for solution exchange*. Lab on a Chip, 2013. **13**(8): p. 1476-1481.
15. Sollier, E., et al., *Rapid prototyping polymers for microfluidic devices and high pressure injections*. Lab on a Chip, 2011. **11**(22): p. 3752-3765.
16. Bomer, J.G., et al., *Wafer-scale fabrication of glass-FEP-glass microfluidic devices for lipid bilayer experiments*. Lab on a Chip, 2014. **14**(23): p. 4461-4464.
17. Halza, E., et al., *Well-Defined Microapertures for Ion Channel Biosensors*. Analytical Chemistry, 2013. **85**(2): p. 811-815.
18. Kendall, E.L., C. Shao, and D.L. DeVoe, *Visualizing the Growth and Dynamics of Liquid-Ordered Domains During Lipid Bilayer Folding in a Microfluidic Chip*. Small, 2012. **8**(23): p. 3613-3619.
19. Abgrall, P., et al., *SU-8 as a structural material for labs-on-chips and micro-electromechanical systems*. ELECTROPHORESIS, 2007. **28**(24): p. 4539-4551.
20. Wodzinska, K., A. Blicher, and T. Heimburg, *The thermodynamics of lipid ion channel formation in the absence and presence of anesthetics. BLM experiments and simulations*. Soft Matter, 2009. **5**(17): p. 3319-3330.
21. Gu, H., M.H.G. Duits, and F. Mugele, *A hybrid microfluidic chip with electrowetting functionality using ultraviolet (UV)-curable polymer*. Lab on a Chip, 2010. **10**(12): p. 1550-1556.
22. Kaufmann, T.C., A. Engel, and H.-W. Rémigy, *A Novel Method for Detergent Concentration Determination*. Biophysical Journal, 2006. **90**(1): p. 310-317.
23. Bodas, D. and C. Khan-Malek, *Hydrophilization and hydrophobic recovery of PDMS by oxygen plasma and chemical treatment—An SEM investigation*. Sensors and Actuators B: Chemical, 2007. **123**(1): p. 368-373.
24. Tan, S.H., et al., *Oxygen plasma treatment for reducing hydrophobicity of a sealed polydimethylsiloxane microchannel*. Biomicrofluidics, 2010. **4**(3): p. 032204.
25. Baba, T., et al., *Formation and characterization of planar lipid bilayer membranes from synthetic phytanyl-chained glycolipids*. Biochimica et Biophysica Acta (BBA) - Biomembranes, 1999. **1421**(1): p. 91-102.

-
26. Lee, J.N., C. Park, and G.M. Whitesides, *Solvent Compatibility of Poly(dimethylsiloxane)-Based Microfluidic Devices*. *Analytical Chemistry*, 2003. **75**(23): p. 6544-6554.
 27. Sajeesh, P., M. Doble, and A.K. Sen, *Hydrodynamic resistance and mobility of deformable objects in microfluidic channels*. *Biomicrofluidics*, 2014. **8**(5): p. 054112.
 28. Wägli, P., A. Homsy, and N.F. de Rooij, *Norland optical adhesive (NOA81) microchannels with adjustable wetting behavior and high chemical resistance against a range of mid-infrared-transparent organic solvents*. *Sensors and Actuators B: Chemical*, 2011. **156**(2): p. 994-1001.
 29. Funakoshi, K., H. Suzuki, and S. Takeuchi, *Lipid Bilayer Formation by Contacting Monolayers in a Microfluidic Device for Membrane Protein Analysis*. *Analytical Chemistry*, 2006. **78**(24): p. 8169-8174.
 30. Nikolov, V., et al., *Electrical measurements of bilayer membranes formed by Langmuir-Blodgett deposition on single-crystal silicon*. *Langmuir*, 2007. **23**(26): p. 13040-13045.
 31. Batishchev, O.V. and A.V. Indenbom, *Alkylated glass partition allows formation of solvent-free lipid bilayer by Montal-Mueller technique*. *Bioelectrochemistry*, 2008. **74**(1): p. 22-25.
 32. Gross, L.C.M., et al., *Determining Membrane Capacitance by Dynamic Control of Droplet Interface Bilayer Area*. *Langmuir*, 2011. **27**(23): p. 14335-14342.
 33. Saha, S.C., et al., *Scalable micro-cavity bilayer lipid membrane arrays for parallel ion channel recording*. *Sensors and Actuators B: Chemical*, 2014. **199**(0): p. 76-82.

3.6 Appendix

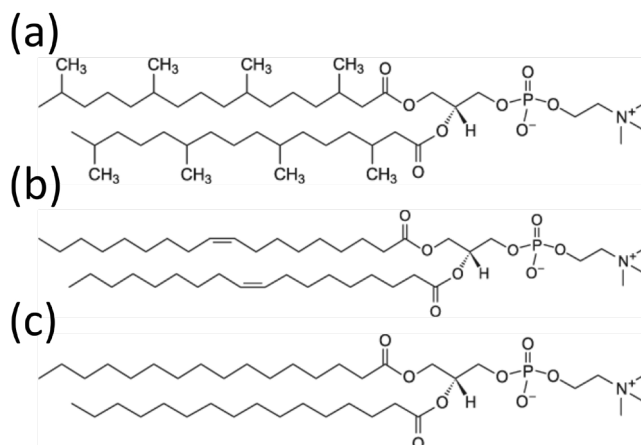


Figure I. Lipid molecules used for assembling of membranes. (a) Lipids (1,2-diphytanoyl-sn-glycero-3-phosphocholine (DPhPC). (b) 1,2-di-(9Z-octadecenoyl)-sn-glycero-3-phosphocholine (DOPC) and (c) 1,2-dihexadecanoyl-sn-glycero-3-phosphocholine (DPPC).

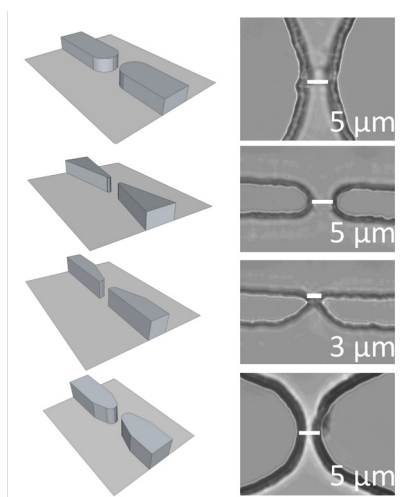


Figure II. Different geometries of the apertures used on PDMS devices. Diameter of the wall right at the aperture is 100 μm , 5 μm , 5 μm and 15 μm from top to bottom respectively.

Chapter 4

Combination of free standing lipid membranes with optical tweezers

Mechanical forces at the cell membrane play a role in a variety of biological processes, such as lipid nanotube formation, cell segregation and endocytosis. Applying and measuring piconewton-level forces can shed light on the interplay between mechanical forces and these bioprocesses. Artificial membrane systems, which mimic cell membranes, enable to control physicochemical conditions for a better quantitative biophysical understanding of such processes. Techniques that combine optical tweezers with free standing lipid membranes often lack of accessibility to both sides of the membrane. In this chapter, a first combination of optical tweezers with free standing lipid bilayers fully accessible from both membrane sides is shown. Lipid membranes are formed in a microfluidic device as described in chapter 3. In order to prevent optical effects hindering optical trapping close to the lipid bilayer, the pockets of solvent surrounding the lipid membrane are reduced in size via a specific combination of solvent and flowcell material. This new method open possibilities for a wide range of application, including the study of molecular motors associated with the membrane and the formation of networks of lipid tubes, as found in cell organelles and intercellular tubular structures for communication*.

*Parts of this chapter is included in: *V. Marin, A. Dols-Perez, R. Kieffer, M.E. Aubin-Tam, submitted (2017).*

4.1 Introduction

Cell membranes host an astonishing amount of proteins and other molecules [1]. Their functions go from signaling [2, 3], structural support [4] to metabolic regulations [5]. Morphological changes of cell membranes are regulated with complex sets of proteins placed onto the extracellular and intracellular surfaces of cell membranes [6]. Additionally, translocation of macromolecules across the membranes occurs in both directions. However, little is known about the mechanisms of such events [7]. Model membranes provide the appropriate conditions to mimic protein membrane interactions [8]. Likewise, model membrane with access to both sides of the membrane offer suitable conditions to study phenomena where control on both membrane sides is required [9]. Free standing lipid membranes assembled on apertures allow access to both side of the membrane, and if combined with force microscopy, can facilitate the study mechanical events at the membrane, as well as rheological properties of membranes.

Biophysical tools that apply and measure piconewton-level forces can help our understanding of mechanical events happening at the membrane. Mechanical deformations using micro-aspiration [10] and optical manipulation [11] are common methods to systematically apply a known force to membranes. Optical tweezers is an optical technique used to manipulate objects at the microscale and to measure forces in real time. The combination of optical tweezers with supported lipid bilayers or giant unilamellar vesicles (GUVs) has contributed to our biophysical understanding of lipid nanotubes formation [12, 13], protein crowding influence on membrane tension [14] and the role of proteins involved in membrane fission [15] and fusion [16]. However, in these systems, it remains challenging to achieve dynamic control over each side of the membrane, asymmetric lipid distribution and zero curvature, which limits the range of biological and biophysical questions that can be addressed. As numerous membrane-bound motor proteins and mechanotransduction systems depend on specific conditions on each side of the membrane, it is beneficial to tune these conditions in real-time, while measuring the system response across the membrane (e.g., current, mechanical force). Little has been explored regarding the combination of optical tweezers and model membranes with easy access to both sides of the membrane like free standing lipid membranes. Contrary to vesicles, free standing lipid membranes assembled in an aperture are flat and mechanical manipulation can be straightforwardly executed on both sides of the membrane.

The assembly of free standing lipid membranes assembled on apertures requires solvents, which results in a solvent remaining between the membranes. Chapter 3 showed that the contact-of-monolayers technique utilizes an interface between an organic solvent and aqueous solution. The function of this interface is to provide an amphipathic interface where lipid molecules can assemble into a monolayer. Different organic solvents are reported to be used for this purpose, as for example ethanol [17], decane [18], octanol [19], squalene [20], mineral oil [21] and chloroform [18] among

others. Compatibility between the organic solvent and the material of the chambers is an important aspect to consider. Chapter 3 demonstrated the importance of selecting a material chemically inert to avoid wear or swelling of the microchambers [22]. The contact-of-monolayers method results in organic solvent trapped in between the two lipidic leaflets and also close to the walls of the microdevice. These pockets of solvent are known as the annulus. The annulus does not represent an inconvenience in performing electrophysiology experiments and confocal microscopy. However, the annulus creates optical aberrations [23] preventing optical trapping close to the membrane. This chapter starts with a description of optical tweezers, followed by a presentation of the technique developed in this thesis to combine optical tweezers with free standing lipid bilayers.

4.1.1 General configuration of optical tweezers

An optical tweezers is a powerful tool to manipulate micron-sized objects in the range of ~ 0.2 to $5 \mu\text{m}$ [24]. It was developed by Arthur Ashkin in the early 70's and showed promising application in the biophysics field in the late 80's. It consists of a single focused laser beam that produces attractive or repulsive forces on dielectric objects. Forces are generated by the transfer of momentum from photons crossing an object with a higher refractive index than the medium. The net force can be described with two components: a *gradient force* that attracts the object towards the center of the trap, and a *scattering force* that pushes the object in direction of the light propagation (Fig. 4.1a-b). Optical tweezers are broadly used by biophysicists to characterize mechanical properties of biological systems or to study motor proteins, such as DNA processing motors [25], kinesin [26], and proteolytic machines like ClpX [27]. To use an optical tweezers, its stiffness must first be calibrated.

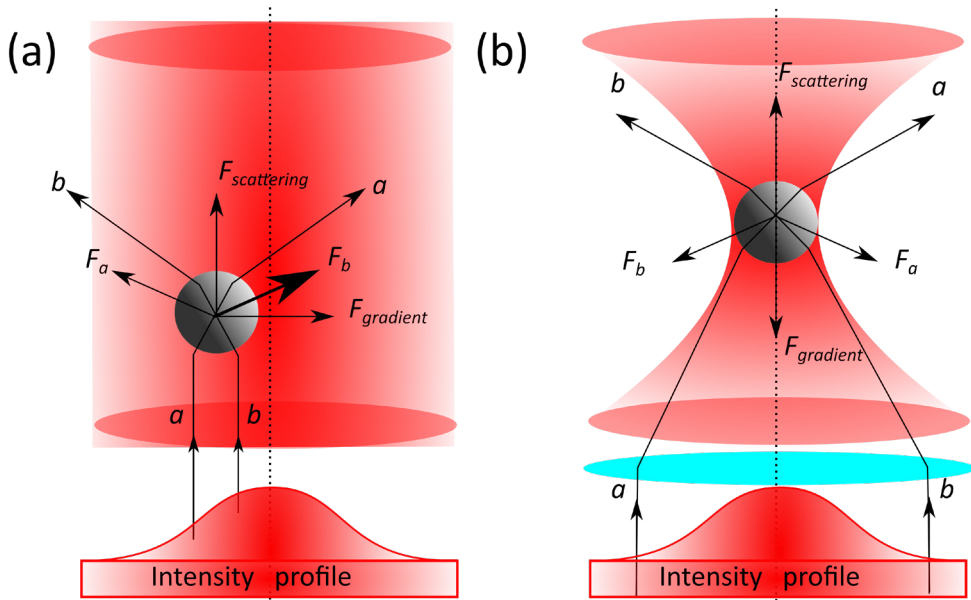


Figure 4.1: Physical principle of optical tweezers using the ray optics regime explanation. (a) Force diagram of a dielectric particle in a collimated beam. This diagram shows the gradient and scattering components affecting its equilibrium position. **(b)** Diagram showing the rays (a , b) inducing momentum on the dielectric particle, in a focused laser beam, which induces a change in the scattering force ($F_{scattering}$) and a gradient force ($F_{gradient}$).

4.1.2 Optical tweezers stiffness calibration

In order to perform force microscopy using optical tweezers, it is crucial to determine the stiffness of the system (k). For small displacements close to the center of the trap, the net force acting on trapped particles behaves as a spring or simple harmonic oscillator. The trap stiffness can be determined with different methods to calibrate an optical tweezers [28-30].

4.1.2.1 Drag force method

Flow on a trapped particle inside the optical tweezers can push a particle away from the trap center (Fig. 4.2). At low Reynolds number [31, 32], inertial effects are neglected while the viscous effects are predominant [33].

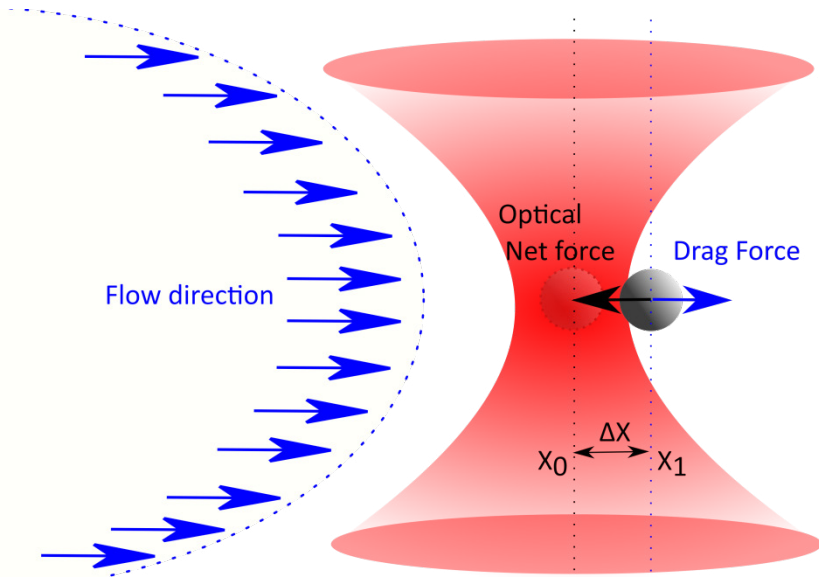


Figure 4.2: Trapped particle displaced using a drag force. The drag force is in equilibrium with the optical net force resulting on a displacement (ΔX) from the center of the trap (X_0) to position (X_1). The drag force is linearly affected by the flow rate and particle radius. Higher flow rates will result on stronger drag forces and thus larger displacements.

Therefore, the drag force acting on a particle can be calculated using Stokes law:

$$F_d = 6\pi\eta Rv \quad (1)$$

where the drag force (F_d) pushes the microparticle outside of the equilibrium region of the trap. The dynamic viscosity and flow velocity are represented by η and v respectively. The radius of the particle is represented as R .

The drag force method is performed at least $10 \mu\text{m}$ above the surface to avoid surface effects. This method is performed in the region of the trap where the optical net force behaves linearly. Excessive drag force can result in the expelling of the microparticle outside of the trap. The optical tweezers stiffness is determined from the slope of the drag force vs microparticle displacement.

4.1.2.2 Power spectrum method

Thermal energy is continuously making water molecules to bump onto a trapped particle inside the optical tweezers, resulting in picometer displacements of the particle [30]. Correlating the relative fluctuations in displacement and thermal energy, it is possible to determine the optical tweezers stiffness [34]. Considering the response of the detector linear to β it is possible to suppose $\beta = x(t)/V(t)$. Where x is the particle displacement and V the response of the sensor in volts, both in function of time (t). The power spectrum in volts of these fluctuations can be expressed as:

$$S_V(f) = \frac{1}{\beta^2} \frac{K_B T}{\gamma \pi^2 (f_c^2 + f^2)} \quad (2)$$

where K_B is the Boltzmann constant, T is temperature, γ is equal to

$$\gamma = 6\pi\eta R \quad (3)$$

where η is the viscous coefficient of the medium, R the radius of the particle and f_c is known as the corner frequency. The stiffness parameter is calculated by:

$$k = 2\pi\gamma f_c \quad (4)$$

The experimental frequency can be accurately obtained with a least-square fitting of the power spectrum as observed in (Fig. 4.3).

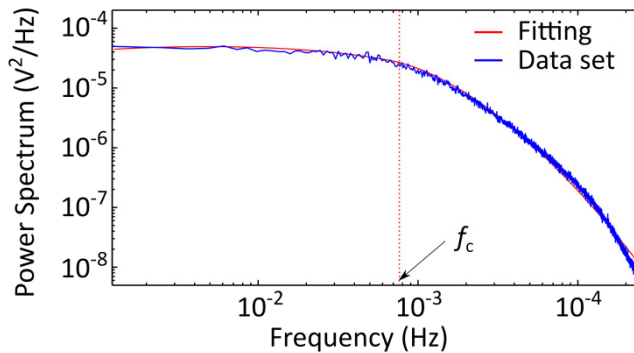


Figure 4.3: Power spectrum of fluctuations of a microparticle within an optical tweezers. A polystyrene particle (1 μm in diameter) is held within an optical tweezers at room temperature. At low frequencies ($f \ll f_c$), the power spectrum is steady, while at high frequencies, it decays. The corner frequency lies at the intersection of these two tendencies (red dash line).

4.1.2.3 Equipartition theorem method

The thermal fluctuations of the trapped bead can give insights into the attraction potential induced by the net optical force. In equilibrium conditions, we can use the average kinetic fluctuations of the particle to calculate the stiffness of the optical tweezers. The equipartition theorem relates the temperature of a system to its average energy and states that particles in thermal equilibrium have the same average energy in every degree of freedom.

The position of a trapped bead during a time interval (Fig. 4.4a) follows a Gaussian distribution centered at the position where the laser beam has the highest intensity (Fig. 4.4b). Considering that the system behaves as a harmonic oscillator, the probability density can be expressed as a Gaussian function such as:

$$p(x, y) = C e^{\frac{-k_x}{2K_B T} (x-x_0)^2} e^{\frac{-k_y}{2K_B T} (y-y_0)^2} \quad (5)$$

where K_B is Boltzmann constant, C is a normalization constant, T temperature, k_x and k_y are the optical tweezers stiffness along the x- and y-axes, and x_0 and y_0 are the hypothetical center of the potential.

The optical trap stiffness can be expressed as:

$$k_x = \frac{K_B T}{\sigma_x^2} \quad (6)$$

where σ_x is the standard deviation of the bead position inside the trap.

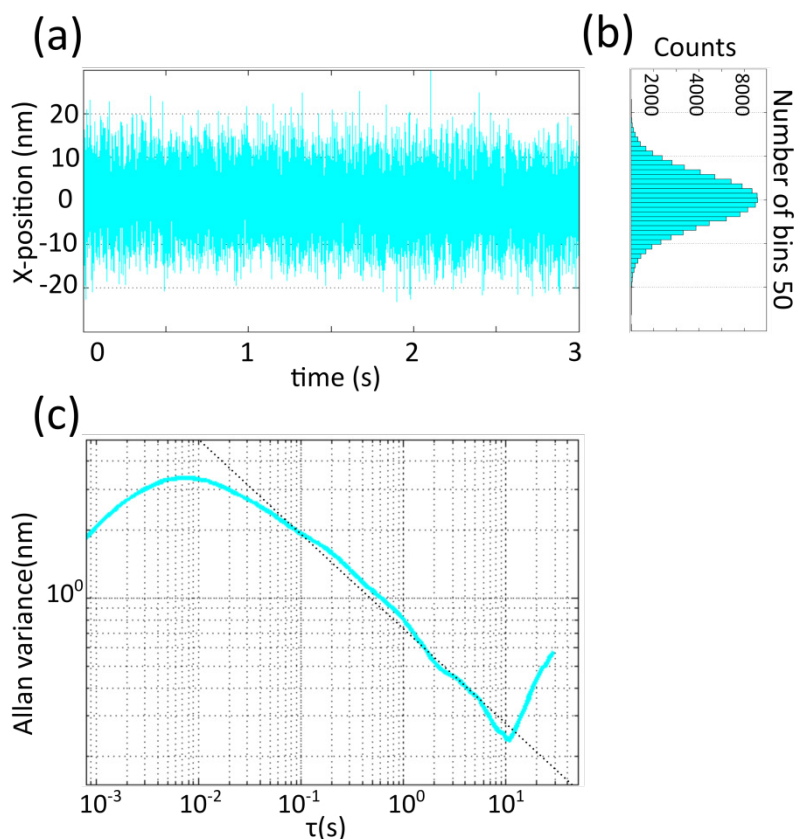


Figure 4.4: Fluctuation analysis of a trapped bead inside an optical tweezers. (a) Time series analysis of a polystyrene particle of $1\ \mu\text{m}$. (b) Histogram of the time series for the same particle showing a Gaussian distribution. (c) Graph of Allan variances analysis of the thermal fluctuation of the bead, dash line denotes the thermal limit.

This is a rapid and straightforward method to determine the stiffness. But it is sensitive to external mechanical fluctuations and stochastic noise.

Classical variance does not converge for stochastic fluctuations which are frequency independent. For example position changes due to a drift are hidden in the fluctuation signal. Optical tweezers are under the influence of different sources of noise, such as electromagnetic noise, mechanical vibrations and even changes in room pressure or temperature. Allan variance is a method that allows characterizing that kind of noise

in such systems. The Allan Variance method is used in molecular measurements to determine to which extent this noise has an influence, even at low frequencies [35, 36]. This is calculated as half the averaged squared mean of the interval neighboring data set (Fig. 4.4c), defined as:

$$\sigma_x^2(\tau) = \frac{1}{2} \left\langle (x_{i+1} - x_i)^2 \right\rangle_{\tau} \quad (7)$$

where τ is the interval of time that determines the amount of elements to be analyzed; x_i is the mean over that interval.

4.2 Material and methods

4.2.1 Microfluidic device description, fabrication and surface functionalization

Parallel microchannels connected by a 85 μm -wide and 100 μm -high aperture are etched on a SU-8 2075 photoresist layer using conventional lithography [37]. Polydimethylsiloxane (PDMS) negative replica is made by curing PDMS onto the SU-8 patterns, and using it as master for a UV soft polymer NOA81 [38].

Liquid NOA81 is poured onto the PDMS replica, and covered with a pre-cleaned microscope glass slide. The NOA81 layer thickness is controlled with thin metal spacers between the glass slide and the PDMS. NOA81 is cured by a 3-min UV exposition at a wavelength of 365 nm, with 36 W of power (Promed UVL-36 with four UV-9W-L bulbs). The PDMS negative replica is then removed from the NOA81 microchannels. Holes are made for inlets/outlets with a sand blaster and the channels are washed with ethanol. To close the microchannels, a clean glass cover slide is coated with a partially cured NOA81 layer. This is done by spin-coating a thin layer of NOA81 during 5 s at 500 rpm followed by 20 s at 4000 rpm (Spin150i POLOS) and partially curing by UV exposition during 30 s. The partially cured NOA81 layer is used as glue to bound the cured NOA81, thus closing the channels. To permanently seal the two layers of NOA81, the device is subject to a final UV exposition during 8 min, followed by heating at 80°C during 12 h. To reduce the surface hydrophilicity of the device, the hydroxyl groups present on the NOA81 are functionalized with tri-chloro(1H,1H,2H,2H-perfluorooctyl) silane (PFOTS, Sigma-Aldrich). For this silanization treatment, a 1.5 % V/V PFOTS solution in isooctane is injected inside clean microchannels and incubated for 15 min. NOA81 microchannels are cleaned after and before silanization by rinsing the channels with ethanol, followed by flowing nitrogen, and drying at 80°C on a hot plate.

4.2.2 Lipid membrane formation

Lipids (1,2-dioleoyl-sn-glycero-3-phosphocholine (DOPC), 1,2-dipalmitoyl-sn-glycero-3-phosphocholine (DPPC), N-(Fluorescein-5-thiocarbonyl)-1,2-dihexadecyl-sn-glycero-3-phosphoethanolamine (Fluor-DHPE), and 1,2-dipalmitoyl-sn-glycero-3-phosphoethanolamine-n-(cap biotinyl) (Biotinyl Cap PE)) were purchased from Avanti lipids in chloroform and used without further purification. Free standing membranes are formed in the inside of the microfluidic devices flowing first an organic phase, followed by an aqueous phase, with the use of a pressure control device, (Fluigent MFCS-EZ). Two different procedures are used to prepare the planar lipid membranes. In both a mixture of DOPC/DPPC 2:1 molar ratio was used. In method 1, the organic phase consists of $\sim 5 \mu\text{l}$ of a mixture of decane, chloroform and methanol in a 7:2:1 (v/v) ratio, and the aqueous phase contains 9 mg/ml of DOPC:DPPC at 2:1 molar ratio in 10 mM HEPES 150 mM KCl pH 7.4. In method 2, the organic phase consists of $\sim 2 \mu\text{l}$ of 37.5 mg/ml of DOPC:DPPC in chloroform at a 2:1 molar ratio and the aqueous phase contains 10 mM HEPES 150 mM KCl pH 7.4. A pressure of 2 mbar is used to flow the organic and the aqueous phases.

4.2.3 Lipid membrane visualization

For visualization of lipid bilayer in the aperture with confocal microscopy, 0.15 mg/ml Fluor-DHPE is added to initial mixture of DOPC/DPPC lipids solution. Imaging of the free standing lipid bilayer is performed by confocal microscopy (Nikon A1R confocal with 60x Plan Apo IR water immersion objective, 488nm laser, GaAsP detector and detection filter 525/50).

4.2.4 Capacitance measurements

Total capacitance (C_T) is monitored with Ag/AgCl electrodes, during the bilayer formation using a 200 Hz triangular signal at 100 mV peak to peak with a waveform generator (BK precision 4040A 20 MHz). A DLPCA 200 (Femto) is used as amplifier and current-potential convertor. After a low-pass filter with a cut-off frequency of 8 kHz, the acquisition is done by one channel of a DAQ USB-6009 (National Instrument) at a 20 kHz rate. A second channel of the DAQ is connected to the waveform generator to determine precisely the period ($2 \cdot dt$) and the amplitude (dV) of the input signal. The capacitance computing is done with a homemade LabView script using the model: $C_T = I \cdot dt / dV$. Constant intrinsic capacitance of the flow cell (C_0) is measured before the formation of the bilayer membrane. This capacitance, C_0 , is subtracted from the total capacitance (C_T) to obtain the membrane capacitance (C_M): $C_M = C_T - C_0$.

4.2.5 Optical tweezers experiments

A dual optical tweezer system is built around an inverted microscope (Eclipse Ti-U, Nikon) using a 1064 nm trapping laser (YLR-10-LP-Y12, IPG Laser) and a 830 nm detection laser (LDT-830-30GC, TOPAG) (Fig. 4.5). Both laser beams are split in two using polarizing beam splitters and focused in the sample with a 60X 1.2NA water-immersion objective (Nikon). An acousto-optic deflector (IntraAction) is used to steer one laser trap and a mirror mounted on a piezo holder (Newport) is used for the other trap. Fine positioning of the microscope stage is done with a piezo stage (NANO-LPS100, Mad City Labs). In all experiments, streptavidin-coated polystyrene beads with a diameter of 1 μm (Kisker biotech) are used. Calibration is performed for every bead before the contact with the membrane. Stiffness determination of the optical tweezers is done by the equipartition method. All measurements are performed at height of 40 μm from the bottom of the flowcell to avoid wall effects.

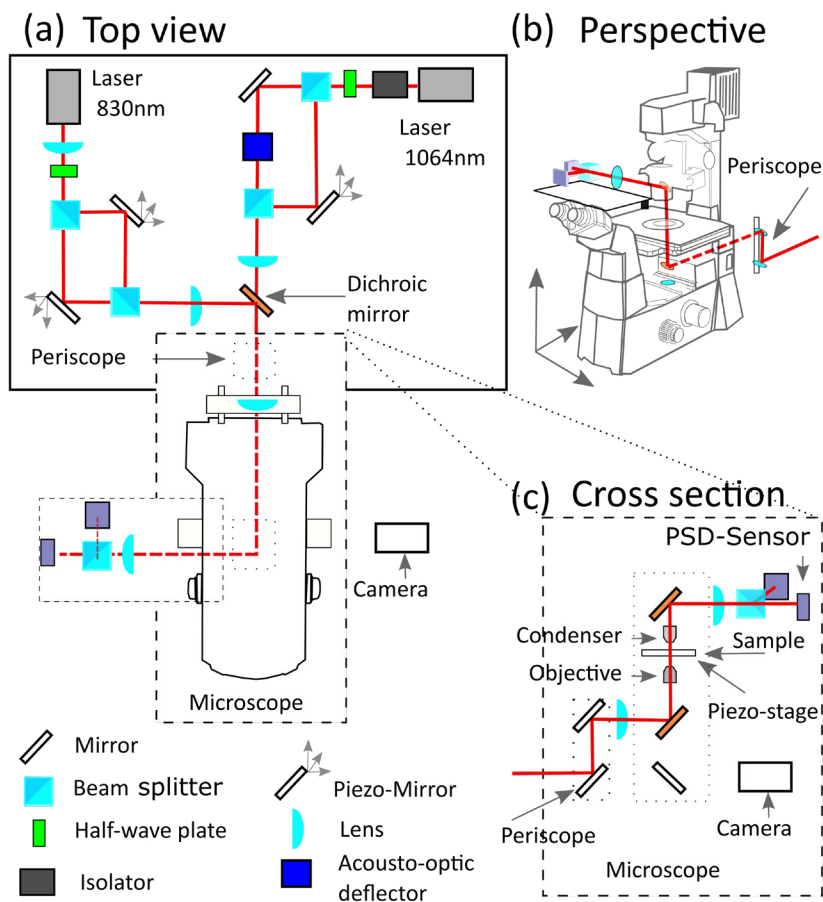


Figure 4.5: Diagram of dual optical tweezers. (a) The optical tweezers is built around an inverted optical microscope. Two lasers of different wavelength are used for trapping (1064 nm infrared) and detection (830 nm infrared). Each laser trap is split in two linear polarizations with a cube beam splitter. Polarization “P” of laser trap is controlled with Acousto-Optic Deflector (AOD) while the other polarization “S” is controlled with a mirror on a piezo electric mount (piezo-mirror). Both polarizations are combined with a cube beam splitter, similar approach is made on laser detection path however position control for each polarization is controlled with piezo-mirrors. Beam expansion is carried out with a set of two lenses right after each beam splitter and before the microscope back opening. (b) Both laser paths are combined on a single path with a dichroic mirror and raised up with a set of mirrors (periscope) to reach the microscope back opening. The final laser path crosses the objective, sample and condenser. (c) The condenser tube contains a dichroic lens to reflect the laser beams towards a Position Sensitive Detector (PSD-Sensor), with the trapping laser beam being blocked with a lens filter. 3D manipulation of the sample is possible with the stage micromanipulators and a piezo-stage.

Bead position is monitored with back focal plane interferometry, which consists of collecting light from the detection laser (after the sample) and projecting the beam path onto a position sensitive detector (PSD, DL100-7-PCBA3, First Sensor) as shown in Figure 4.6 [39]. The PSD collects the incident beam and changes it into an analog electric signal to further be transformed into a digital signal for analysis. Moving the particle across the beam along a certain direction changes the beam profile projected on the PSD, resulting in changes in the electrical signal, which can be used to calculate the displacement of the particle. This means that the relative distance between the particle and the center of the laser beam can be determined via changes in the intensity profile.

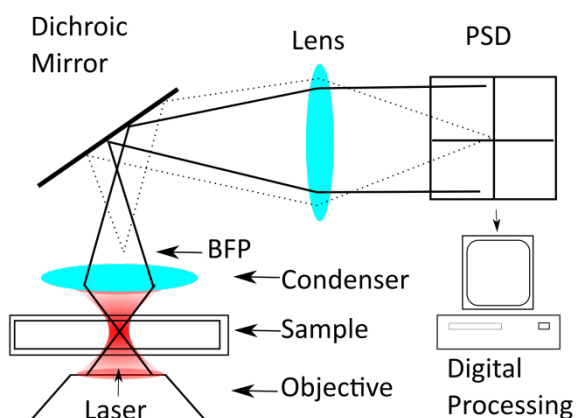


Figure 4.6: Setup for displacement detection using BFP. Light is collected with an optical condenser and a dichroic mirror directs the light path towards a lens to adjust an almost collimated image onto a PSD. Analog signals are turned into digital for further processing of bead displacement inside the optical tweezers [39].

4.3 Results and discussion

The lipid membranes are formed in a microfluidic device following a simple, low-cost and reproducible method. We find that the photopolymerised thiolene resin Norland Optical Adhesive 81 (NOA81) is a favoured flow cell material to form stable free standing lipid bilayers into microfluidic devices. In a first approach, lipid membranes are formed by subsequently flowing an organic solvent (a mixture of decane, chloroform and methanol) [40, 41] and an aqueous solution containing lipids (DOPC:DPPC), into

two parallel microchannels connected by one or several rectangular apertures ($100\ \mu\text{m} \times 85\ \mu\text{m}$), as shown in chapter 3. The membranes are formed by the contact of two lipid monolayers at the water-solvent interface over the aperture(s) that connect(s) the two channels. These flow cells can be washed and used multiple times to form membranes. In such made membranes, the annulus is easily observable with bright-field and fluorescence microscopy (Figure 4.7a) at the edges of lipid membrane. Here, as opposed to GUVs, both sides of the membrane are readily accessible and conditions can be changed in real-time. However, we find that optical trapping is impossible in the vicinity of these membranes. An important decay in stiffness of the optical tweezers is measured when the trap approaches the membrane (Fig. 4.8c, in cyan). The optically trapped bead is brought as close as possible to the membrane. While stiffness values remain constant (at $\sim 0.8\ \text{pN/nm}$) for bead-membrane distances above $50\ \mu\text{m}$, it is not possible to stably trap a particle at a distance shorter than $18\ \mu\text{m}$ from the lipid bilayer. It is also observed difficulty in optical visualization close to these membranes (Figure 4.8a).

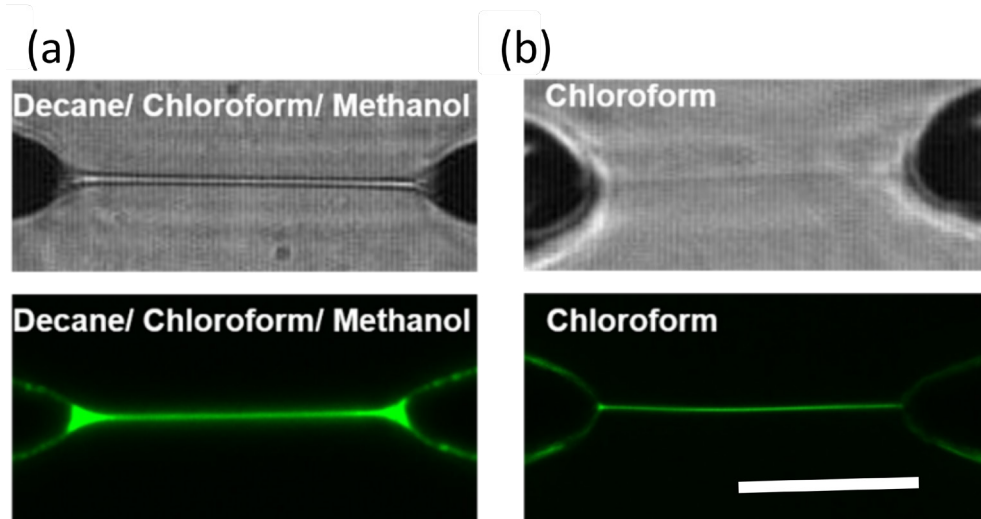


Figure 4.7: Microscope imaging of the lipid membrane and the annulus. Bright field (top) and confocal fluorescence optical microscopy (bottom) images of lipid membranes formed using (a) a mixture of decane/chloroform/methanol as organic phase, or (b) only chloroform as organic phase. Scale bar $50\ \mu\text{m}$

Interestingly, the size of the annulus can be dramatically reduced by simply using chloroform as organic solvent. In the DOPC:DPPC membranes formed using only chloroform as organic solvent, no apparent annulus is observed (Figure 4.7b). The negligible size of the annulus is likely due to chloroform penetrating into NOA81 [42], which is also consistent with the slight swelling of the walls of the microdevice that we observe (Figure 4.7b). Remarkably, the trap stiffness remains relatively constant for beads trapped at distances of 1 μm to 200 μm from the lipid bilayer (Fig. 4.8c), in magenta). The same observation is made with different laser powers, where there is no significant change in trap stiffness close to the bilayer (Fig. 4.9).

These observations confirm that a considerably smaller annulus improves trapping stiffness in the vicinity of the membrane, likely because of a reduction in the optical aberrations [43] affecting the profile of the trapping laser beam. This is consistent with the optical appearance of the beads as they approach the membranes (Fig. 4.8a-b). An additional advantage is the nearly complete removal of biologically incompatible solvent from the system.

While it was almost impossible to observe residues of solvent with confocal microscopy when chloroform alone is used, large variations in annulus size were observed when a mixture of chloroform, decane and methanol is used.

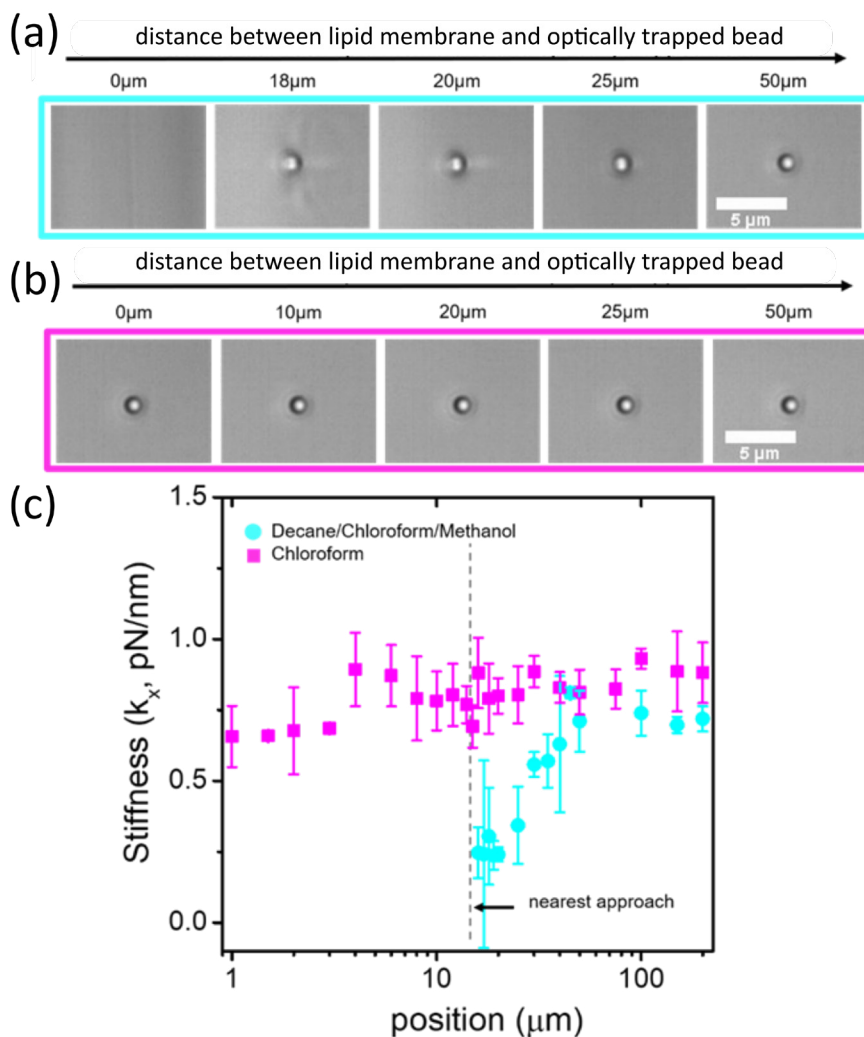


Figure 4.8: Effect of the annulus on optical imaging and on optical trap stiffness. (a) Pictures of trapped bead near a membrane prepared using the decane/chloroform/methanol mixture. (b) Pictures of trapped bead near a membrane prepared with chloroform. The distances between the bead and the membrane are indicated on top of the pictures. (c) Optical trap stiffness as a function of the trap position with respect to the membrane. Trap stiffness measurements are all done with a laser power of 1.3 W (measured before entering microscope objective) near the membranes formed using decane/chloroform/methanol (cyan) and chloroform (magenta). These measurements are done using a total of 94 beads and 7 membranes, and the bars represent the standard deviation between measurements.

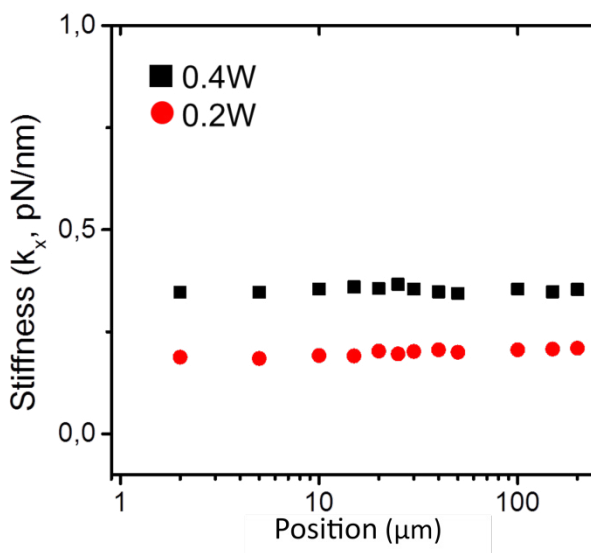


Figure 4.9. Optical trap stiffness as a function of the trap position with respect to the membrane. Trap stiffness measurements are all done with a laser power of 0.2 W and 0.4W , as measured before entering microscope objective), near the membranes formed using only chloroform. These measurements are all done with a same bead and a same membrane.

Capacitance measurements are done to further compare the size of the annulus in both kinds of membranes and to follow the kinetics of membrane formation. A lipid bilayer spanning over a larger area will have a higher capacitance, if it has a same composition and thickness. The DOPC:DPPC membranes with the large annulus (formed with the solvent mixture) show a wide variation in capacitance values, varying between $C_M \sim 20\text{pF}$ and $C_M \sim 50\text{pF}$ between different membranes (Fig. 4.10, in black). The broad variation in measured capacitance is in agreement with the wide variation of annulus sizes observed with bright field microscopy. Most of these membranes form in more than 1 minute and show also large fluctuations of

capacitance values in time, suggesting that the size of the lipid bilayer fluctuates in time. In comparison, the DOPC:DPPC membranes with the small annulus (formed with simply chloroform) have an average steady capacitance value of $C_M = 49.2$ pF, with a standard deviation of 2.4 pF (Fig. 4.10, in blue).

The larger capacitance results from of the larger membrane area, due to an annulus nearly absent, in agreement with the bright field and fluorescence observations. Membranes with a small annulus form much more quickly, within a few seconds, and a steady capacitance value is reached in 16 ± 10 seconds.

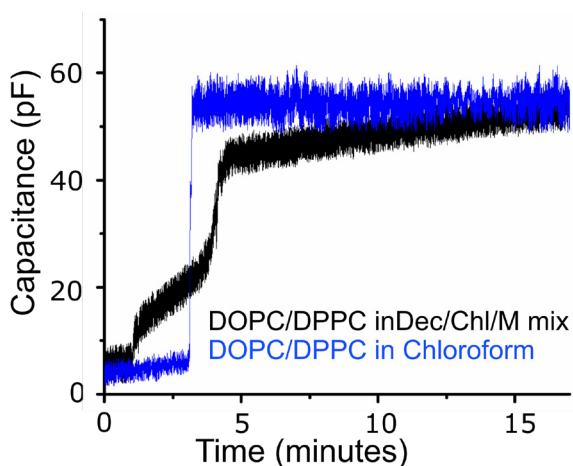


Figure 4.10: Capacitance comparison between lipid membranes with different solvent. Representative capacitance traces of DOPC/DPPC dissolved in chloroform (blue trace) and same lipid composition but dissolved in a solvent mixture of chloroform/decane/methanol (black trace). 11 and 7 experiments are performed with black and blue capacitance traces respectively.

Both types of membranes can be stable over several days when formed in flow cells with multiple apertures (Fig. 4.11 a-b).

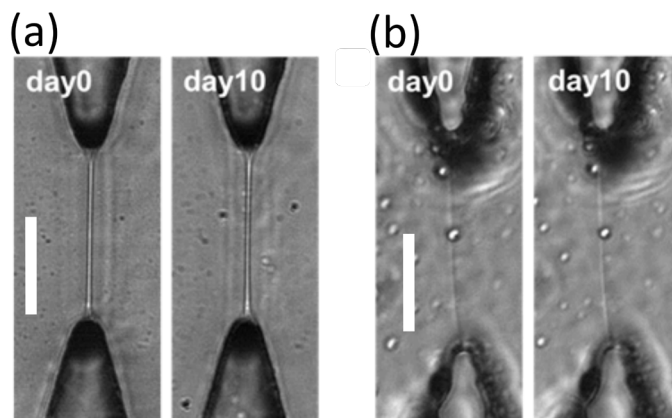


Figure 4.11. Stability of membranes. Bright-field microscopy image of membranes on the day it was formed (day 0) and 10 days later (day 10) for (a) membranes prepared with the solvent mixture, and (b) membranes prepared with chloroform. Polystyrene beads can be seen in the solution. Scale bar 50 μm .

4.4 Conclusion

In this work, we demonstrate the use of optical tweezers for the nanomanipulation of objects at the interface of free standing lipid membranes fully accessible on both sides. The lipid membranes assembled in NOA81 microfluidics devices are characterized.

An annulus is formed during the assembly of such membranes, which can be controlled with the right selection of solvent. Such annulus creates optical aberrations, which prevents optical trapping in the vicinity of the lipid bilayers. Loss of optical trapping capability is seen at distances shorter of $\sim 18 \mu\text{m}$. A significant reduction in annulus size is observed when using chloroform alone as solvent. These small annulus are difficult to visualize using bright field microscopy. A comparison of lipid membranes with large or small annulus is performed with confocal microscopy and capacitance measurements. Capacitance experiments show different dynamic formation for both membranes. Membranes using mixture of solvents show values of capacitance ranging from 20 pF to 43 pF when fully formed, in agreement with large variation in annulus size observed with confocal microscopy. Membranes with small annulus form significantly more rapidly and show a stable capacitance value of 49 pF demonstrating a larger lipid membrane area formed due to the almost absence of annulus as observed in the confocal studies. Lipid membranes with small annulus showed to be suitable for combination with optical tweezers. The stiffness of the

optical tweezer remained almost unchanged at distances as close as 1 μm to 50 μm from the membrane.

A large number of cellular processes depend on unequal conditions on each side of the membrane, such as protonmotive force dependent processes. It is therefore often critical to control each side of the lipid bilayers independently. Optical tweezers are frequently used by biophysicists for high precision 3D nanomanipulation and high resolution force measurements, but their combination with lipid bilayers readily accessible on both sides had not been yet achieved. This new approach presents the important advantage of a straightforward dynamic control over conditions on each membrane side, which is crucial to properly reproduce the cellular environment. Furthermore, as the membrane plane is perpendicular to the imaging focal plane, morphological changes in the membrane are easily visualized. Optical tweezers have considerably pushed forward the mechanistic understanding of cytoplasmic motor proteins [44]. Interfacing optical tweezers with membrane systems accessible on both leaflets enables their use for the study of *membrane associated* motor proteins, such as translocation machines that transport biopolymers across membranes [45, 46]. More generally, we expect that this approach will further our understanding of biomechanical processes at the membrane (e.g., mechanosensitivity involved in cell motility, signaling, or muscle, auditory or tactile functions).

4.5 References

1. Dufrene, Y.F., et al., *Five challenges to bringing single-molecule force spectroscopy into living cells*. Nat Meth, 2011. **8**(2): p. 123-127.
2. Shaw, A., et al., *Spatial control of membrane receptor function using ligand nanocalipers*. Nat Meth, 2014. **11**(8): p. 841-846.
3. Langton, M.J., et al., *Controlled membrane translocation provides a mechanism for signal transduction and amplification*. Nat Chem, 2017. **9**(5): p. 426-430.
4. Sheetz, M.P., *Cell control by membrane–cytoskeleton adhesion*. Nat Rev Mol Cell Biol, 2001. **2**(5): p. 392-396.
5. Wu, W., X. Shi, and C. Xu, *Regulation of T cell signalling by membrane lipids*. Nat Rev Immunol, 2016. **16**(11): p. 690-701.
6. Knorr, R.L., et al. *Membrane morphology is actively transformed by covalent binding of the protein Atg8 to PE-lipids*. PloS one, 2014. **9**, e115357 DOI: 10.1371/journal.pone.0115357.
7. Park, E. and T.A. Rapoport, *Preserving the membrane barrier for small molecules during bacterial protein translocation*. Nature, 2011. **473**(7346): p. 239-242.
8. Peetla, C., A. Stine, and V. Labhasetwar, *Biophysical Interactions with Model Lipid Membranes: Applications in Drug Discovery and Drug Delivery*. Molecular Pharmaceutics, 2009. **6**(5): p. 1264-1276.
9. Bartsch, P., et al., *Horizontal Bilayer for Electrical and Optical Recordings*. Materials, 2012. **5**(12).
10. Henriksen, J.R. and J.H. Ipsen, *Measurement of membrane elasticity by micro-pipette aspiration*. The European Physical Journal E, 2004. **14**(2): p. 149-167.
11. Poole, C. and W. Losert, *Laser Tweezer Deformation of Giant Unilamellar Vesicles*, in *Methods in Membrane Lipids*, A.M. Dopico, Editor. 2007, Humana Press: Totowa, NJ. p. 389-404.
12. Koster, G., et al., *Force Barriers for Membrane Tube Formation*. Physical Review Letters, 2005. **94**(6): p. 068101.
13. Valentino, F., et al., *Fluctuations of a membrane nanotube revealed by high-resolution force measurements*. Soft Matter, 2016. **12**(47): p. 9429-9435.

14. Sorre, B., et al., *Nature of curvature coupling of amphiphysin with membranes depends on its bound density*. Proceedings of the National Academy of Sciences, 2012. **109**(1): p. 173-178.
15. Roux, A., et al., *Membrane curvature controls dynamin polymerization*. Proceedings of the National Academy of Sciences, 2010. **107**(9): p. 4141-4146.
16. Brouwer, I., et al., *Direct quantitative detection of Doc2b-induced hemifusion in optically trapped membranes*. 2015. **6**: p. 8387.
17. Nizza, D.T. and K. Gawrisch, *A Layer Model of Ethanol Partitioning into Lipid Membranes*. General physiology and biophysics, 2009. **28**(2): p. 140-145.
18. Watanabe, R., et al., *High-throughput formation of lipid bilayer membrane arrays with an asymmetric lipid composition*. Scientific Reports, 2014. **4**: p. 7076.
19. Elliott, J.R. and D.A. Haydon, *The interaction of n-octanol with black lipid bilayer membranes*. Biochimica et biophysica acta, 1979. **557**(1): p. 259-263.
20. White, S.H., *Formation of "solvent-free" black lipid bilayer membranes from glyceryl monooleate dispersed in squalene*. Biophysical Journal, 1978. **23**(3): p. 337-347.
21. Dixit, S.S., et al., *Droplet Shape Analysis and Permeability Studies in Droplet Lipid Bilayers*. Langmuir : the ACS journal of surfaces and colloids, 2012. **28**(19): p. 7442-7451.
22. Lee, J.N., C. Park, and G.M. Whitesides, *Solvent Compatibility of Poly(dimethylsiloxane)-Based Microfluidic Devices*. Analytical Chemistry, 2003. **75**(23): p. 6544-6554.
23. Ries, R.S., et al., *Black Lipid Membranes: Visualizing the Structure, Dynamics, and Substrate Dependence of Membranes*. The Journal of Physical Chemistry B, 2004. **108**(41): p. 16040-16049.
24. Neuman, K.C. and S.M. Block, *Optical trapping*. The Review of scientific instruments, 2004. **75**(9): p. 2787-2809.
25. Wickham, S.F.J., et al., *A DNA-based molecular motor that can navigate a network of tracks*. Nat Nano, 2012. **7**(3): p. 169-173.
26. Verhey, K.J. and J.W. Hammond, *Traffic control: regulation of kinesin motors*. Nat Rev Mol Cell Biol, 2009. **10**(11): p. 765-777.

-
27. Aubin-Tam, M.-E., et al., *Single-molecule protein unfolding and translocation by an ATP-fueled proteolytic machine*. *Cell*, 2011. **145**(2): p. 257-267.
 28. Capitanio, M., et al., *Calibration of optical tweezers with differential interference contrast signals*. *Review of Scientific Instruments*, 2002. **73**(4): p. 1687-1696.
 29. Tolić-Nørrelykke, S.F., et al., *Calibration of optical tweezers with positional detection in the back focal plane*. *Review of Scientific Instruments*, 2006. **77**(10): p. 103101.
 30. Visscher, K., S.P. Gross, and S.M. Block, *Construction of multiple-beam optical traps with nanometer-resolution position sensing*. *IEEE Journal of Selected Topics in Quantum Electronics*, 1996. **2**(4): p. 1066-1076.
 31. Amini, H., et al., *Engineering fluid flow using sequenced microstructures*. 2013. **4**: p. 1826.
 32. Duncombe, T.A., A.M. Tentori, and A.E. Herr, *Microfluidics: reframing biological enquiry*. *Nat Rev Mol Cell Biol*, 2015. **16**(9): p. 554-567.
 33. Zhang, J., et al., *Fundamentals and applications of inertial microfluidics: a review*. *Lab on a Chip*, 2016. **16**(1): p. 10-34.
 34. Berg-Sørensen, K. and H. Flyvbjerg, *Power spectrum analysis for optical tweezers*. *Review of Scientific Instruments*, 2004. **75**(3): p. 594-612.
 35. Czerwinski, F., A.C. Richardson, and L.B. Oddershede, *Quantifying Noise in Optical Tweezers by Allan Variance*. *Optics Express*, 2009. **17**(15): p. 13255-13269.
 36. Lansdorp, B.M. and O.A. Saleh, *Power spectrum and Allan variance methods for calibrating single-molecule video-tracking instruments*. *The Review of Scientific Instruments*, 2012. **83**(2): p. 025115.
 37. Qin, D., Y. Xia, and G.M. Whitesides, *Soft lithography for micro- and nanoscale patterning*. *Nat. Protocols*, 2010. **5**(3): p. 491-502.
 38. Sollier, E., et al., *Rapid prototyping polymers for microfluidic devices and high pressure injections*. *Lab on a Chip*, 2011. **11**(22): p. 3752-3765.
 39. Gittes, F. and C.F. Schmidt, *Interference model for back-focal-plane displacement detection in optical tweezers*. *Optics Letters*, 1998. **23**(1): p. 7-9.
 40. Marin, V., et al., *Stable free-standing lipid bilayer membranes in Norland*

-
- Optical Adhesive 81 microchannels*. Anal. Chem., 2016. **88**(15): p. 7466-7470.
41. Wodzinska, K., A. Blicher, and T. Heimburg, *The thermodynamics of lipid ion channel formation in the absence and presence of anesthetics. BLM experiments and simulations*. Soft Matter, 2009. **5**(17): p. 3319-3330.
 42. Sheppard, G., et al., *Thiolene-based microfluidic flow cells for surface plasmon resonance imaging*. Biomicrofluidics, 2011. **5**(2): p. 026501.
 43. Berestovsky, G.N., et al., *Voltage-induced reflectivity relaxation of bilayer lipid membranes: On changes of bilayer thickness*. J. Membr. Biol., 1978. **43**: p. 107-126.
 44. Spudich, J.A., et al., *Optical traps to study properties of molecular motors*. Cold Spring Harb Protoc., 2011: p. 1305-1318.
 45. Tomkiewicz, D., N. Nouwen, and A.J.M. Driessen, *Pushing, pulling and trapping - Modes of motor protein supported protein translocation*. FEBS Lett., 2007. **181**(15): p. 2820-2828.
 46. Burton, B. and D. Dubnau, *Membrane-associated DNA transport machines*. Cold Spring Harb Perspect Biol., 2010. **2**(7): p. a000406.

Chapter 5

Lipid nanotube formation on planar lipid membranes

Lipid nanotubes are cylindrical cellular structures, which are thought to play a role for the communication and transport between organelles and cells. The use of artificial lipid membranes in controlled conditions facilitates the study of lipid nanotubes. This chapter introduces an application of the free standing lipid bilayers interfaced with optical tweezers: studying the formation of lipid nanotubes from planar membranes. Several lipid nanotubes can be simultaneously pushed or pulled from the membrane, and their dynamics can be studied with force spectroscopy. This method open possibilities for a wide range of application, for example for studying the networks of lipid tubes found in cell organelles.

5.1. Introduction

Cell lipid membranes are the host of several vital processes involving mechanical forces [1, 2]. For instance, membrane-associated motor proteins drive molecular motion leading to a variety of biomechanical processes such as lipid nanotube formation [3], endocytosis [4] or protein translocation [5]. To fully understand the fundamental mechanisms driving such biomechanical processes, it is often necessary to tune physical and chemical parameters in an *in vitro* reconstituted system. *In vitro* membrane systems (e.g., supported lipid bilayers, black lipid membranes, lipid vesicles) are simplified cell membrane mimics that minimize the complexity, while enabling control over physicochemical conditions, and study specific phenomena.

Mechanical properties of lipid membranes enable them to adopt a conformation similar to cylindrical hollow structures, called lipid nanotubes or nanotubules. The observations of such structures being formed *in vivo* have puzzled biologists for a long time [6]. Their first pictures from electron microscopy suggested an intrinsic intercommunication function between organelles compartments. Since then, membrane tubules have attracted a great interest, mainly due to their structural importance in different cellular organelles such as the endoplasmic reticulum [3, 7], the mitochondria [8] and Golgi apparatus [9, 10], but also, for their role in inter- and intracellular exchanges and cellular transport [9].

Lipids nanotubes are formed by the application of an external force or by spontaneous curvature on lipid membranes [11]. *In vivo*, lipid tubes formation is induced by proteins like cytoskeleton motors or via cytoskeleton polymerization [12]. Simplified systems like model lipid membranes with known lipid composition and controlled conditions can give a better understanding of the physics of tube formation. In *in vitro* studies, forces are usually applied with an external device. Common approaches include optical tweezers [13-17] or micropipette manipulation [18] combined with GUVs.

Interfacing optical tweezers with free standing lipid membranes formed in a microfluidic device, as described in chapter 4, presents several advantages, such as straightforward modification of the composition or surface area of the membrane, dynamic control and monitoring over conditions on both sides of the membrane, and ease in performing electrophysiological measurements. To observe morphological changes in the lipid membrane (e.g., lipid tube formation), it is advantageous for the lipid bilayer plane to be parallel to the trapping laser beam and perpendicular to the microscope focal plane.

5.1.1 Lipid nanotubes in cells

Communication among cells can be mediated by the release of chemical compounds, for example in synaptic clefts and gap junctions. Communication can also be mediated with lipid connecting bridges. Essentially these mechanical connections are lipid tubes that transport water, ions [19] and even bigger molecules, like viruses that can travel

through these tubular structures [9, 20]. The formation of lipid tubes *in vivo*, which have diameters from 50 nm to 200 nm, are attributed to spontaneous curvature and forces induced on lipid membranes. Forces generated by microtubules and proteins are responsible (Fig. 5.1a) for the deformation of lipid membranes and the formation of lipid nanotubes. The Golgi apparatus contains lipid nanotubes, which are thought to play an important role in intracellular trafficking. These nanotubes grow together with the cytoskeleton. In addition, molecular motors were shown to generate pulling forces that can result in lipid nanotubes formation (Fig. 5.1b).

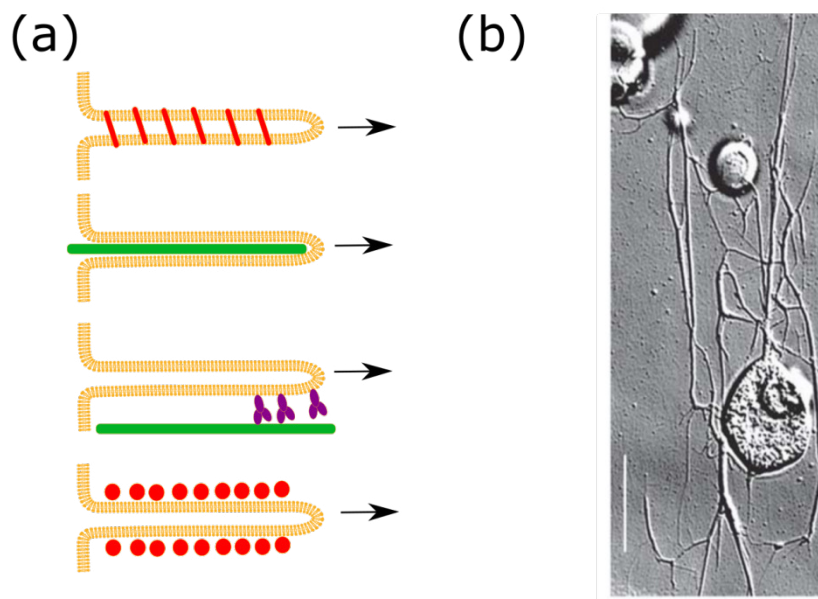


Figure 5.1: Lipid nanotubes formation in cells. (a) Different mechanisms to form lipid nanotubes in cells. From top to bottom: Polymerization of scaffold proteins, showed with red lines, coil around the membranes to induce an elongation of the membrane. Cytoskeleton polymerization, showed as long green tube, can push and deform the membrane. The cytoskeleton can also act as a rail for motor proteins like kinesin (purple figures) that pull the tube. Proteins on the membrane (red circles) can induce spontaneous curvature triggering membrane protrusions. (b) Membrane lipid tubes pulled from a giant liposome along microtubules by the action of kinesins. Image taken using Differential interference contrast (DIC). Scale bar 10 μm . Figure adapted from [21].

5.1.2 Lipid nanotube formation triggered by an external force

Force measurements during tube formation can be achieved with different methodologies. Such methods generally consist of applying an external force to the membrane of cells or to model lipid membranes. The drag force produced inside a microchannel

can trigger the formation of lipid nanotubes [22]. This method consists of applying a high speed shear flow to a lipid reservoir acting as a hydrodynamic tweezers for pulling lipid nanotubes (Fig. 5.2a). However this method is not well-controlled, because the flow is pulling the lipid nanotube with poor control over the length of the lipid nanotube.

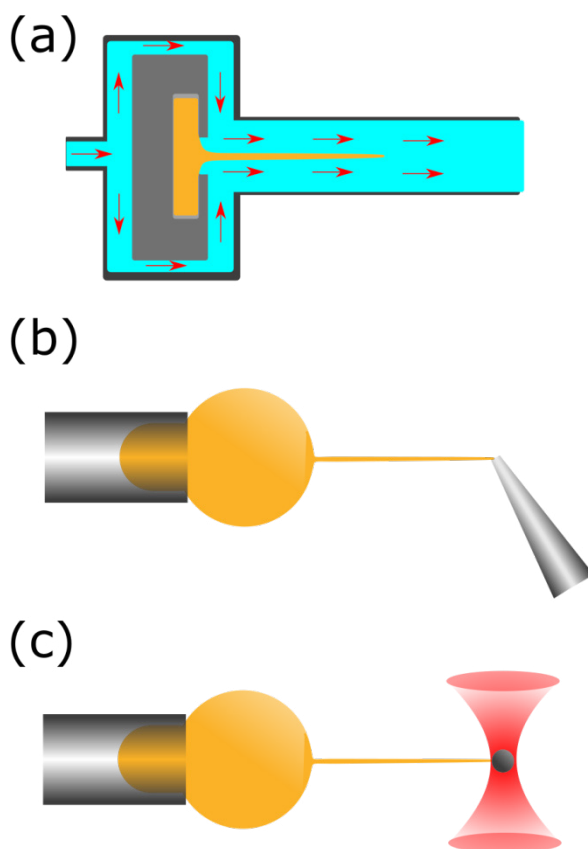


Figure 5.2: Formation of lipid nanotubes in vitro systems. (a) Schematics of microfluidic device for the formation of a lipid nanotube from a reservoir of lipid and solvent. The pulling force is generated by applying drag force from a continuous surrounding flow. (b) Manipulation and formation of lipid nanotubes is also achieved with micropipettes [19, 23]. (c) A lipid tube is formed by pulling an optically trapped bead from a lipid vesicle held by pipette aspiration [14, 24]. This method allows the formation, manipulation and force characterization, all at the same time. By knowing the displacement of the microparticle from the center of the laser beam, it is possible to determine the force required to form a lipid nanotube.

The most common model membranes used for the study lipid nanotubes are GUVs [19, 24-26]. Various methods have been developed to manipulate and pull lipid nanotubes from GUVs. Lipid nanotubes can be pulled with a micropipette [23] from a GUV held by a larger pipette. The micropipette sucks a tiny patch of membrane and pulls it to extend a lipid nanotube (Fig. 5.2b). This technique shows precise control in lipid nanotube length and in membrane tension (as shown in chapter 1). Another common method used by biophysicists to form lipid nanotubes is by combining optical tweezers [27, 28] with GUVs (Fig. 5.2c) [13]. This method typically uses a biotin-streptavidin interaction to attach the membrane to a dielectric particle for pulling lipid nanotubes. Likewise, inwards and outwards lipid nanotubes are accessible using this approach. This tool allows real time mechanical and dynamic measurements of lipid tubes. However, as stated in chapter 4, these approaches do not fully reproduce and do not offer control over biologically relevant conditions, because they lack dynamic control over conditions on each side of the membrane. As a large number of cellular processes depend on unequal conditions on each side of the membrane (e.g., protonmotive force dependent processes), we benefit from a strategy that enables optical tweezers nanomanipulation of lipid bilayers fully accessible from both sides.

Interfacing optical tweezers with free standing lipid membranes formed in a microfluidic device (Fig. 5.3a) presents several advantages: dynamic control and monitoring over conditions on both sides of the membrane, straightforward modification of the composition or surface area of the membrane, and ease in performing electrophysiological measurements. The control over the protein composition on each side of the membrane, as well as the gradient of pH and voltage, enables to mimic the intracellular and extracellular side of biological membranes. Observing morphological changes in the lipid membrane like lipid tube formation is facilitated by the fact that the membrane is perpendicular to the microscope focal plane (Fig. 5.3b).

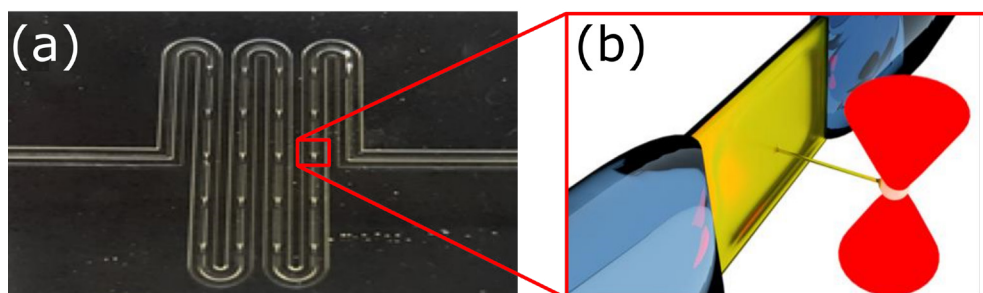


Figure 5.3: Optical tweezers at the interface with free standing lipid membrane. (a) Picture of microfluidic device. Free standing lipid bilayers are formed over the gaps connecting two microchannels. (b) Schematic representation of optical tweezers (red) integrated to free standing lipid membranes forming a lipid nanotube. The system consists of an artificial lipid bilayer (yellow) assembled on a rectangular aperture (blue) allowing free access to both sides of the membrane.

5.2 Material and Methods

5.2.1 Microfluidic device fabrication

Microfluidic devices are prepared as previously described in chapters 3 and 4 with NOA81 polymer (Norland Products). In summary, two parallel 100 μm -high rectangular microchannels are connected by 85 μm -wide and 100 μm -high apertures. Microchannel device is functionalized by flowing a solution of tri-chloro(1H,1H,2H,2H-perfluorooctyl) silane (PFOTS, Sigma-Aldrich) at a concentration of 1.5 % v/v in isooctane in the channels. After 15 minutes incubation, the microchannels are thoroughly rinsed with pure ethanol, followed by nitrogen flow, and a complete drying step at 80°C on a hot plate. After this process, PDMS perforated blocks are glued with non-polymerized PDMS to the surface coinciding with the previously formed inlets/outlets and baked for their full attachment.

5.2.2 Free standing lipid membrane formation

Lipids (1,2-dioleoyl-sn-glycero-3-phosphocholine (DOPC), 1,2-dipalmitoyl-sn-glycero-3-phosphocholine (DPPC), N-(Fluorescein-5-thiocarbonyl)-1,2-dihexadecyl-sn-glycero-3-phosphoethanolamine (Fluor-DHPE), and 1,2-dipalmitoyl-sn-glycero-3-phosphoethanolamine-n-(cap biotinyl) (Biotinyl Cap PE)) were purchased from Avanti lipids in chloroform and used without further purification. Free standing membranes are formed in the inside of the microfluidic devices flowing first an organic phase, followed by an aqueous phase, with the use of a pressure control device, (Fluigent MFCS-EZ). The organic phase consists of 37.5 mg/ml of DOPC:DPPC in chloroform at a 2:1 molar ratio and the aqueous phase contains 10mM HEPES 150mM KCl pH 7.4.

For optical tweezers experiments, of Biotinyl Cap PE is added to the organic phase to a final concentration of 0.625mg/ml. After membrane formation, a solution of 1 μm diameter streptavidin-coated polystyrene beads (Kisker biotech) in 10 mM HEPES 150 mM KCl pH 7.4 is flowed into both channels.

5.2.3 Optical tweezers experiments

A dual optical tweezer system is built around an inverted microscope (Eclipse Ti-U, Nikon) using a 1064 nm trapping laser (YLR-10-LP-Y12, IPG Laser) and a 830 nm detection laser (LDT-830-30GC, TOPAG). Both laser beams are split in two using polarizing beam splitters and focused in the sample with a 60X 1.2NA water-immersion objective (Nikon). An acousto-optic deflector (IntraAction) is used to steer one laser trap and a mirror mounted on a piezo holder (Newport) is used for the other trap. Bead position is monitored with back focal plane interferometry using position sensitive detectors (PSD, DL100-7-PCBA3, First Sensor). Fine positioning of the microscope stage is done with a piezo stage (NANO-LPS100, Mad City Labs). In all experiments, streptavidin-coated polystyrene beads with a diameter of 1 μm (Kisker

biotech) were used. Calibration is performed for every bead before the contact with the membrane. Stiffness of the optical tweezers is calculated by the equipartition method. All measurements are performed at height of 40 μm from the bottom of the flowcell to avoid wall effects.

5.2.4. Image particle tracking of retracting lipid nanotubes

Lipids nanotubes are formed by pushing microparticles across the membrane and extended for specific distances from the membrane, followed by the release of the bead trapped inside the optical tweezers. Video recordings of the particle being pulled back towards the membrane by the retracting lipid tube are taken with a sCMOS camera (PCO.edge 5.5) at 1981 frames per second. Tracking of the microparticles position is performed using TrackMate from Fiji project [29]. Coordinates for each frame-time are acquired and exported to matlab for retraction speed determination with a custom matlab script (Section 5.5.1, Appendix).

5.3 Results and discussion

The newly developed free standing lipid bilayers interfaced with optical tweezers (chapter 4) are used to form lipid membrane nanotubes. *In vitro*, they are typically formed in many studies via direct micromanipulation using an optical tweezers interfaced with a lipid vesicle. Here, because of an easy access to both sides of the membrane [31], lipid nanotubes are formed by two different ways: (1) by *pulling* a tube with a trapped streptavidin coated microparticle from a membrane containing biotinylated lipids (Fig. 5.4a), and (2) by *pushing* a trapped microparticle across the membrane (Fig. 5.4b).

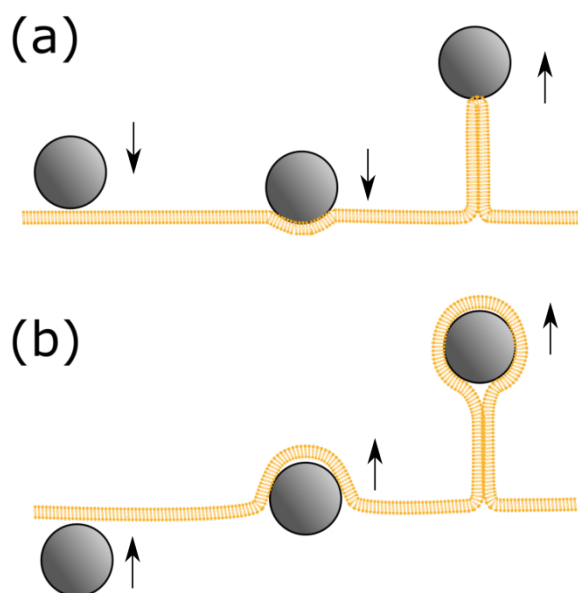


Figure 5.4: Representation of lipid nanotubes formation with two different methods. (a) Formation of lipid tube by pulling a membrane patch attached onto the surface of the microparticle. (b) Formation of lipid tube by pushing a microparticle against the lipid membrane [15]. The microparticle is first wrapped by the lipid membrane, then the microparticle is pushed further until the tube is formed.

The *pushing* approach results in nanotube formation in all attempts (Fig. 5.5a), while the *pulling* approach requires a few trials for biotin-streptavidin bonds between the free standing membrane and the bead to be created (Fig. 5.5b). When the bead is pushed across the membrane at a speed of $2 \mu\text{m/s}$ with a trap stiffness of 0.13 pN/nm , a force of $\sim 12 \text{ pN}$ is required to form the tube (Fig. 5.5c). The extension of the tube necessitates a force of $\sim 4 \text{ pN}$, which is close to values found to extend tubes pulled from vesicles [13, 30]. During force measurements, lipid nanotubes are

extended up to 15 μm .

An advantage of this method is the possibility to manipulate particles on both sides of the membrane. Through the use of multiple optical traps, networks of tubes can be created in a straightforward manner. To demonstrate this capability, two neighboring tubes are formed by the use of two optical traps and the coalescence of the tubes is observed in real-time (Figure 5.5d). Networks of lipid nanotubes with increasing complexity can be easily created. Furthermore, lipid nanotubes as long as 250 μm are formed, which corresponds to the width of the channels in the microdevice. Longer nanotubes are probably achievable with wider channels. Hypothetically, the lipid nanotube formed here can grow in length due to a source of lipid coming from the large membrane and from lipids spread onto the surface of the microchannels. Tubes pulled or pushed from a free standing lipid bilayer can be considerably longer than tubes formed from vesicles where the maximum tube length is limited by the vesicle diameter [15].

An additional advantage of this method is the possibility to create networks of tubes [31-33] in a straightforward manner, through the use of multiple optical traps [34]. For instance, several neighboring tubes can be formed by the use of several optical traps (Fig. 5.5d), their coalescence behavior can be studied, and complex networks of lipid nanotubes can be created.

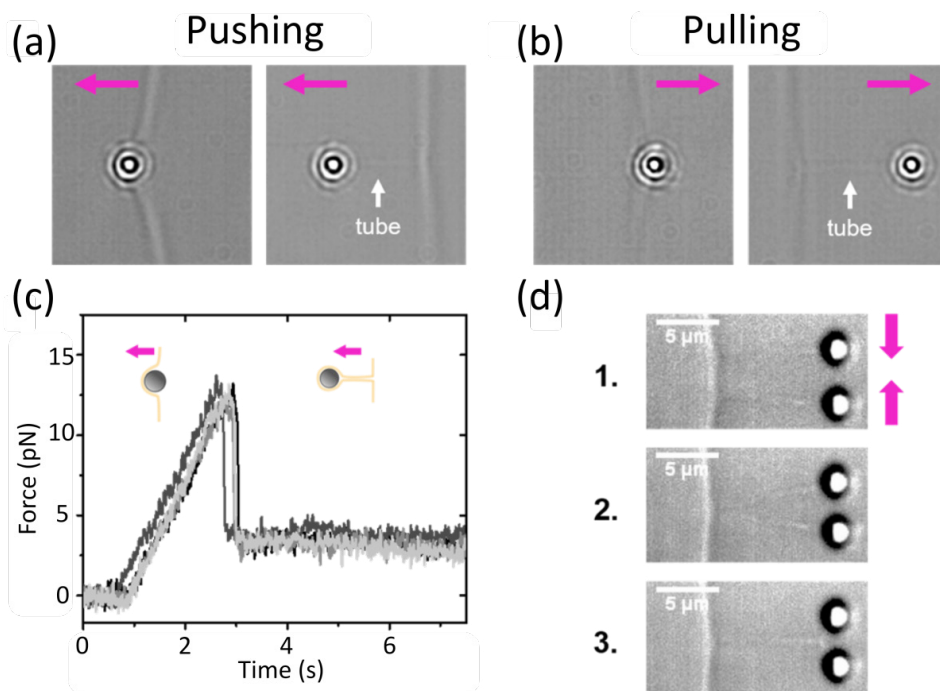


Figure 5.5: Membrane tube formation by pushing and pulling beads. Bright field images of a membrane tube formed by (a) pushing a bead across the membrane, and (b) touching the membrane with a streptavidin bead and pulling the bead away from the membrane. (c) 4 force curves during tube formation by pushing a bead across the membrane. (d) Bright-field image of two separate membrane tubes held in two optical traps (1). The traps are brought closer to one another until the tubes enter in contact (2). Coalescence of the two tubes is then observed (3).

Interestingly, every time that the particles are released from the optical tweezer, they are dragged backward towards the membrane. To elucidate the mechanism of retraction, several lipid tubes are formed with different lengths and their retraction speed is studied. The retraction speed corresponds to the speed of the particle as it is pulled towards the membrane during the retraction. The particle position is tracked and plotted vs time in order to extract the speed (Fig. 5.6a).

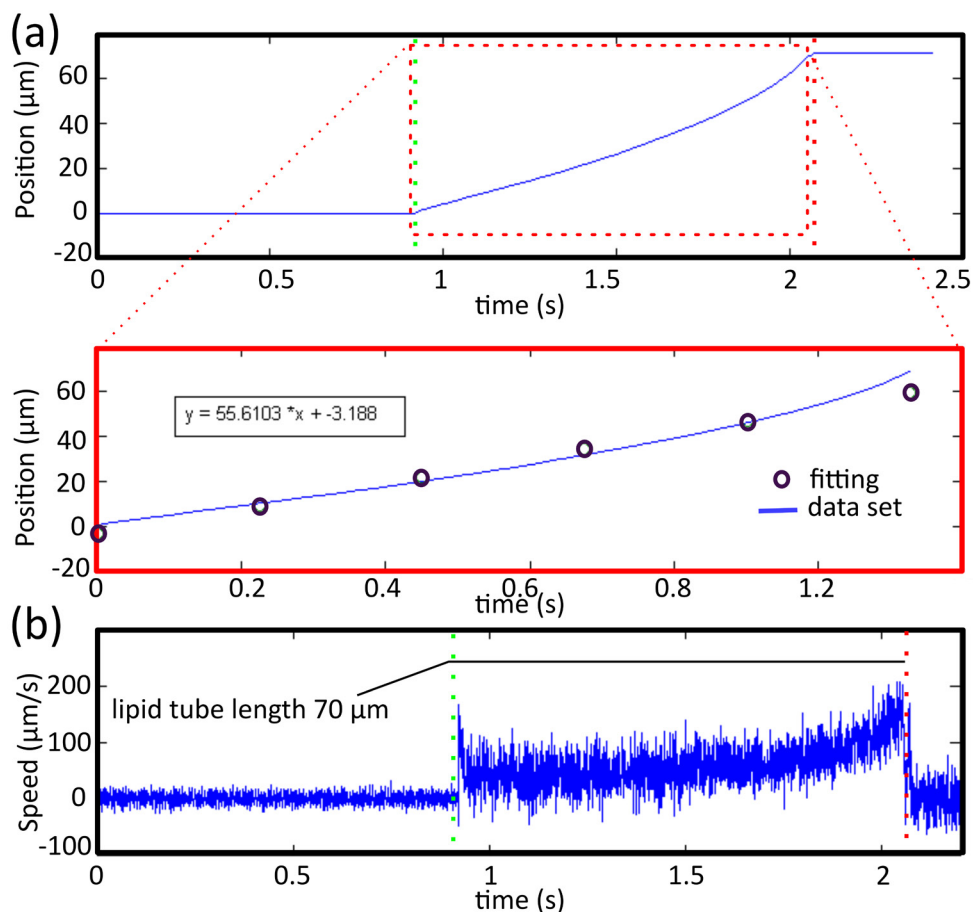


Figure 5.6: Speed particle determination. (a) Position of particle while it moves backward the membrane. Speed of the particle is extracted between the moments the particle is trapped (green dash line) until it gets to the membrane (red dash line). Linear fitting (red purple) is used to calculate the slope that interval. (b) Speed variation during retraction interval. Big part of the noise could be originated by the tracking software.

The retraction speed is determined from the slope of the interval corresponding to the instant the particle is released from the optical trap until it reaches the membrane.

A linear fit is used to determine the slope for such interval which provides insight of the overall speed for this process. However, it should be noted that at positions near to the membrane, the bead position does not change linearly anymore (Fig. 5.6b).

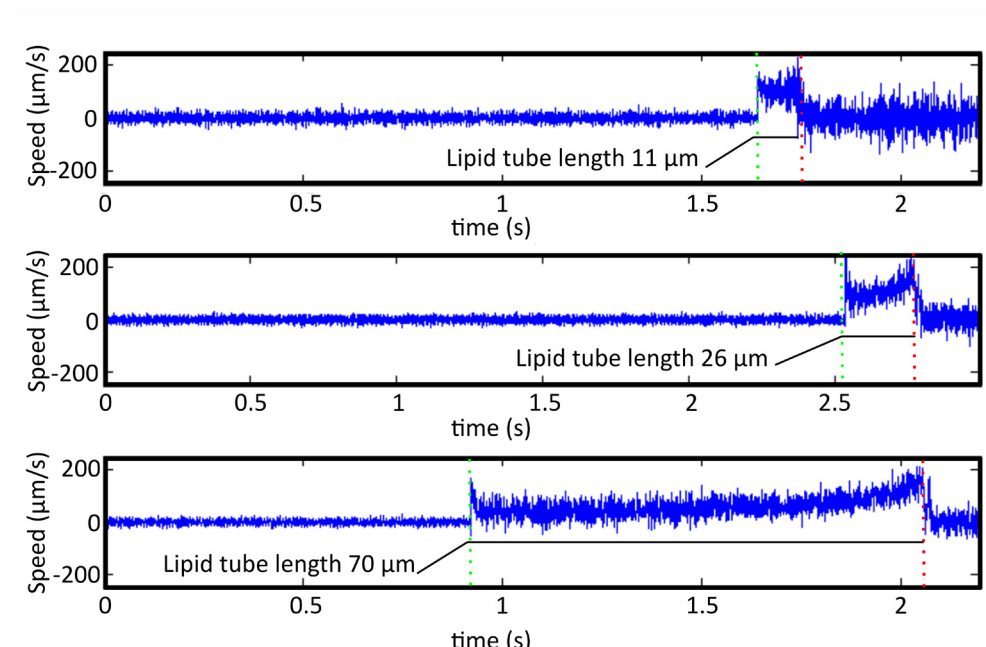


Figure 5.7: Speed variation, comparison among different tube lengths. Particle speeds increase near to the membrane (red dash line). The maximum speed near the membrane is about 180 $\mu\text{m/s}$.

As soon as the bead is released, a sudden change in speed is observed, after which the retraction speed stays mostly constant, until the bead approaches the membrane and an acceleration is observed, to reach a maximum speed of $\sim 180 \mu\text{m/s}$ (Fig. 5.7) This is also observed when comparing the speed of the process with the length of the lipid tube resulting in a decreased speed with longer lipid tubes (Fig. 5.8).

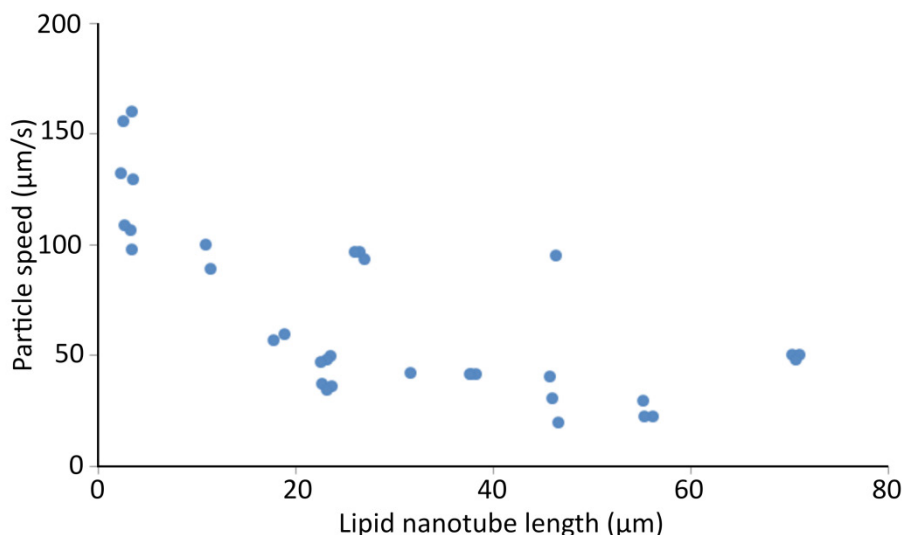


Figure 5.8: Dynamics of lipid nanotube retraction. The speed of the particles is plotted as a function of the lipid tube length. Five different lipid membranes are tested with a total of 33 different microparticles. The maximum lipid nanotube length is limited by the maximum of the area of the CMOS sensor for a suitable frame rate. The minimum length is the minimum tube length for which it is still possible to track bead displacement during retraction.

Let's first consider the force pulling the particle towards the membrane when the particle is released from the optical trap to be equal to the drag force exerted on the particle (Dp) being $Dp=6\pi R_p \eta \dot{L}(t)$, where R_p is the radius of the particle, η the viscosity of the medium and $\dot{L}(t)$ the speed of the particle over time. The drag force associated with the long lipid nanotube is neglected here.

At the highest velocity $\dot{L}(t) \sim 180 \mu\text{m/s}$, a drag force of $\sim 1.7 \text{ pN}$ is obtained. This value is smaller than the force measured to extend a lipid nanotube using the optical tweezers. This is possibly caused by the friction between the lipid monolayers as proposed previously in a similar approach using vesicles [16].

Interestingly, it is observed that the particle speeds up near the membrane. This

can be hypothetically explained with different scenarios. The fluctuations of the membrane when the lipid nanotube moves can lead to a dissipative force due to interleaflet friction [35]. The longer the lipid nanotube, the more this effect becomes important. Another factor might be due to the “pinching” of the membrane at the tube-freestanding membrane junction. In these experiments, the membranes have probably low tension due to a large lipid reservoir. For lipid nanotubes pulled from vesicles with floppy membranes (with low membrane tension), a stem or “pinching” section of the membrane have been observed at the tube-vesicle junction [36, 37]. When the bead reaches the stem junction, it would accelerate due to the larger cross-section of the pinned membrane compared to the lipid nanotube.

5.4 Conclusion

Force spectroscopy on free standing lipid membranes is carried out by combining optical tweezers with the technique developed in this thesis to assemble lipid membranes in microfluidics devices. Lipid nanotubes are formed from free standing lipid membranes. Due to the advantageous access to both sides of the membranes, lipid nanotubes are not only pulled from the membrane, but tubes are also pushed with an optically trapped bead crossing the membrane. Due to an almost unlimited pool of lipids, the tubes are extended to lengths above 200 μm , and can probably reach much longer lengths in wider microchannels. A more complex network of tubes is formed using this technique. Two particles trapped with a dual optical tweezers configuration are used to push two lipid nanotubes simultaneously from the same side of the membrane, which demonstrated the possibility to study the coalescences of such structures. The retraction speed of the tube increases as the length of the tube decreases.

This newly developed method is expected to complement tools available to quantify forces in cell biomechanical processes [38], for instance to study the mechanosensitivity associated with cell motility, auditory or tactile functions. It also opens up new possibilities for the creation and the study of artificial lipid tube networks mimicking biological structures, i.e. lipid tubes part of cell organelles [39] and lipid tubes that extend from cells for communication [6].

5.5 References

1. Dufrene, Y.F., et al., Five challenges to bringing single-molecule force spectroscopy into living cells. *Nat Meth*, 2011. 8(2): p. 123-127.
2. Yang, N.J. and M.J. Hinner, Getting Across the Cell Membrane: An Overview for Small Molecules, Peptides, and Proteins. *Methods in molecular biology* (Clifton, N.J.), 2015. 1266: p. 29-53.
3. Leduc, C., et al., Mechanism of membrane nanotube formation by molecular motors. *Biochimica et Biophysica Acta (BBA) - Biomembranes*, 2010. 1798(7): p. 1418-1426.
4. Grant, B.D. and J.G. Donaldson, Pathways and mechanisms of endocytic recycling. *Nat Rev Mol Cell Biol*, 2009. 10(9): p. 597-608.
5. Agarraberes, F.A. and J.F. Dice, Protein translocation across membranes. *Biochimica et Biophysica Acta (BBA) - Biomembranes*, 2001. 1513(1): p. 1-24.
6. Baker, M., How the Internet of cells has biologists buzzing. *Nature*, 2017. 549(7672): p. 322-324.
7. Cole, N.B. and J. Lippincottschwartz, ORGANIZATION OF ORGANELLES AND MEMBRANE TRAFFIC BY MICROTUBULES. *Current Opinion in Cell Biology*, 1995. 7(1): p. 55-64.
8. Li, T., et al., Fission yeast mitochondria are distributed by dynamic microtubules in a motor-independent manner. *Scientific Reports*, 2015. 5: p. 11023.
9. Gerdes, H.-H., N.V. Bukoreshtliev, and J.F.V. Barroso, Tunneling nanotubes: A new route for the exchange of components between animal cells. *FEBS Letters*, 2007. 581(11): p. 2194-2201.
10. Polishchuk, E.V., et al., Mechanism of constitutive export from the Golgi: Bulk flow via the formation, protrusion, and en bloc cleavage of large trans-golgi network tubular domains. *Molecular Biology of the Cell*, 2003. 14(11): p. 4470-4485.
11. Liu, Y.G., et al., Patterns of flexible nanotubes formed by liquid-ordered and liquid-disordered membranes. *ACS Nano*, 2016. 10(1): p. 463-474.
12. Raviv, U., et al., Cationic liposome–microtubule complexes: Pathways to the formation of two-state lipid–protein nanotubes with open or closed ends. *Proceedings of the National Academy of Sciences of the United States of America*, 2005. 102(32): p. 11167-11172.

-
13. Koster, G., et al., Force Barriers for Membrane Tube Formation. *Physical Review Letters*, 2005. 94(6): p. 068101.
 14. Koster, G., et al., Membrane tube formation from giant vesicles by dynamic association of motor proteins. *Proceedings of the National Academy of Sciences of the United States of America*, 2003. 100(26): p. 15583-15588.
 15. Meinel, A., et al., Induced phagocytic particle uptake into a giant unilamellar vesicle. *Soft Matter*, 2014. 10(20): p. 3667-3678.
 16. Raktim, D. and D. Rumiana, Inward and outward membrane tubes pulled from giant vesicles. *Journal of Physics D: Applied Physics*, 2014. 47(28): p. 282001.
 17. Roux, A., et al., Membrane curvature controls dynamin polymerization. *Proceedings of the National Academy of Sciences*, 2010. 107(9): p. 4141-4146.
 18. Jesorka, A., et al., Generation of phospholipid vesicle-nanotube networks and transport of molecules therein. *Nat. Protocols*, 2011. 6(6): p. 791-805.
 19. Zhang, H., et al., Artificial nanotube connections and transport of molecular cargo between mammalian cells. *Nano Communication Networks*, 2013. 4(4): p. 197-204.
 20. Davis, D.M. and S. Sowinski, Membrane nanotubes: dynamic long-distance connections between animal cells. *Nat Rev Mol Cell Biol*, 2008. 9(6): p. 431-436.
 21. Roux, A., The physics of membrane tubes: soft templates for studying cellular membranes. *Soft Matter*, 2013. 9(29): p. 6726-6736.
 22. West, J., A. Manz, and P.S. Dittrich, Lipid Nanotubule Fabrication by Microfluidic Tweezing. *Langmuir*, 2008. 24(13): p. 6754-6758.
 23. Karlsson, M., et al., Micropipet-Assisted Formation of Microscopic Networks of Unilamellar Lipid Bilayer Nanotubes and Containers. *Langmuir*, 2001. 17(22): p. 6754-6758.
 24. Roux, A., et al., Intracellular Transport. *Annals of the New York Academy of Sciences*, 2008. 1123(1): p. 119-125.
 25. Bo, L. and R.E. Waugh, Determination of bilayer membrane bending stiffness by tether formation from giant, thin-walled vesicles. *Biophysical Journal*, 1989. 55(3): p. 509-517.
 26. Shitamichi, Y., M. Ichikawa, and Y. Kimura, Mechanical properties of a giant liposome studied using optical tweezers. *Chemical Physics Letters*, 2009. 479(4-6):

p. 274-278.

27. Reiner, J.E., et al. Optical manipulation of lipid and polymer nanotubes with optical tweezers. 2004.
28. Qian, F., et al., Combining optical tweezers and patch clamp for studies of cell membrane electromechanics. *The Review of scientific instruments*, 2004. 75(9): p. 2937-2942.
29. Tinevez, J.-Y., et al., TrackMate: An open and extensible platform for single-particle tracking. *Methods*, 2017. 115: p. 80-90.
30. Derényi, I., F. Jülicher, and J. Prost, Formation and Interaction of Membrane Tubes. *Physical Review Letters*, 2002. 88(23): p. 238101.
31. Karlsson, A., et al., Molecular engineering: Networks of nanotubes and containers. *Nature*, 2001. 409(6817): p. 150-152.
32. Lobovkina, T., et al., Mechanical tweezer action by self-tightening knots in surfactant nanotubes. *Proceedings of the National Academy of Sciences of the United States of America*, 2004. 101(21): p. 7949-7953.
33. Karlsson, M., et al., Formation of geometrically complex lipid nanotube-vesicle networks of higher-order topologies. *Proceedings of the National Academy of Sciences*, 2002. 99(18): p. 11573-11578.
34. Cuvelier, D., et al., Coalescence of Membrane Tethers: Experiments, Theory, and Applications. *Biophysical Journal*, 2005. 88(4): p. 2714-2726.
35. Shi, Z. and T. Baumgart, Dynamics and instabilities of lipid bilayer membrane shapes. *Advances in Colloid and Interface Science*, 2014. 208(Supplement C): p. 76-88.
36. Rossier, O., et al., Giant Vesicles under Flows: Extrusion and Retraction of Tubes. *Langmuir*, 2003. 19(3): p. 575-584.
37. Bar-Ziv, R., E. Moses, and P. Nelson, Dynamic Excitations in Membranes Induced by Optical Tweezers. *Biophysical Journal*, 1998. 75(1): p. 294-320.
38. Roca-Cusachs, P., V. Conte, and X. Trepat, Quantifying forces in cell biology. *Nat Cell Biol*, 2017. 19(7): p. 742-751.
39. Sackmann, E., Endoplasmatic reticulum shaping by generic mechanisms and protein-induced spontaneous curvature. *Advances in Colloid and Interface Science*, 2014. 208(Supplement C): p. 153-160.

5.6 Appendix

Matlab script

```
clear
```

```
clc
```

```
points=dlmread('FileName.txt');
```

```
x=(points(:,1)-min(points(:,1)))*108.6/1000;%conversion pxl to  
nm using 108.64 nm/pxl measured by Msc DA 15/08/16
```

```
y=(points(:,2)-min(points(:,1)))*107.6/1000;%conversion pxl to  
nm using 107.64 nm/pxl measured by Msc DA 15/08/16
```

```
[m n] =size(points);%empty matrix for loop
```

```
steptime=1/1981;%Time-step for time axes, 1981 fps
```

```
time=(steptime:steptime:(steptime*m));
```

```
time=time';
```

```
for i=1:m-1
```

```
    displacementX(i)=x(i+1)-x(i);
```

```
    Speed(i)= displacementX(i)/steptime;
```

```
end
```



```
%%%%%%%%%%%%%%%%%%%%%%%%%%%%%%%%%%%%%%%%%%%%%%%%%%%%%%%%%%%%%%%%%%%%%%%%%
```

```
[w, r]=size(slope);
p = polyfit((time(1:r))',slope,1);
time2 = 0:(time(r)/5):time(r);
FitSlope=polyval(p,time2);
```

```
%%%%%%%%%%%%%%%%%%%%%%%%%%%%%%%%%%%%%%%%%%%%%%%%%%%%%%%%%%%%%%%%%%%%%%%%%
```

```
%%%%%%%%%%%%%%%%%%%%%%%%%%%%%%%%%%%%%%%%%%%%%%%%%%%%%%%%%%%%%%%%%%%%%%%%%      Plots      %%%%%%%%%%%%%%%%%%%%%%%%%%%%%%%%%%%%%%%%%%%%%%%%%%%%%%%%%%%%%%%%%%%%%%%%%%
```

```
figure
subplot (2,1,1)
plot (time(1:(m-1)),distance);title('Position vs time')
xlabel('time (sec)') % x-axis label
ylabel('position (um)') % y-axis label
```

```
%%%%%%%%%%%%%%%%%%%%%%%%%%%%%%%%%%%%%%%%%%%%%%%%%%%%%%%%%%%%%%%%%%%%%%%%%
```

```
%%%%%%%%%%%%%%%%%%%%%%%%%%%%%%%%%%%%%%%%%%%%%%%%%%%%%%%%%%%%%%%%%%%%%%%%%
```

```
subplot (2,1,2)
plot(time(1:r),slope,time2,FitSlope,'o'); title('Position vs
time ')
xlabel('time (sec)') % x-axis label
ylabel('position (um)') % y-axis label
```

```
dim = [.2 .075 .3 .3];  
%%%Optional overlap fitting  
polyfit_str = ['y = ' num2str(p(1)) ' *x + ' num2str(p(2))];  
annotation('textbox',dim,'String',polyfit_str,'FitBoxTo-  
Text','on');
```

Chapter 6

Conclusion and Outlook

Artificial lipid membranes are frequently used in biophysical studies to investigate for instance, the mechanical properties of lipid membranes or protein-membrane interactions. Free standing artificial membranes with access to both sides of the membrane can facilitate the study of the mechanical behavior of lipid membranes when combined with force spectroscopy technologies. In this thesis, it was demonstrated that the formation of artificial lipid membranes in microfluidic devices combined with optical tweezers is not only a suitable approach to perform mechanical studies on lipid membranes, but that it enables new possibilities because of the direct access to both leaflets of the membrane. This final chapter summarizes the general contributions of this research to the field and proposes future directions.

6.1 Summary

Several vital cell processes are carried out at the lipid membrane [1, 2]. Artificial lipid bilayers are used as model lipid membranes to study membrane-associated processes [3]. Combination of model membranes with force spectroscopy allows understanding the mechanics of these processes. Current model membranes constrain the dynamic real-time access to one side of the membrane. Free standing lipid artificial bilayers assembled on apertures allow easier access to both sides of the membrane, making them suitable model membranes to combine with force spectroscopy techniques like optical tweezers, while enabling dynamic control on the solution on each side of the membrane.

The self-assembly of lipid membranes in microfluidics devices was explored in chapter 3. Several materials were tested: polydimethylsiloxane (PDMS), glass and a UV curable polymer called NOA81. Hydrophobicity of the microchannels (with a water droplet contact angle above $\sim 100^\circ$) turned to be crucial to form membranes. The formation of membrane lipid bilayers was confirmed by performing electrophysiology tests on pore proteins inserted on the lipid membranes of 1,2-dihexadecanoyl-sn-glycero-3-phosphocholine (DPhPC). In addition, a visual characterization of the lipid membrane on the aperture is carried out via confocal microscopy as well as a general study of the dynamic of bilayer formation, measured with capacitance recordings. In order to form lipid membranes composed of a mixture of DOPC (1,2-Dioleoyl-sn-glycero-3-phosphocholine) and DPPC (1,2-dihexadecanoyl-sn-glycero-3-phosphocholine), both lipids were dissolved in either a mixture of organic solvents (chloroform, decane and methanol) or in purely chloroform. The choice of solvent had an impact on the resulting structure of the lipid membranes. In chapter 4, a deeper look into the differences between these two types of membranes revealed that the membrane total area was affected by the choice of solvent. Furthermore, it was found that pockets of solvent at the edge of the membrane prevented optical trapping close to the membrane. Interestingly, the membranes formed with only chloroform had (almost) no pocket of solvent, likely because of the chloroform being absorbed by NOA81. Then, chapter 5 showed that the combination of optical tweezers with the free standing lipid bilayers previously described enabled the formation cylindrical lipid nanotubes, either by pushing or pulling a trapped bead. Tubes of several hundreds of microns were formed and the dynamics of tube coalescing could be recorded.

6.2 Contributions to the field

6.2.1 Development of artificial lipid membranes in microfluidics

Model membranes mimic lipid cell membranes [4]. Common model membranes [5, 6] can be categorized into supported lipid bilayers, vesicles [7], free standing bilayers spanned on apertures [8], and water emulsion droplets submerged in solvent [9]. Several technologies are being developed for the formation of different model

membranes. Despite the fact that model lipid membranes studied in the lab usually have a surface area of a few microns, the assembly process often requires the use of chambers at the scale of centimeters, as well as multiple steps of thawing and extrusion. Recent developments in manufacturing microtechnologies have helped to reduce dimensions and process times.

This thesis presents a reliable technology to assemble free standing lipid membranes using microfabricated devices. A microfluidic cartridge consisting of parallel channels connected with a rectangular aperture was designed and characterized to assemble artificial membranes. This methodology resulted on a system capable of assembling lipid bilayer membranes of different lipid composition. Using decane as organic solvent, ~70% of the aperture was covered by the lipid bilayer, while the remaining area was occupied by a pocket of solvent (annulus). An almost complete depletion of the annulus can be achieved by choosing a solvent (chloroform) capable of being absorbed by the flowcell material. In comparison with other methods, this approach is an important contribution to the field as it allows real-time control over conditions (voltage, molecules in solution, pH) over both leaflets of the membrane. Furthermore, the lipid bilayer plane is perpendicular to the microscope focal plane, allowing observation of morphological changes in the lipid membrane and straightforward combination with optical techniques. Other advantages are the easier manufacturing and the cost effectiveness.

6.2.2 Optical tweezers combined with artificial lipid membrane

Force spectroscopy at the interface of lipid membranes enables the study of lipid membranes rheology as well as membrane-protein interactions and the mechanism of motor proteins inserted in the membrane. Atomic force spectroscopy (AFM) [10, 11], optical tweezers [12], micropipette aspiration [13, 14] and microfluidics [15, 16] are common techniques to carry out studies on artificial and cell lipid membranes. Most often, supported lipid bilayers or GUVs are used with these force spectroscopy techniques, however, such artificial membranes systems are typically limited to only one side of the membrane when interfaced with optical tweezers or AFM. Also, supported lipid bilayers can be influenced by surface effects. Therefore, the use of free standing lipid bilayers spanning over apertures in microdevices present advantages over other model membranes in force spectroscopy studies.

This work shows the first successful operation of optical tweezers combined with planar lipid membranes accessible from both sides. Direct manipulation of the membrane is demonstrated with membranes with a reduced annulus. One of the microfluidic devices designed in this thesis can host several membranes simultaneously, which are all accessible with an optical tweezers. This device facilitates optical tweezers studies of by allowing to work with different membranes of same lipid composition in a same device with access to both sides of the membranes. Direct mechanical manipulation and adjustable buffer conditions both simultaneously are

highly desired features that this technique offers, enabling the study of biological processes that depend on asymmetric conditions on each membrane sides. In addition, the easy access facilitates the study of the formation of lipid nanotube via the intrusion of objects on a flat membrane. The long lifetimes of the membranes contained in reusable cartridge-like devices enables the study lipid membranes in a more reproducible manner compared with others models like GUVs where their manipulation and size is restricted.

6.3 Future work

The methodology developed in the context of this thesis can be used for combined electrophysiology and force spectroscopy of lipid membranes. To reach the full potential of this technique, a more complete descriptive model of the membrane is needed. More complex lipid membranes could also be implemented.

Here, two types of membranes have been formed: membranes with a single type of lipid (DPhPC) and membranes with a mixture of lipids (DOPC and DPPC). The study of a cocktail of different lipids (DMPC and glycolipids), cholesterol and plus the addition of transmembrane proteins (translocon proteins like Sec61[17] or toxin proteins[18]) would represent a model membrane that approximate better to a real cell lipid membrane. A further increase in complexity would be to assemble asymmetric membranes, which are lipid membranes with different lipid composition in each leaflet of the bilayer and are more accurate models of cell membranes. Flowing different lipids on each side of the channels would enable the assembly of asymmetric bilayers via contacting monolayers of different lipid compositions. In a similar way, a different type of asymmetry can be achieved by placing a network of protein filaments on one side of the membrane mimicking a simple cytoskeleton.

A mathematical model to describe this system can help in predicting certain properties like tension and bending rigidity. The addition of a reservoir of lipids (i.e. continuous source of lipids) and the wall boundaries should be added to the current model of flat lipid membranes. Determination of tension by a non-invasive method must be developed. A good approach for this is the analysis of fluctuations of the membrane, which was previously used on giant unilamellar vesicles. Studying the fluctuations of the membrane could help in understanding the tension and bending rigidity for asymmetric membranes or the effect of different concentrations of cholesterol.

Lipid nanotubes were formed with easy access to both sides of the membrane. It is desired to perform a deeper comparative study of the two different methods used to form lipid nanotubes: pushing a microparticle across the membrane and pulling a patch formed between the lipid bilayer and the microparticle. The effect of the microparticle diameter and surface chemistry should be investigated. The potential of this technique can be further explored by studying single molecule events like the translocation of biopolymers (protein, DNA) across the membrane mediated by transmembrane transporters.

6.4 References

1. Dufrene, Y.F., et al., *Five challenges to bringing single-molecule force spectroscopy into living cells*. Nat Meth, 2011. **8**(2): p. 123-127.
2. Richter, R.P., J.L.K. Him, and A. Brisson, *Supported lipid membranes*. Materials Today, 2003. **6**(11): p. 32-37.
3. Chan, Y.-H.M. and S.G. Boxer, *Model Membrane Systems and Their Applications*. Current opinion in chemical biology, 2007. **11**(6): p. 581-587.
4. Li, L.B., I. Vorobyov, and T.W. Allen, *The role of membrane thickness in charged protein–lipid interactions*. Biochimica et Biophysica Acta (BBA) - Biomembranes, 2012. **1818**(2): p. 135-145.
5. Khan, M.S., N.S. Dosoky, and J.D. Williams, *Engineering Lipid Bilayer Membranes for Protein Studies*. International Journal of Molecular Sciences, 2013. **14**(11): p. 21561-21597.
6. Peetla, C., A. Stine, and V. Labhasetwar, *Biophysical Interactions with Model Lipid Membranes: Applications in Drug Discovery and Drug Delivery*. Molecular Pharmaceutics, 2009. **6**(5): p. 1264-1276.
7. Akbarzadeh, A., et al., *Liposome: classification, preparation, and applications*. Nanoscale Research Letters, 2013. **8**(1): p. 102.
8. Jeong, D.-W., et al., *Enhanced stability of freestanding lipid bilayer and its stability criteria*. Scientific Reports, 2016. **6**: p. 38158.
9. Leptihn, S., et al., *Constructing droplet interface bilayers from the contact of aqueous droplets in oil*. Nat. Protocols, 2013. **8**(6): p. 1048-1057.
10. Garcia-Manyes, S., G. Oncins, and F. Sanz, *Effect of Temperature on the Nanomechanics of Lipid Bilayers Studied by Force Spectroscopy*. Biophysical Journal, 2005. **89**(6): p. 4261-4274.
11. Steltenkamp, S., et al., *Mechanical Properties of Pore-Spanning Lipid Bilayers Probed by Atomic Force Microscopy*. Biophysical Journal, 2006. **91**(1): p. 217-226.
12. Ayala, Y.A., et al., *Rheological properties of cells measured by optical tweezers*. BMC Biophysics, 2016. **9**(1): p. 5.
13. Oh, M.-J., et al., *Micropipette Aspiration of Substrate-attached Cells to Estimate Cell Stiffness*. Journal of Visualized Experiments : JoVE, 2012(67): p. 3886.

-
14. Raktim, D. and D. Rumiana, *Inward and outward membrane tubes pulled from giant vesicles*. Journal of Physics D: Applied Physics, 2014. **47**(28): p. 282001.
 15. Li, X., et al., *Probing red blood cell mechanics, rheology and dynamics with a two-component multi-scale model*. Philosophical transactions. Series A, Mathematical, physical, and engineering sciences, 2014. **372**(2021): p. 20130389.
 16. Honerkamp-Smith, A.R., et al., *Membrane Viscosity Determined from Shear-Driven Flow in Giant Vesicles*. Physical Review Letters, 2013. **111**(3): p. 038103.
 17. Goder, V. and M. Spiess, *Topogenesis of membrane proteins: determinants and dynamics*. FEBS Letters, 2001. **504**(3): p. 87-93.
 18. Thoren, K.L., et al., *Lethal factor unfolding is the most force-dependent step of anthrax toxin translocation*. Proceedings of the National Academy of Sciences, 2009. **106**(51): p. 21555-21560.

Glossary

Abbreviations

Small unilamellar vesicle	(SUV)
Giant unilamellar vesicle	(GUV)
Multilamellar vesicle	(MLV)
Atomic force microscopy	(AFM)
Free black lipid membrane	(BLM)
Polydimethylsiloxane	(PDMS)
Norland optical adhesive 81	(NOA81)
Endoplasmic reticulum	(ER)
Poly(methylmethacrylate)	(PMMA)
Tetraethoxysilane	(TEOS)
Tri-chloro(1H,1H,2H,2H-perfluorooctyl)silane	(PFOTS)
Trichloro(octyl)silane	(OTS)
Methyltriesilane	(MTES)
deionized water	(D.I.)
Ultraviolet	(UV)
Lipids (1,2-diphytanoyl-sn-glycero-3-phoscholine	(DPhPC)
1,2-di-(9Z-octadecenoyl)-sn-glycero-3-phosphocholine	(DOPC)
1,2-dihexadecanoyl-sn-glycero-3-phosphocholine	(DPPC)
N-(Fluorescein-5-thicarbonyl)-1,2-dihexadecyl-sn-gycero-3- phosphoethanolamine (Fluor-DHPE)	
1,2-dipalmitoyl-sn-glycero-3-phosphoethanolamine-n- (cap biotinyl)	(Biotinyl Cap PE)

Acousto-Optic Deflector (AOD)
Position Sensitive Detector (PSD-Sensor)
Back focal plane interferometry (BFP)
pressure (ΔP)
pipette aperture (L_p)
Giga seal or resistances (R_{memb})
Clamp voltage (V_{clamp}).
Stiffness (K)
Flow velocity (v)
Boltzmann constant (K_B)
Temperature (T)
Total capacitance (C_T)
Membrane capacitance (C_M)
Viscosity (η)
Speed of the particle $L'(t)$

Acknowledgements

Thank you lord because without you anything of this would be possible.

I want to thank enormously to Dr. Marie-Eve Aubin-Tam who gave me the opportunity to turn my ideas into a reality. Thank you for your supervision during my Ph.D. I will always admire your determination, energy and professionalism. I feel very thankful of have been part of your group.

My sincere gratitude to my promotor Prof. S. Tans for his good advice during this years, and to the members of the committee Prof. M. Dogterom, Prof. C. Wyman, Prof. M. Prins and Dr. L. Segerink for accepting to review my work. During this project I have the opportunity to explore different scientific disciplines, it was not easy but it was enjoyable thanks to the advice of many experts. I would like to thank to Dr. Christophe Danelon for your time, you always had a good suggestion and disposition to help. I also want to thank Dr. Andreas Engel for his sharp-eyed and accurate comments during the group meetings.

During my Ph.D. I realized that friendship is one of the things that makes you giving the little extra at the end of a tough day. Thank you Dr. Roland Kieffer, I will remember your advises, good attitude and commitment for your work; your ideas are also part of this project. Vanessa many thanks for your support, I admire your strength, I learned from you to always have my feet on the ground. I will miss the nice talks during the dinners with you and Nuno, thank you for sharing important moments in life. Organization and discipline are great skills that I learned from my friend Dominik, thank you very much for sharing your friendship and good humor. A mi amigo Da, I still remember the rainy midnight when I meet you. A lucky friendly guy with non fears of making new friends. Thank you for helping me to improve the setup, I always enjoyed the philosophical, crazy and science fiction talks. I also want to thank to Jochem, Ewa, Benjamin and Lisa for your friendship. I would like to thank to Simon, Michaela, Aurora and Yaron, friends that kindly offered experience, expertise and advice while working as postdocs in the department.

Honestly speaking, no one else can understand a PhD better than another PhD. To my PhD friends, brothers in resistance and conviction, colleagues in seminars, family in christmas time, support during incertitude and comrades in party time. I want to thank to Nuria, Seungkyou and Mahipal for sharing your experiences and friendship in the PhD. As well as Alicia, Jonas, Johannes, Duco and Ilja, thank you for your warm attitude and amazing humor sense. Thank you Laura, Mathia, Carsten, Luuk (for the graduation tips too), Viktorija and Mohamed, you guys are so friendly that sometimes I felt like if I were part of your lab. I want to thank to Stephanie, Adithya, Siddharth and Daniel for sharing your enthusiasm while hard working in clean room. Orkide, Sumit, Nicole, Helena, Ferhat, Marek, Louis and Richard for the nice chats and sharing your time.

A PhD student learns a lot during this period and frequently needs to get out of the comfort zone. I think passing this knowledge is the best way to consolidate and challenge yourself. Saying that, I want to thank to the great students I had the opportunity of supervise. Thank you Reymond, Rosalie, Igor, Anthea and Ruben for you dedication and hard work.

I want to thank to the staff of the department for your professional work, Amanda, Jolijn, Dijana, Dimitri, Margreet, Roland Dries, Sacha and to Jeremie for their friendship and help.

One of the most fantastic experiences of carrying out a PhD abroad was making new friends. For all those wonderful moments, trips, dinners and parties, I want to thank to Roy, Erandi, Carlos y Laura, Isaac, Victor and Aura, Luis and Linda, Adonis and Tania, Moises, and last but not least Steffano. Thank you for opening your hearts.

The biggest achievements in my life could not be possible without the love of my family for that I want to thank to my father Victor Marin, my mother Cándida Lizarraga and my sister Angélica for their support and unconditional love. Mom, I did not make a telescope to look the macrocosm but instead, I made a microscope to study what hides the micro world.

No matter how difficult the situation was you were there for good, you are the source of big adventures of my life, you challenge me to be myself better every day. You are my support and my confident. For that and countless reasons I dedicate this work to you, Fabiola Gutiérrez.

Curriculum vitae

Victor Manuel Marin Lizarraga was born in Merida city, Mexico on 11 of March of 1986. In 2010 he graduated from the Merida institute of technology in Mexico with a major in engineering biochemistry. Later he was awarded with a scholarship to study a MSc in Biomedical Engineering and Physics at the Centre for Research and Advanced Studies campus Monterrey, Mexico. In 2012 he obtained the Master's degree for the study of the spiral micro sorters in microfluidics devices. From November 2012 to March 2017 he worked on a PhD project at Delft University of Technology, The Netherlands within the Applied Physics faculty at the Bionanoscience department. Under the supervision of Marie-Eve Aubin-Tam, he developed a new technology to assemble artificial lipid membranes in microfluidics devices combined with optical tweezers.

Publications

Dols-Perez A, **Marin V**, Aubin-Tam ME. Optical tweezers investigation of the coalescence of lipid nanotubes formed from a planar free standing membrane. (in preparation)

Marin V, Dols-Perez A, Kieffer R, Aubin-Tam ME. Optical tweezers nanomanipulation at the interface of free-standing lipid bilayers. (Submitted).

Marin V, Kieffer R, Padmos R, Aubin-Tam ME. Stable free-standing lipid bilayer membranes in Norland Optical Adhesive (NOA81) microchannels. *Analytical Chemistry*, 88, 7466-7470, 2016